





**A spectroscopic study of Nd<sup>3+</sup> and Pr<sup>3+</sup>  
doped fluorozirconate glass**

A thesis submitted

by

**Ian Robert Mitchell**

for the degree of

**Doctor of Philosophy**



Optical Technology Research Laboratory,  
School of Communications and Informatics,  
Victoria University

1999

22489257

FTS THESIS  
621.36 MIT  
30001005559044  
Mitchell, Ian Robert  
A spectroscopic study of  
Nd<sup>3+</sup> and Pr<sup>3+</sup> doped  
fluorozirconate glass

For Anne

“Every passing hour brings the Solar System forty-three thousand miles closer to Globular Cluster M13 in Hercules – and still there are some misfits who insist that there is no such thing as progress.

Ransom K. Ferm.”

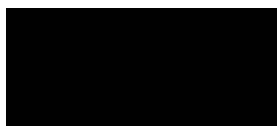
From “The Sirens of Titan” by Kurt Vonnegut

# Declaration

I, Ian Robert Mitchell, declare that this thesis titled,

“A spectroscopic study of Nd<sup>3+</sup> and Pr<sup>3+</sup> doped fluorozirconate glass”

is my own work and has not been submitted previously, in whole or in part, in respect of any other academic award.

A solid black rectangular box used to redact the signature of Ian Mitchell.

Ian Mitchell,

dated the 9<sup>th</sup> day of August, 1999.

# Acknowledgements

There are many people, without whom, this thesis would never have been completed. Foremost in this group of people are Dr Peter Farrell, who has given me superb guidance and Professor David Booth who had the initial faith in me and has provided me with the opportunity to complete this work. Both of these people have always given me tremendous support and encouragement and I cannot thank them enough for this. Later to this group is Professor Min Gu who has provided me with the opportunity to continue this work and has backed that up with financial support.

Some of the glass materials used in this work were provided by the Photonics Section, Telstra Research Laboratories, Clayton, Victoria.

Significant and helpful discussions have been had with Professor Min Gu, Dr Greg Baxter, Dr Ken Peard, Valentine Bogdanov, Scott Wade, Darol Garchev, Puchun Ke, Christina Vergara and Christopher Vale and for this I thank them whole-heartedly.

I would like to thank all members of the OTRL for their help and friendship over the past few years. I would also like to thank the undergraduate students for keeping life entertaining, especially Dale, Kon and Tass.

There are two people who cannot bear witness to the completion of this thesis but who will always be in my memory, Dr Ssenyomo Kaddu and Dr James Wilkie, may they rest in peace.

Special thanks go to Colin and Patricia for their faith and encouragement.

Finally, to the two most significant people in my life. Anne, thank you for all your support both financial and emotional and to Jessica, thanks for being my inspiration and thank you both for all the love.

# Abstract

This work is an investigation of praseodymium and neodymium doped fluorozirconate glasses with consideration given to applications in medicine, optical data storage and printing, communications and research. In order to study the feasibility of these applications a rate equation model has been developed, utilising a 795nm-pump source, that describes excited state populations for a variety of parameters. Parameters to be varied are the input pump power, the spot size of the input beam and the concentration of praseodymium and neodymium. Spectroscopic parameters are determined for the model by observation of absorption spectra, time dependent fluorescence and steady state fluorescence. The model is used to predict the performance of the glasses as well as being an integral part of a novel imaging technique. The analysis performed in this work is equally applicable to other rare earth doped materials.

The initial analysis of these materials utilised Judd-Ofelt theory whereupon deficiencies were noted with the theory as applied to praseodymium. Modified techniques have been developed for application to praseodymium by other workers but these, for the most part, only correct the unphysical aspects of predictions made utilising the original theory. An attempt to further enhance the theory by the inclusion of lifetime information in the fitting process is made here. The lifetime of a state, among other things, depends on radiative decay rates to states other than the ground state. While this does not improve the reliability of the Judd-Ofelt theory as applied to praseodymium, it is thought that this new technique will improve the precision and accuracy of

predictions made for other rare earth doped materials. The temperature dependence of the Judd-Ofelt parameters is investigated to validate or otherwise the approximation made by Judd and Ofelt that ions in a state are evenly distributed across the sub-states. While variations with temperature are noted for the Judd-Ofelt parameters, the spectroscopic parameters predicted from the theory do not show significant variation. The excited state absorption cross-section of the  $^4F_{3/2}$  state of neodymium for 795nm excitation has been determined to be  $0.15 \pm 0.02$  of the ground state absorption cross-section.

Time dependent fluorescence has been used to investigate the energy transfer processes both within and between species of ions for the significant radiative states. The parameter for cross-relaxation from the  $^3P_0$  state of praseodymium,  $\alpha_1$ , is  $(18 \pm 3) \times 10^{-23} \text{ m}^3/\text{s}$ . For two ion energy transfer from the  $^3P_0$  state of praseodymium to neodymium, the energy transfer parameter,  $\alpha_2$ , has been determined to be  $(6.6 \pm 0.8) \times 10^{-23} \text{ m}^3/\text{s}$ . The parameter for cross-relaxation from the  $^4F_{3/2}$  state of neodymium,  $\alpha_5$ , is  $(0.34 \pm 0.06) \times 10^{-23} \text{ m}^3/\text{s}$ . The energy transfer parameter describing the two ion transfer process from the  $^4F_{3/2}$  state of neodymium to praseodymium,  $\alpha_6$ , is  $(1.9 \pm 0.4) \times 10^{-23} \text{ m}^3/\text{s}$ . While three-ion energy transfer processes can be observed at higher dopant concentrations, it is necessary to utilise a different technique to quantify the parameter associated with these.

The variation of steady state fluorescence output for varying pump power has been used to determine further parameters required for the model. The parameter describing three ion energy transfer from the  $^3P_0$  state of praseodymium,  $\alpha_4$ , is  $(1.6 \pm 0.2) \times 10^{-43} \text{ m}^6/\text{s}$ . Co-operative upconversion is a feature of the  $^4F_{3/2}$  state of neodymium and the parameter

for quantifying this process,  $\alpha_7$ , has been determined to be  $(500\pm 100)\times 10^{-23}\text{m}^3/\text{s}$ . Finally, the parameter that quantifies the rate of energy transfer from the  ${}^2\text{G}_{11/2}$  state of neodymium to praseodymium,  $\alpha_9$ , is  $(17\pm 5)\times 10^{-23}\text{m}^3/\text{s}$ .

The completed model is used to predict gain for the existing glass samples but gains of less than one are the result, which is duly confirmed by experiment. The poor performance of the glasses in this respect dismisses most of the initially envisaged applications. The temperature dependence of energy transfer parameters has been investigated for temperature sensor applications involving the  ${}^3\text{P}_0$  state of praseodymium. Further, a lifetime based temperature sensor has been proposed utilising the  ${}^1\text{G}_4$  state of praseodymium and a 795nm pump source. The model is also used to create a relatively high resolution image of dopant concentration in a fibre core.

While the overall performance of the glass has been disappointing with regard to initially proposed applications, the techniques for analysis have revealed a great deal. The techniques used here are equally applicable to all rare earth ions opening the way for better modelling of amplifiers and lasers as well as allowing higher precision images of dopant concentration to be made.

# Table of contents

<b>Declaration</b> .....	i
<b>Acknowledgements</b> .....	ii
<b>Abstract</b> .....	iii
<b>Table of contents</b> .....	vi
<b>Chapter 1. Introduction</b> .....	1-1
1.1 Introduction .....	1-2
1.2 Applications .....	1-2
1.2.1 Medical.....	1-2
1.2.2 Optical data storage and printing .....	1-3
1.2.3 Communications .....	1-4
1.2.4 Research .....	1-5
1.3 Blue lasers .....	1-5
1.4 Praseodymium.....	1-6
1.5 Rate equation technique .....	1-9
1.6 Basic model .....	1-9
1.7 Scope of the thesis.....	1-11
<b>Chapter 2. Absorption</b> .....	2-1
2.1 Introduction .....	2-2
2.2 The Samples .....	2-3
2.3 Ion density calculations .....	2-4
2.4 Transmittance.....	2-5
2.5 Oscillator strength .....	2-5
2.6 Actual concentrations .....	2-10
2.7 Oscillator strengths of the codoped glass.....	2-11

2.8	Judd-Ofelt.....	2-12
2.8.1	Oscillator strength calculations .....	2-13
2.8.2	Determination of Judd-Ofelt parameters.....	2-14
2.8.3	Judd-Ofelt parameters .....	2-15
2.8.4	Lifetimes and Judd-Ofelt.....	2-17
2.9	Temperature dependence of Judd-Ofelt parameters.....	2-22
2.10	Spectroscopic parameters.....	2-23
2.10.1	Relaxation rates.....	2-23
2.10.2	Radiative emission rate $\omega_{N_4}$ .....	2-24
2.10.3	Phonon diffusion relaxation rate $\omega_{N_{12}}$ .....	2-24
2.10.4	Excited state absorption cross-section $\sigma_{esa}$ .....	2-25
2.10.5	Ground state absorption cross-section $\sigma_{gsa}$ .....	2-28
2.11	Conclusion.....	2-28
<b>Chapter 3.</b>	<b>Time dependent fluorescence .....</b>	<b>3-1</b>
3.1	Introduction .....	3-2
3.2	The rate equation approach .....	3-2
3.3	Applying the rate equation approach. ....	3-7
3.4	Experimental arrangement .....	3-10
3.5	Fitting of decay data.....	3-11
3.6	Energy transfer and concentration.....	3-14
3.7	Applications of $\alpha_1, \alpha_2, \alpha_5, \alpha_6$ .....	3-16
3.8	Conclusion.....	3-17
<b>Chapter 4.</b>	<b>Steady state fluorescence .....</b>	<b>4-1</b>
4.1	Introduction .....	4-2
4.2	Spot size determination .....	4-3
4.3	Power in the spot.....	4-3

4.4	Pumping rate ( $\overline{\omega_p}$ ) .....	4-4
4.5	Measurement of fluorescence.....	4-5
4.6	$\alpha_4$ .....	4-6
4.7	465.8nm pump experiment.....	4-7
4.8	$\alpha_7$ and $\alpha_9$ . .....	4-10
4.9	795nm pump experiment.....	4-17
4.10	Other processes .....	4-20
4.11	Pumping approximations .....	4-23
4.12	Conclusion.....	4-24
<b>Chapter 5.</b>	<b>Applications</b> .....	<b>5-1</b>
5.1	Introduction .....	5-2
5.2	Gain .....	5-4
5.2.1	Determination of loss in the system for 635nm light.....	5-5
5.2.2	Prediction of gain .....	5-5
5.3	Optimal concentrations .....	5-7
5.4	Concentration determination.....	5-10
5.5	Imaging.....	5-11
5.6	1300nm amplifiers .....	5-17
5.7	Temperature sensors.....	5-19
5.8	The future for Nd:Pr codoping .....	5-25
5.9	Conclusion.....	5-27
<b>Chapter 6.</b>	<b>Conclusion</b> .....	<b>6-1</b>
6.1	Conclusion.....	6-2

<b>References</b> .....	R-1
<b>Publications</b> .....	P-1

# 1. Introduction

Section.....	Page
1.1 Introduction .....	1-2
1.2 Applications .....	1-2
1.2.1 Medical.....	1-2
1.2.2 Optical data storage and printing.....	1-3
1.2.3 Communications .....	1-4
1.2.4 Research .....	1-5
1.3 Blue lasers .....	1-5
1.4 Praseodymium .....	1-6
1.5 Rate equation technique .....	1-9
1.6 Basic model .....	1-9
1.7 Scope of the thesis.....	1-11

## 1.1 Introduction

In recent years, photonic devices have become an integral part of life. The challenge for researchers is to find new and better photonic devices that can be produced more economically, with better specifications. The aim of this work is to investigate the potential of neodymium ( $\text{Nd}^{3+}$ ) and praseodymium ( $\text{Pr}^{3+}$ ) codoped fluorozirconate glass as the basis for future photonic devices. Of particular interest are the multiple transitions from the  $^3\text{P}_0$  state and a transition from the  $^1\text{G}_4$  state of  $\text{Pr}^{3+}$ . A device utilising the appropriate transitions from these states would have potential applications in medicine, optical data storage, printing, communications and research.

## 1.2 Applications

### 1.2.1 Medical

The use of lasers in the medical field has a growing list of applications from surgery to the treatment of cancers [Arons I. J., 1994; Li J. *et al.*, 1998]. At present argon ( $\text{Ar}^+$ ) lasers are utilised in surgery involving coloured tissue and  $\text{CO}_2$  lasers for white tissue. The  $\text{Ar}^+$  laser is large and expensive but produces high output powers at blue wavelengths. An inexpensive blue device would mean that this cutting edge technology would become widely available to the medical community.

The use of optical fibres as temperature sensors is highly desirable for medical applications as the fibres are electrically isolated and are immune from electromagnetic interference. Conventional temperature sensors involve thermocouples or thermistors which can cause interference during radiative treatments such as hypothermia [Culshaw B. *et al.*, 1988]. There are at least two possible techniques that can be

employed with rare earth doped glasses to produce a temperature sensor. One technique involves the measurement of a temperature dependent fluorescence lifetime (FL). The second technique requires the existence of thermally linked states from which relaxation produce two different wavelengths, the intensity ratio of which is dependent on temperature (FIR) [Berthou H. *et al.*, 1990; Collins S. F. *et al.*, 1999; Maurice E. *et al.*, 1997; Sun T. *et al.*, 1999].

Lasers are also useful for spectroscopic studies in medical research. For example, human colon tissue will fluoresce when pumped with blue, green or red wavelengths. The resulting fluorescence spectra are used for the detection of precancerous changes to colon tissue [Huang Z. *et al.*, 1998]. An inexpensive laser that could be tuned to produce each of the wavelengths would be an invaluable tool.

### **1.2.2 Optical data storage and printing**

The principle restriction regarding the resolution of high quality printing, whether it be with a laser printer or photocopier, is the size to which a light source can be focussed. Current technology employs red or infrared laser sources as they are compact, common and inexpensive. However, the spot size to which these sources can be focussed is directly proportional to the wavelength of the source. Shorter wavelength sources can be focussed to smaller spot sizes improving the overall resolution of the printing device.

Current technology for optical data storage such as compact disks also employ red or infrared laser sources. Information is stored in the form of pits that either reflect or do not reflect light. The capacity of the disks is limited to the number of pits that can be located on the surface of the disk. The pits are the size of the wavelength of the

photonic device, shorter wavelength devices require smaller pits thus allowing greater storage capacity. The most common aim is to produce a blue laser, this has a wavelength around half that of the current red and infra-red devices which would lead to a four fold increase in the storage capacity of a disk [Bucholtz C., 1995].

### **1.2.3 Communications**

The application of fibre optics to communications provides a low loss, broad bandwidth transmission path that has revolutionised many communication systems. In spite of the low loss, signal deterioration over large distances still limit the transmission range of systems [Shimada S. *et al.*, 1994]. To overcome this loss, amplification of the signal at regular intervals is required. Amplification has been performed utilising repeaters where the incoming signal is detected, converted to an electrical signal, amplified and then re-transmitted as an optical signal. The speed and bandwidth of the system are limited to that of the electronics of the repeater. This consequently represents a significant restriction to the performance of the system. An optical amplifier uses stimulated emission to amplify signals and can be placed in line with the system, requiring no signal conversions to be made. Erbium doped fibre amplifiers have proven to be of great significance for the optimisation of communications in the 1550nm window [Shimada S. *et al.*, 1994]. At present there are few commercially available optical amplifiers for the second communications window around 1300nm [Fibercore; NTT Electronics]. With a large proportion (90%) of currently installed fibre systems optimised for 1300nm operation, it is of considerable interest to develop optical amplifiers for this window [Nishida Y. *et al.*, 1998].

#### **1.2.4 Research**

The development of an inexpensive, multiple wavelength laser is of interest to researchers and would provide significant opportunities for institutions that lack funding for large and expensive laser systems. Optical amplifiers are also of interest to researchers where weak signals need to be observed.

#### **1.3 Blue lasers**

There is significant interest in the production of compact, blue photonic devices for most of the above applications. At present there are several technologies being researched including laser diodes [Nakamura S., 1998; Hecht J., 1996; Fasol G., 1997], frequency doubling of infra-red sources [Hemmerlich A. *et al.*, 1994; Webjorn J. *et al.*, 1998] and upconversion of rare earth doped glasses [Tohmon G. *et al.*, 1997; Zhao Y. *et al.*, 1997; Zellmer H. *et al.*, 1998]. Commercial interest seems to be more focussed on laser diodes but they are yet to achieve the operational lifetimes required for many applications. The frequency doubling of infrared laser diodes requires complicated cavities, which may limit their commercial viability. Blue lasers from rare earth doped fibre require some sort of upconversion process in the pumping scheme. Two different wavelength pump sources can be utilised but this again leads to a complex configuration [Zhao Y. *et al.*, 1995; Tohmon G. *et al.*, 1997]. Single pump wavelength lasers often require the use of a codopant to facilitate the necessary upconversion process. This scheme is simple but threshold powers are remarkably high [Zellmer H. *et al.*, 1998].

## 1.4 Praseodymium

Praseodymium ( $\text{Pr}^{3+}$ ) has transitions that have the potential to be the solution for all of the previously mentioned applications. Radiative transitions in  $\text{Pr}^{3+}$  include 488nm, 520nm, 605nm, 635nm, 695nm, 715nm, 910nm,  $1\mu\text{m}$  and  $1.3\mu\text{m}$  [Goh S. C. *et al.*, 1995; Grattan K. T. V. *et al.*, 1998]. The blue (488nm) transition is of interest for applications concerning optical data storage and printing. The  $1.3\mu\text{m}$  transition is of particular interest for optical amplifiers operating in the 1300nm window [Nishida Y. *et al.*, 1998]. The  $^3\text{P}_0$  state and the  $^3\text{P}_1+^1\text{I}_6$  states are thermally linked giving rise to possible FIR temperature sensor applications [Maurice E. *et al.*, 1997]. The lifetime of the state that gives rise to the  $1.3\mu\text{m}$  transition is highly dependent on the phonon diffusion rate making it an ideal candidate for an FL temperature sensor.

The major obstacle to the realisation of these applications is the method for pumping the  $\text{Pr}^{3+}$  to the appropriate excited state. For example, if a single pump source were to be used, then the wavelength of that source would need to be in the blue region of the spectrum to populate the  $^3\text{P}_0$  state of  $\text{Pr}^{3+}$ . This requires an inexpensive blue light source to exist to produce an inexpensive blue light source so clearly an alternative scheme is required where  $\text{Pr}^{3+}$  is not directly pumped. One particular scheme of interest was proposed by Goh [Goh S. C. *et al.*, 1995] where neodymium ( $\text{Nd}^{3+}$ ) was codoped with the  $\text{Pr}^{3+}$  to produce an excited state population in the  $^3\text{P}_0$  state. The scheme allows for pumping with a readily available and inexpensive infrared laser diode source.

The first work on  $\text{Pr}^{3+}$  and  $\text{Nd}^{3+}$  was by Mosander in 1842 but at that time it was believed to be a single element, didymium [Reisfeld R. *et al.*, 1977]. The first mention of the possibility of excitation of  $\text{Pr}^{3+}$  via  $\text{Nd}^{3+}$  was by Stanley [Stanley A. T. *et al.*,

1993] who were investigating upconversion processes in  $\text{Nd}^{3+}$  but observed fluorescence from a transition that they attributed to traces of  $\text{Pr}^{3+}$  in their glass samples. The processes required for the observation of such a transition is the absorption of a pump photon exciting a  $\text{Nd}^{3+}$  to the  $^4\text{F}_{5/2}$  state. The ion relaxes quickly to the relatively long-lived  $^4\text{F}_{3/2}$  state by phonon diffusion. A further pump photon is required exciting the  $\text{Nd}^{3+}$  to the  $^2\text{D}_{5/2}$  state. The  $^2\text{D}_{5/2}$  state of  $\text{Nd}^{3+}$  is short lived and will decay quickly through other states back to the  $^4\text{F}_{3/2}$  state. Some of the states that the  $\text{Nd}^{3+}$  decay through,  $^4\text{G}_{11/2}$ ,  $^2\text{D}_{3/2}$  and  $^2\text{D}_{9/2}$  are in near resonance with the  $^3\text{P}_1+^1\text{I}_6$  and  $^3\text{P}_0$  states of  $\text{Pr}^{3+}$ , allowing the possibility of energy transfer from the  $\text{Nd}^{3+}$  to the  $\text{Pr}^{3+}$ . The complete system is illustrated in figure 1.4.1 where only a few of the possible output transitions are represented. Other energy transfers from the  $^4\text{F}_{3/2}$  state of  $\text{Nd}^{3+}$  to the  $^1\text{G}_4$  state of  $\text{Pr}^{3+}$  give rise to populations suitable for  $1.3\mu\text{m}$  amplification as well as for an FL temperature sensor. The work in this thesis is the study of the processes that are required to populate these excited states.

The host material selected for this study is a fluorozirconate glass as this has the advantage of a broader absorption spectrum when compared to crystalline hosts. The broader absorption lines facilitate the use of less expensive, broader bandwidth pump sources. In comparison to other glass hosts, fluorozirconate has the advantage of having low phonon energies so that losses in the excited state populations through phonon diffusion are minimized. Specifically, the host material chosen for this work is ZBLANP and this differs from the standard fluorozirconate glass (ZBLAN) by the inclusion of lead fluoride ( $\text{PbF}_2$ ). This is the usual additive for raising the refractive index of the core material in comparison to that of the cladding for optical fibres.

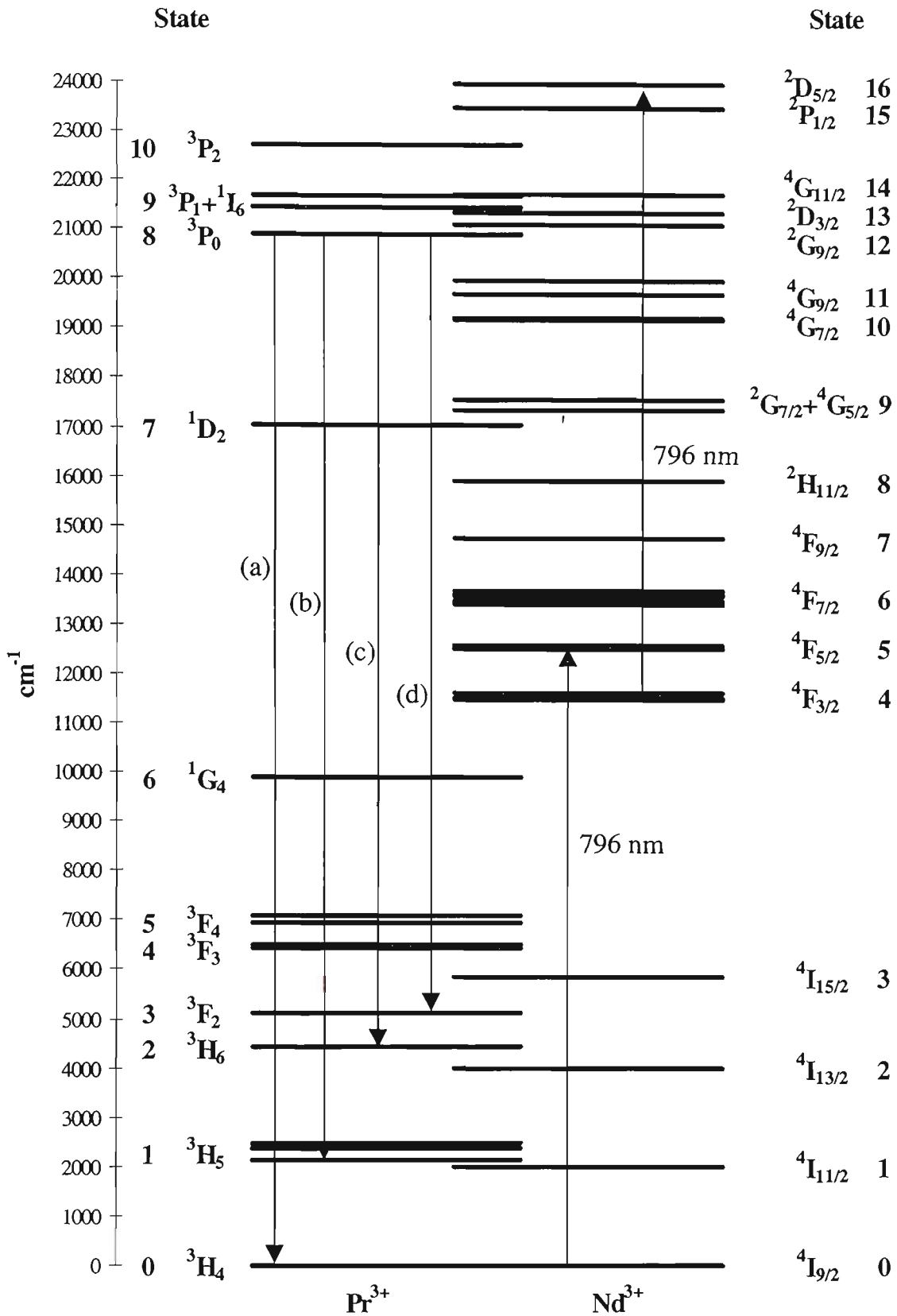


**Figure 1.4.1** Energy levels of Pr<sup>3+</sup> and Nd<sup>3+</sup> ions in a ZBLANP host showing the proposed pumping scheme and some of the possible visible transitions of Pr<sup>3+</sup>. (a) 488 nm, (b) 536 nm, (c) 605 nm and (d) 635 nm. Spectroscopic states are assigned after Carnall [Carnall W. T. *et al.*, 1968].

## 1.5 Rate equation technique

The use of rate equations is a particularly useful analysis tool for modelling lasers and amplifiers, see for example [Tropper A. C. *et al.*, 1994; Remillieux A. *et al.*, 1996]. The rate equations as applied here are for a lightly pumped regime in which the ground state populations can be approximated to the dopant concentration. This approximation allows for the determination of energy transfer parameters, which can be utilised in the quantification of energy transfer rates [Petreski B. P. *et al.*, 1995; Mitchell I. R. *et al.*, 1998]. The technique involves writing rate equations that include terms for the relaxation processes where energy is transferred between ions. This energy transfer term consists of the population of the excited state, the population of the state with which the excited ion is interacting (usually the ground state) and a constant. In this thesis these constants (energy transfer parameters) are determined for energy transfers in and between  $\text{Nd}^{3+}$  and  $\text{Pr}^{3+}$ . They are then used to study the population dynamics of the codopants to determine the viability and uses of such a scheme. The technique is widely applicable to all the rare-earth doped glasses and crystals, providing a useful analysis tool for many laser systems and amplifiers. The energy transfer parameters can also be utilised to determine the dopant concentration of host materials. One technique involves lifetime measurements and has been demonstrated by Petreski [Petreski B. P. *et al.*, 1997]. A new technique is demonstrated here which can be utilised with a scanning confocal microscope to produce images of dopant concentration density across a fibre.

## 1.6 Basic model

The initial rate equation model is based around the energy level diagram for the codoped

glass, figure 1.4.1. This diagram was compiled from absorption spectra of a nominal 2% Nd and 2% Pr codoped ZBLANP glass. Where absorption lines from each species of dopant coincided, the energies of absorption lines from singly doped ZBLANP samples were used. In a complete rate equation model, an equation would be required for each state of each ion, which would lead to a very complicated solution and require knowledge of a large number of parameters. To simplify the model it is assumed that there are only five states that have significant populations. The  $^3P_0$  and the  $^3P_1+^1I_6$  states of  $Pr^{3+}$  are thermally linked and will be treated as a single state. There are a few states of  $Nd^{3+}$  from which energy can transfer to the  $^3P_0$  ensemble of states in  $Pr^{3+}$ . These will also be treated as a single state, the decay rate of which is determined by the slowest rate of the states  $^2D_{5/2}$ ,  $^2P_{1/2}$ ,  $^4G_{11/2}$ ,  $^2D_{3/2}$  and  $^2G_{9/2}$ . The other states that are considered to have significant populations are the ground states of  $Pr^{3+}$  and  $Nd^{3+}$  and the  $^4F_{3/2}$  state of  $Nd^{3+}$ . All ions that are not in any of these states relax quickly down to these population reservoirs giving the simplified rate equations of the system as

$$N_{N_T} = N_{N_0} + N_{N_4} + N_{N_{12}}, \quad (1.6.1)$$

$$\frac{\partial N_{N_4}}{\partial t} = \omega_{gsa} N_{N_0} + \omega_{N_{12}} N_{N_{12}} + \omega_{ET_8} N_{P_8} - (\omega_{esa} + \omega_{N_4} + \omega_{ET_4}) N_{N_4}, \quad (1.6.2)$$

$$\frac{\partial N_{N_{12}}}{\partial t} = \omega_{esa} N_{N_4} - (\omega_{N_{12}} + \omega_{ET_{12}}) N_{N_{12}}, \quad (1.6.3)$$

$$N_{P_T} = N_{P_0} + N_{P_8}, \quad (1.6.4)$$

$$\frac{\partial N_{P_8}}{\partial t} = \omega_{ET_{12}} N_{N_{12}} - (\omega_{P_8} + \omega_{ET_8}) N_{P_8}, \quad (1.6.5)$$

where  $N_{X_n}$  are the time dependent populations of state n of species X (N for  $Nd^{3+}$  and P for  $Pr^{3+}$ ),  $\omega_{gsa}$  is the ground state absorption rate,  $\omega_{esa}$  is the excited state absorption

rate,  $\omega_{x_n}$  is the relaxation rate of state  $n$  of species  $X$  and  $\omega_{ET_n}$  is the energy transfer rate from state  $n$ .  $N_{x_T}$  is the total population of species  $X$  and is generally replaced by  $\rho_x$ , the concentration of species  $X$ .

## 1.7 Scope of the thesis

This thesis consists of five chapters, the first being of an introductory nature where a basic rate equation model has been presented. In Chapter 2 spectroscopic parameters, which are required for the determination of the energy transfer parameters and for the model, are determined from absorption measurements. Time dependent fluorescence measurements are utilised to produce the first of two sets of energy transfer parameters in Chapter 3. The second set of energy transfer parameters are determined in Chapter 4 from steady state fluorescence measurements. In Chapter 5, the complete rate equation model is used to predict gain and optimal concentrations. Also, the energy transfer parameters are utilised in a novel imaging technique that allows the quantification of dopant concentrations. The applications proposed in the earlier part of this chapter will be addressed with regard to Nd:Pr:ZBLANP glasses. Overall conclusions will be drawn in Chapter 6.

## 2. Absorption

Section.....	Page
2.1 Introduction .....	2-2
2.2 The Samples .....	2-3
2.3 Ion density calculations .....	2-4
2.4 Transmittance .....	2-5
2.5 Oscillator strength .....	2-5
2.6 Actual concentrations .....	2-10
2.7 Oscillator strengths of the codoped glass .....	2-11
2.8 Judd-Ofelt.....	2-12
2.8.1 Oscillator strength calculations .....	2-14
2.8.2 Determination of Judd-Ofelt parameters.....	2-14
2.8.3 Judd-Ofelt parameters .....	2-15
2.8.4 Lifetimes and Judd-Ofelt.....	2-17
2.9 Temperature dependence of Judd-Ofelt parameters.....	2-22
2.10 Spectroscopic parameters.....	2-23
2.10.1 Relaxation rates .....	2-23
2.10.2 Radiative emission rate $\omega_{N_4}$ .....	2-24
2.10.3 Phonon diffusion relaxation rate $\omega_{N_{12}}$ .....	2-24
2.10.4 Excited state absorption cross-section $\sigma_{esa}$ .....	2-25
2.10.5 Ground state absorption cross-section $\sigma_{gsa}$ .....	2-28
2.11 Conclusion.....	2-28

## 2.1 Introduction

This is the first of three chapters of which the aim is to determine the spectroscopic parameters required for a rate equation model of a Nd:Pr:ZBLANP glass. The parameters presented in this chapter are based on absorption measurements of the glass samples.

Initial work is centred on the determination of dopant concentrations followed by the determination of the required spectroscopic parameters. One particular technique employed is the application of Judd-Ofelt theory to the absorption spectra. This technique has been successfully applied to rare-earth doped materials with the exception  $\text{Pr}^{3+}$ , which has required the invention of several modified techniques. The modified techniques have provided limited improvements to individual predictions that can be made using Judd-Ofelt theory but fail to provide an overall improvement. Another modified approach is attempted here with the inclusion of lifetime information in the fitting process. A further investigation as to a possible weakness in the Judd-Ofelt theory is undertaken with the determination of parameters at an elevated temperature. Also included is the first application and study known to the author of Judd-Ofelt theory as applied to a  $\text{Pr}^{3+}$  and  $\text{Nd}^{3+}$  codoped glass.

Spectroscopic parameters to be measured or predicted in this chapter are the radiative decay rate for the  ${}^4\text{F}_{3/2}$  state of  $\text{Nd}^{3+}$ , the decay rate attributed to the  ${}^2\text{D}_{5/2}$  state of  $\text{Nd}^{3+}$ , excited state absorption cross-section from the  ${}^4\text{F}_{3/2}$  state of  $\text{Nd}^{3+}$  for 795nm radiation and ground state absorption cross-sections for 795nm ( ${}^4\text{I}_{9/2} \rightarrow {}^4\text{F}_{5/2}$ ), 465.8nm ( ${}^3\text{H}_4 \rightarrow {}^3\text{P}_1$ ) and 476.5nm ( ${}^3\text{H}_4 \rightarrow {}^3\text{P}_0$ ) radiation.

## 2.2 The Samples

Several doped ZBLANP samples have been provided by the Telstra Research Laboratories for the experimental work of this project. The samples are of various shapes, sizes and nominal concentrations and include one singly doped Pr:ZBLANP sample, one singly doped Nd:ZBLANP sample and six Nd:Pr:ZBLANP codoped samples as shown in table 2.2.1. There are two codoped samples with the same nominal concentration of 0.2% NdF<sub>3</sub> 0.2% PrF<sub>3</sub> and it should be noted that these are essentially the same piece of glass. One of these pieces is the bulb taken from the top of a fibre pre-form and the second piece of glass is the pre-form itself with a core diameter of 400 $\mu$ m.

The composition of the ZBLANP host material is 53% ZrF<sub>4</sub>, 15% BaF<sub>2</sub>, (4-X-Y)% LaF<sub>3</sub>, 3% AlF<sub>3</sub>, 20% NaF and 5% PbF<sub>2</sub>. The dopants are in the form of PrF<sub>3</sub> and NdF<sub>3</sub>, represented by X and Y respectively, in the previous formulation and they are substituted for LaF<sub>3</sub> in the host material [France P. W., 1990]. It is common to refer to the dopant concentrations in terms of parts per million (ppm) and it should be noted that this refers to the parts per million of the molecules (i.e. PrF<sub>3</sub>) and not ppm of the individual ions (Pr<sup>3+</sup>).

Glass Composition	Nominal dopant concentration
Pr:ZBLANP	1% PrF <sub>3</sub>
Nd:ZBLANP	1% NdF <sub>3</sub>
Nd:Pr:ZBLANP	0.1% NdF <sub>3</sub> 0.2% PrF <sub>3</sub>
Nd:Pr:ZBLANP	0.2% NdF <sub>3</sub> 0.2% PrF <sub>3</sub>
Nd:Pr:ZBLANP	0.2% NdF <sub>3</sub> 0.2% PrF <sub>3</sub>
Nd:Pr:ZBLANP	0.4% NdF <sub>3</sub> 0.2% PrF <sub>3</sub>
Nd:Pr:ZBLANP	2.0% NdF <sub>3</sub> 0.2% PrF <sub>3</sub>
Nd:Pr:ZBLANP	2% NdF <sub>3</sub> 2% PrF <sub>3</sub>

**Table 2.2.1** Glass samples with nominal dopant concentrations as supplied by Telstra Research Laboratories.

### 2.3 Ion density calculations

As an essential part of later calculations, it is necessary to know the dopant concentrations in terms of concentration density (ions/m<sup>3</sup>). The shape of the Nd<sup>3+</sup> doped glass sample is irregular, making it difficult to determine the density of the glass. Using the 1.0% Pr:ZBLANP sample, the density of the glass was measured to be 4.14g/cm<sup>3</sup>. The atomic weight of Pr (140.91 g/mole) and Nd (144.24 g/mole) are approximately the same, the difference causing only a trivial variation to the final concentration determination. The total atomic weight of the glass as calculated by the weighted summation of the atomic weights of the constituents of ZBLANP is 14593.01 g/mole. The dopant ion concentration is then  $1.71 \times 10^{26}$  ions/m<sup>3</sup> for the 1% (10,000ppm) samples.

## 2.4 Transmittance

Transmittance is the ratio of the power transmitted through the material to the power entering the material. This ratio is related to the cross-section of the material at a particular wavelength by

$$\frac{P_{\text{out}}}{P_{\text{in}}}(\lambda) = \exp\left(-l\sigma_{\text{ab}}(\lambda)(N_{\text{a}} - N_{\text{b}})\right), \quad (2.4.1)$$

where  $P_{\text{out}}$  and  $P_{\text{in}}$  are the output and input powers respectively,  $l$  is the length through which the incident light passes,  $\sigma_{\text{ab}}$  is the cross-section for the transition and  $N_{\text{a}}$  is the population density of the initial and final states [Svelto O., 1990]. When the absorbing transition involves ions from the ground state and  $P_{\text{in}}$  is relatively small, then  $N_{\text{a}}$  can be approximated to the dopant ion concentration ( $\rho_{\text{x}}$ ) and the excited state population ( $N_{\text{b}}$ ) can be approximated to zero, giving

$$\frac{P_{\text{out}}}{P_{\text{in}}}(\lambda) = \exp\left(-l\sigma_{\text{ab}}(\lambda)\rho_{\text{x}}\right). \quad (2.4.2)$$

A simple experiment to measure the transmittance spectrum of a sample involves a collimated white light source, the sample and a wavelength discriminating measurement device. In this work, a fibre coupled white light source was collimated with a microscope objective. The sample was placed in the collimated beam with the transmitted light captured by a second microscope objective, focussing the beam into a fibre coupled optical spectrum analyser.

## 2.5 Oscillator strength

Oscillator strength ( $f$ ) is the ratio of the response of an atomic transition to that of the classic electron oscillator of the same frequency. Absorption oscillator strength is a

relatively easy parameter to measure and gives a good indication as to the strength of a transition.

To measure absorption oscillator strength, the transmittance spectrum of the required transition is used in the determination of the integrated absorption cross-section. The integrated cross-section is then related to the measured oscillator strength ( $f_m$ ) by

$$f_m = 4\pi\epsilon_0 \frac{mc}{\pi e^2} \int \sigma(\nu) d\nu, \quad (2.5.1)$$

where  $\epsilon_0$  is the permittivity of free space,  $m$  is the mass of an electron,  $e$  is the charge of an electron,  $c$  is the speed of light,  $\int \sigma(\nu) d\nu$  is the integrated cross-section and  $\nu$  is the frequency of the transition [Hilborn R. C., 1982]. Absorption spectra are often measured with respect to wavelength ( $\lambda$ ) so a more convenient form for equation 2.5.1 is

$$f_m = 4\pi\epsilon_0 \frac{mc^2}{\pi e^2} \int \frac{\sigma(\lambda)}{\lambda^2} d\lambda. \quad (2.5.2)$$

The measured transmittance spectra can include lines that overlap so it is convenient to least squares fit particular lineshapes to the spectra, usually Gaussian or Lorentzian, figure 2.5.1. By separating the lines, more data becomes available for the Judd-Ofelt fitting process [Medeiros Neto J. A. *et al.*, 1995]. The best fit has been found using a Lorentzian function to fit the  $^3P_0$  absorption (~480nm) while the other absorption lines are fitted with Gaussian functions. Scattering and background losses are removed from the spectra by subtraction. Integrating the fitted lineshape and dividing by the product of the concentration and the length of the sample results in the integrated absorption cross-section. As part of the lineshape fitting process, there is an associated

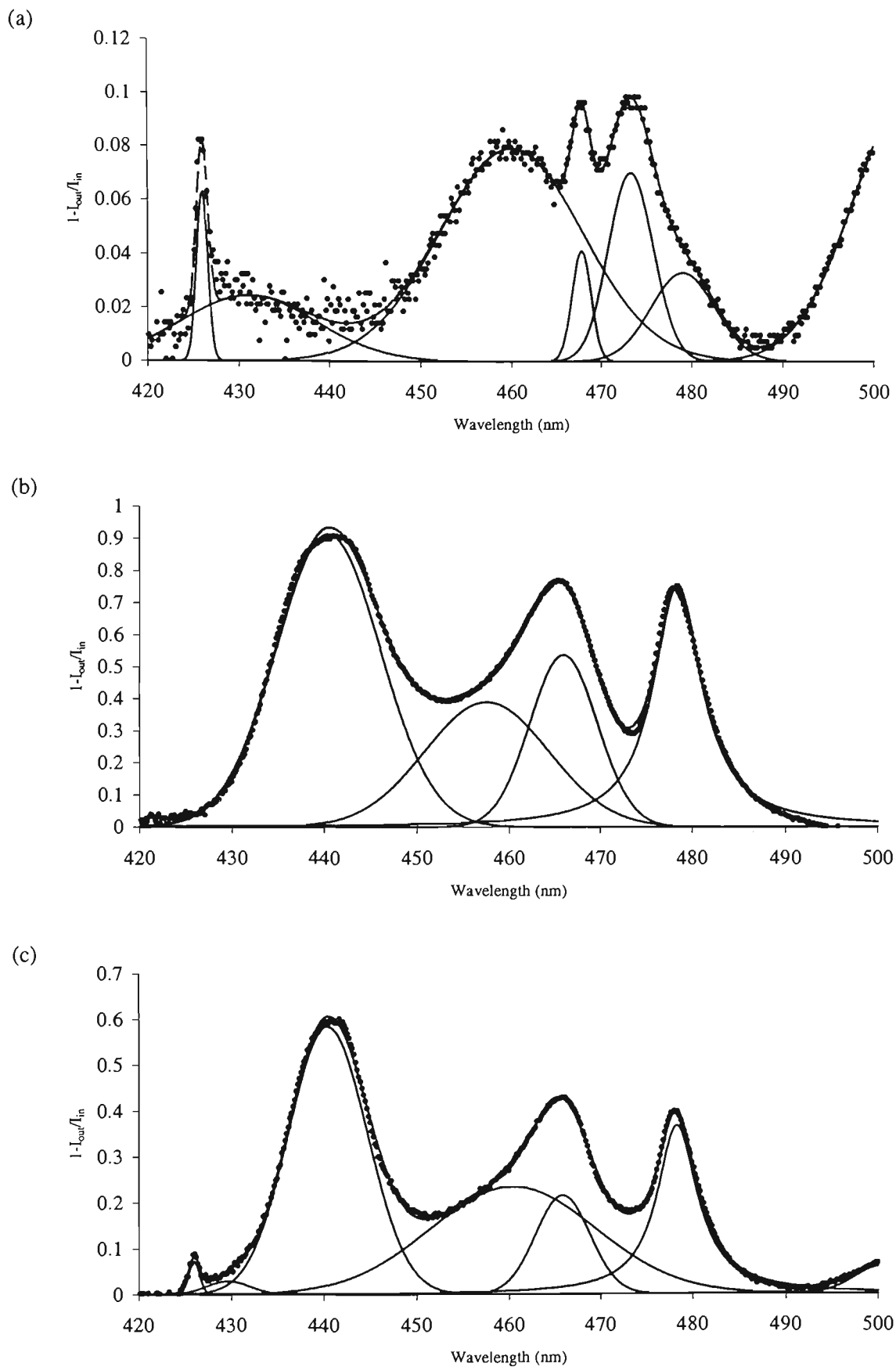


**Figure 2.5.1** Selected absorbance (1-transmittance) spectra for (a) Nd:ZBLANP, (b) Pr:ZBLANP and (c) Nd:Pr:ZBLANP glasses as fitted with Gaussian and Lorentzian lineshape functions. Samples are of differing dopant concentration and dimension.

uncertainty with each of the lineshape fitting parameters. There are also uncertainties in the concentration as well as in the length of the optical path within the sample. The uncertainty of the measured oscillator strength is related to these uncertainties by

$$\Delta f_m^2 = \sum_i \left( \Delta \varphi_i \frac{\partial f_m}{\partial \varphi_i} \right)^2 + \left( \Delta \rho \frac{\partial f_m}{\partial \rho} \right)^2 + \left( \Delta l \frac{\partial f_m}{\partial l} \right)^2, \quad (2.5.3)$$

where  $\varphi_i$  are the lineshape fitting parameters,  $\Delta \varphi_i$  are the uncertainties in the lineshape fitting parameters,  $\rho$  is the dopant concentration,  $\Delta \rho$  is the uncertainty in the dopant concentration,  $l$  is the length of the optical path through the sample and  $\Delta l$  is the uncertainty in the length of the optical path.

The singly doped samples are initially chosen for absorption oscillator strength measurements, tables 2.5.1 and 2.5.2. Not all oscillator strengths have been measured due to a lack of appropriate detectors and light sources for the longer wavelengths. Some lines were too weak to identify from the noise and so in both cases, no oscillator strengths were recorded for them. Of the lines that could be determined, some could not be separated by fitting an appropriate lineshape function and so they appear in the tables as a summation of the appropriate oscillator strengths.

Transition	Nominal Wavelength (nm)	$f_m \times 10^8$	$f_{Balda} \times 10^8$
${}^4I_{9/2} \rightarrow {}^4F_{3/2}$	866	$150 \pm 30$	140
${}^4F_{5/2} + {}^2H_{9/2}$	794	$440 \pm 40$	541
${}^4F_{7/2} + {}^4S_{3/2}$	740	$450 \pm 10$	538
${}^4F_{9/2}$	678	$41 \pm 4$	34
${}^2H_{11/2} + {}^4G_{5/2} + {}^2G_{7/2}$	577	$950 \pm 20$	1166
${}^2K_{13/2} + {}^4G_{7/2} + {}^4G_{9/2}$	520	$430 \pm 50$	451
${}^2K_{15/2} + {}^2G_{9/2} + {}^2D_{3/2} + {}^4G_{11/2}$	460	$190 \pm 20$	135

**Table 2.5.1** Oscillator strengths for ground state absorption in Nd:ZBLANP at room temperature compared to Balda R. *et al.*, 1994.

Direct comparison of the measured oscillator strengths to those of other authors is more for qualitative rather than for quantitative purposes as they do not provide uncertainties with their measurements. However, since the measurement of the absorption cross-section requires knowledge of the concentration of the sample, a comparison of cross-sections can be used to indicate the actual concentrations of the samples. The initial assumption for both the  $\text{Pr}^{3+}$  and  $\text{Nd}^{3+}$  doped samples was that they are of their nominal dopant value ie 1%. Any variations in the oscillator strengths measured here should be due to a deviation from the nominal value of dopant concentration. By taking the ratio of the oscillator strengths measured here to those of the other authors for each absorption line, possible deviations from the nominal dopant concentration can be determined. From table 2.5.1, the average ratio of  $f_m/f_{Balda}$  is 1.01, indicating that 1% is a good indication of the actual dopant concentration. The average of the ratios with Medeiros Neto [Medeiros Neto J. A. *et al.*, 1995] and Quimby [Quimby R. S. *et al.*, 1994], table 2.5.2, are 0.85 and 0.98, respectively. The average of these two average

ratios is 0.92 indicating that the nominal value for Pr<sup>3+</sup> concentration is a reasonable indication as to the actual dopant concentration.

Transition	Nominal Wavelength (nm)	$f_m \times 10^8$	$f_{Medeiros\ Neto} \times 10^8$	$f_{Quimby} \times 10^8$
$^3H_4 \rightarrow ^3F_3 + ^3F_4$	1548	880 ± 90	852	865
$^1G_4$	1010	23 ± 2	25	25
$^1D_2$	588	200 ± 20	233	196
$^3P_0$	478	280 ± 30	296	215
$^3P_1 + ^1I_6$	466	440 ± 80	601	470
$^3P_2$	440	730 ± 80	1031	920

**Table 2.5.2** Oscillator strengths for ground state absorption in Pr:ZBLANP at room temperature compared to Medeiros Neto J. A. *et al.*, 1995 and Quimby R. S. *et al.*, 1994.

## 2.6 Actual concentrations

In order to check the validity of the nominal concentration values for the codoped samples, a comparison of peak absorptions is used. The peak absorption is measured at the wavelength of maximum absorption for the transition. The most clearly defined and most stable absorption oscillator strengths, when comparing transitions in the singly doped to the codoped sample, were to the  $^3P_2$  state of Pr<sup>3+</sup> and the  $^4F_{3/2}$  state of Nd<sup>3+</sup> so these will be used for determination of the actual concentrations. Rearranging equation 2.4.2 and by using the 1% singly doped samples as a reference, the dopant concentration for the codoped samples can be determined from

$$\rho_x = \frac{\ln\left(\frac{P_{out}}{P_{in}}\right)_{ref} \rho_{xref}}{\ln\left(\left(\frac{P_{out}}{P_{in}}\right)_{ref}\right) l}, \quad (2.6.3)$$

the results for which are listed in table 2.6.1. The experimentally determined concentrations differ from the nominal concentrations supplied with the glass samples. In the ensuing work where the magnitude of the dopant concentration is required, the experimentally determined results will be utilised.

Nominal concentration %		$\frac{P_{out}}{P_{in}}$		Actual concentration %	
Nd <sup>3+</sup>	Pr <sup>3+</sup>	<sup>4</sup> F <sub>3/2</sub>	<sup>3</sup> P <sub>2</sub>	Nd <sup>3+</sup>	Pr <sup>3+</sup>
1	1	0.62 ± 0.01	0.08 ± 0.01	1.0 ± 0.1	1.0 ± 0.1
0.1	0.2	0.93 ± 0.01	0.87 ± 0.01	0.15 ± 0.03	0.14 ± 0.02
0.2	0.2	0.76 ± 0.01	0.63 ± 0.01	0.31 ± 0.04	0.24 ± 0.03
0.4	0.2	0.10 ± 0.01	0.41 ± 0.01	0.8 ± 0.1	0.15 ± 0.02
2.0	0.2	0.01 ± 0.01	0.68 ± 0.01	2.1 ± 0.5	0.08 ± 0.01
2.0	2.0	0.62 ± 0.01	0.40 ± 0.01	2.3 ± 0.3	2.0 ± 0.2

**Table 2.6.1** Experimentally determined dopant concentrations using the singly doped samples as a reference.

## 2.7 Oscillator strengths of the codoped glass

The 2.3% Nd -2.0% Pr codoped glass is used for the oscillator strength measurement due to the high dopant concentration producing strong absorption lines, table 2.7.1. Coincident absorption lines from both Nd<sup>3+</sup> and Pr<sup>3+</sup> could not be separated by the fitting of lineshape functions so in this case, only a single entry has been made in the table. At the shorter wavelength end of the spectrum, the absorption lines for the <sup>2</sup>K<sub>15/2</sub>, <sup>2</sup>G<sub>9/2</sub>, <sup>2</sup>D<sub>3/2</sub> and <sup>4</sup>G<sub>11/2</sub> states have been ignored as these lines coincide with the considerably stronger absorption lines of Pr<sup>3+</sup> (<sup>3</sup>P<sub>0</sub>, <sup>3</sup>P<sub>1</sub>+<sup>1</sup>I<sub>6</sub> and <sup>3</sup>P<sub>2</sub>). Unfortunately,

absorption to the  $^1G_4$  state of  $\text{Pr}^{3+}$  could not be separated from the background noise so it is omitted from the table.

Transition	$f_m \times 10^8$
$^3H_4 \rightarrow, ^4I_{9/2} \rightarrow$ $^4I_{11/2} + ^3H_5$	$300 \pm 100$
$^4I_{13/2} + ^3H_6 + ^3F_2$	$550 \pm 90$
$^4I_{15/2} + ^3F_3 + ^3F_4$	$1000 \pm 400$
$^4F_{3/2}$	$160 \pm 40$
$^4F_{5/2} + ^2H_{9/2}$	$440 \pm 60$
$^4F_{7/2} + ^4S_{3/2}$	$480 \pm 10$
$^4F_{9/2}$	$45 \pm 6$
$^1D_2 + ^2H_{11/2} + ^4G_{5/2} + ^2G_{7/2}$	$1100 \pm 100$
$^2K_{13/2} + ^4G_{7/2} + ^4G_{9/2}$	$500 \pm 80$
$^3P_0$	$270 \pm 40$
$^3P_1 + ^1I_6$	$650 \pm 80$
$^3P_2$	$770 \pm 90$
$^2P_{1/2}$	$24 \pm 6$

**Table 2.7.1** Oscillator strengths for ground state absorption in Nd:Pr:ZBLANP at room temperature.

## 2.8 Judd-Ofelt

Judd-Ofelt analysis is a semi-empirical method for predicting spectroscopic parameters such as absorption and emission cross-sections and emission rates using three phenomenological parameters ( $\Omega_2$ ,  $\Omega_4$  and  $\Omega_6$ ). Separately developed by Judd and Ofelt in 1962 [Judd B. R., 1962; Ofelt G. S., 1962], it is common to refer to the phenomenological parameters as Judd-Ofelt parameters. It is an approximation to the crystal field interaction where from a number of assumptions, found in the

aforementioned papers, the integrated electric-dipole strength of a transition reduces to a simple expression involving the three Judd-Ofelt parameters [Digonnet M. J. F., 1993].

The Judd-Ofelt technique has been applied to all rare earths allowing highly successful predictions to be made. An exception to this is praseodymium ( $\text{Pr}^{3+}$ ) where several modified techniques have been devised [Kornienko A. A. *et al.*, 1990; Quimby R. S. *et al.*, 1994; Goldner P. *et al.*, 1996] but have met with limited success. The modified techniques were deemed necessary as the original technique produced a negative Judd-Ofelt parameter ( $\Omega_2$ ). The negative parameter causes some unphysical predictions to be made such as negative lifetimes.

Traditionally, determining Judd-Ofelt parameters involves the least squares fitting of calculated oscillator strengths to measured oscillator strengths. Previous workers have not allowed for the uncertainty in their oscillator strength measurements so that less well defined lines contribute equally with well defined lines to the fit. Recently, Goldner [Goldner P. *et al.*, 1996] applied a common fractional uncertainty to their measured oscillator strengths in a weighted fitting procedure. This, unfortunately, negates the effect of weighting the fit so here, individual uncertainties will be used in the determination of Judd-Ofelt parameters.

In earlier work, when applying the Judd-Ofelt technique, it was not uncommon to provide an uncertainty associated with each Judd-Ofelt parameter. This would seem to be a necessary part of the technique if useful predictions of spectroscopic parameters are to be made. The lack of uncertainties also makes it difficult to compare the results of other workers. Bearing both of these in mind, the practice of providing uncertainties has been resumed here.

### 2.8.1 Oscillator strength calculations

According to Judd-Ofelt theory, the oscillator strength due to an electric dipole transition, can be calculated from

$$f_c = \frac{8\pi^2 m \chi_{ed}}{3h(2J+1)n^2 e^2} \frac{c}{\lambda} S, \quad (2.8.1.1)$$

where  $\chi_{ed}$  is the local field correction factor for electric dipole radiation,

$$\chi_{ed} = \frac{n(n^2 + 2)^2}{9},$$
  $n$  is the index of refraction of the medium,  $h$  is Planck's constant,  $J$

is the angular momentum quantum number of the initial level of the transition and  $S$  is the transition line strength.

$$S = e^2 \sum_{t=2,4,6} \Omega_t \left| \langle a \| U^{(t)} \| b \rangle \right|^2, \quad (2.8.1.2)$$

where  $\Omega_t$  are the Judd-Ofelt parameters and  $\langle a \| U^{(t)} \| b \rangle$  are doubly reduced matrix elements of the tensor operator  $U^{(t)}$  [Medeiros Neto J. A. *et al.*, 1995]. The tensor operator  $U^{(t)}$  is the quantum mechanical operator for an electric dipole transition from state  $|a\rangle$  to state  $|b\rangle$ , a large number of evaluations of which are readily available in literature, see for example [Carnall W. T. *et al.*, 1968].

### 2.8.2 Determination of Judd-Ofelt parameters

To determine the Judd-Ofelt parameters, it is necessary to use a method of maximum probability to match the calculated oscillator strengths to those that have been measured.

The maximum probability solution is found by minimising

$$\chi^2 = \sum_{p=1..q} \left( \frac{f_{m_p} - f_{c_p}}{\Delta f_{m_p}} \right)^2, \quad (2.8.2.1)$$

where  $f_m$  is the measured oscillator strength,  $f_c$  is equation 2.8.1.1 containing the Judd-Ofelt parameters,  $\Delta f_m$  is the uncertainty in the measured oscillator strength and  $q$  is the number of absorption lines. Solving for the maximum probability solution, least squares fitting, is found by minimising equation 2.8.2.1. The Judd-Ofelt parameters are found by solving for  $\Omega_2$ ,  $\Omega_4$  and  $\Omega_6$  when

$$\frac{\partial \chi^2}{\partial \Omega_2} = 0, \frac{\partial \chi^2}{\partial \Omega_4} = 0, \frac{\partial \chi^2}{\partial \Omega_6} = 0. \quad (2.8.2.2)$$

The uncertainty in the established Judd-Ofelt parameters is then

$$\Delta \Omega_t^2 = \sum_{p=1..q} \left( \Delta f_{m_p} \frac{\partial \Omega_t}{\partial f_{m_p}} \right)^2. \quad (2.8.2.3)$$

### 2.8.3 Judd-Ofelt parameters

Using the oscillator strengths measured in section 2.5 and 2.7, tables 2.5.1, 2.5.2 and 2.7.1, equation 2.8.2.2 can be solved to produce Judd-Ofelt parameters, table 2.8.3.1. There are two sets of Judd-Ofelt parameters for the codoped glass, one set for each dopant. These must be determined concurrently as some of the  $\text{Nd}^{3+}$  absorption lines overlap with those of  $\text{Pr}^{3+}$  and are not separable by fitting appropriate lineshape functions.

Nd:ZBLANP $\times 10^{-24} \text{m}^2$	Nd:Pr:ZBLANP $\times 10^{-24} \text{m}^2$	Pr:ZBLANP $\times 10^{-24} \text{m}^2$
$\Omega_2 = 0.9 \pm 0.3$	$\Omega_2 = 1.1 \pm 0.6$	
$\Omega_4 = 4.4 \pm 0.5$	$\Omega_4 = 3.9 \pm 0.8$	
$\Omega_6 = 3.2 \pm 0.2$	$\Omega_6 = 3.4 \pm 0.2$	
	$\Omega_2 = 1 \pm 2$	$\Omega_2 = 20 \pm 10$
	$\Omega_4 = 5.1 \pm 0.5$	$\Omega_4 = 4.7 \pm 0.4$
	$\Omega_6 = 12 \pm 1$	$\Omega_6 = 7.6 \pm 0.7$

**Table 2.8.3.1** Judd-Ofelt parameters for the 1% Nd:ZBLANP, 2.3%:2.0% Nd:Pr:ZBLANP and 1% Pr:ZBLANP glass samples.

A comparison of the Judd-Ofelt parameters for the singly doped samples to the codoped sample shows that there are no significant changes to the Judd-Ofelt parameters for  $\text{Nd}^{3+}$ . This is expected as the substitution of  $\text{PrF}_3$  for  $\text{LaF}_3$  should not greatly change the structure of the glass. However, when comparing the parameters for Pr:ZBLANP to those of the codoped sample, a significant change is noted for two of the three parameters. This was not the expected result as this implies that substituting  $\text{NdF}_3$  for  $\text{LaF}_3$  significantly changes the structure of the glass. For  $\text{Pr}^{3+}$ , the  $\Omega_4$  parameter did not show any variation within the determined uncertainty. This is understandable from observing the matrix elements where only the  $U^{(4)}$  elements are non-zero for absorptions to the  $^3\text{P}_0$  and  $^3\text{P}_1$  states. This tends to hold the  $\Omega_4$  parameter stable as it is only this parameter that can adjust  $f_c$  for the  $^3\text{P}_0$  and  $^3\text{P}_1$  absorptions. A large degree of instability can be expected for the  $\Omega_2$  parameter as the  $U^{(2)}$  matrix elements for  $\text{Pr}^{3+}$  tend to be small thus requiring greater changes in the parameter to affect changes in  $f_c$ . The instability of both the  $\Omega_2$  and  $\Omega_6$  parameters show that even with the weighted least

squares fitting technique, standard Judd-Ofelt theory is not suitable for the prediction of spectroscopic parameters of  $\text{Pr}^{3+}$ .

#### 2.8.4 Lifetimes and Judd-Ofelt.

The quality of determined Judd-Ofelt parameters is often stated by comparing an overall deviation of measured to calculated oscillator strengths. The relative success of the Judd-Ofelt technique is then determined by the ability to predict lifetimes for states. In  $\text{Pr}^{3+}$ , these predictions have been poor [Medeiros Neto J. A. *et al.*, 1995]. Modified techniques show some improvement in the prediction of lifetime for one state or another but when the technique is used to predict lifetimes of the other radiative states, the predictions seem to be just as weak as those of the original technique.

The lifetime of the state is the inverse of the sum of radiative and non-radiative rates from the state. The non-radiative rate is the sum of the total phonon diffusion rate and the concentration dependent energy transfer rates, both of which will be discussed later. The electric dipole radiative rate ( $A_{ed}$ ) of a state, in the limit of low (zero) concentration, can be determined using the Judd-Ofelt theory from

$$A_{ed} = \frac{64\pi^4 \chi_{ed}}{4\pi\epsilon_0 \lambda^3 3h(2J+1)} S. \quad (2.8.4.1)$$

Thus far, the technique used here, when applied to the singly doped and codoped samples, produces the predicted lifetimes for the  ${}^4F_{3/2}$  state of  $\text{Nd}^{3+}$  and the  ${}^1G_4$ ,  ${}^1D_2$  and  ${}^3P_0$  states of  $\text{Pr}^{3+}$  as shown in table 2.8.4.1. The lifetimes,  $\tau$ , have been calculated from

$$\tau = \frac{1}{\sum (A_{ed} + \omega_{pd})}, \quad (2.8.4.2)$$

where the sum is over all possible transitions to lower energy states and  $\omega_{pd}$  is the

phonon diffusion rate as discussed in section 2.10.3. The concentration dependent processes are neglected as these effects are considered negligible by the authors referred to in table 2.8.4.1.

State	Nd:ZBLANP	Nd:Pr:ZBLANP	Pr:ZBLANP	Measured
${}^4F_{3/2}$	$480 \pm 30 \mu s$	$500 \pm 50 \mu s$		$430 \mu s$ [1]
${}^1G_4$		$137 \pm 2 \mu s$	$113 \pm 2 \mu s$	$110 \mu s$ [2]
${}^1D_2$		$400 \pm 100 \mu s$	$140 \pm 20 \mu s$	$387 \pm 2 \mu s$ [3]
${}^3P_0$		$34 \pm 5 \mu s$	$16 \pm 7 \mu s$	$50 \pm 1 \mu s$ [4]

**Table 2.8.4.1** Predicted lifetimes for the longer lived states of  $Nd^{3+}$  and  $Pr^{3+}$  when doped into ZBLANP glass, compared to measured lifetimes from literature. [1] Balda R. *et al.*, 1994. [2] Sugawa T. *et al.*, 1991. [3] Medeiros Neto J. A. *et al.*, 1995. [4] Petreski B. P. *et al.*, 1996.

Two of the measured values do not have an uncertainty associated with them so only a qualitative comparison can be made. Of these, the  ${}^1G_4$  state of  $Pr^{3+}$  is highly temperature dependent due to a significant phonon diffusion rate; this will be discussed in a later chapter. The prediction for the  ${}^4F_{3/2}$  state is consistent within the two glass samples and is not too different from the value measured by Balda [Balda R. *et al.*, 1994]. The predicted lifetime however does not allow for concentration dependent processes which can greatly effect measured lifetimes. Predictions of lifetimes for the remaining two states ( ${}^1D_2$  and  ${}^3P_0$ ) are still less than impressive although the codoped predictions appear to be better than for the singly doped sample. However, it has already been noted that the addition of  $NdF_3$  to the glass effects the  $Pr^{3+}$  Judd-Ofelt parameters and hence effects the lifetime predictions made with these parameters. It is considered by Medeiros Neto [Medeiros Neto J. A. *et al.*, 1995] that concentration dependent processes are not significant in their measurements and this being the case, their results present a valid comparison to the lifetimes predicted in table 2.8.4.1.

Petreski [Petreski B. P. *et al.*, 1996] determined the lifetime of the  $^3P_0$  state of  $Pr^{3+}$  in the limit of zero concentration and also presents a valid comparison.

Since Judd-Ofelt theory can be used to predict lifetimes, so measured lifetimes can be used to determine Judd-Ofelt parameters. The lifetime of a state is the inverse sum of radiative and non-radiative rates to all lower energy states, while the oscillator strength only involves the two states of the transition. Any measurement of the lifetime of a state contains more information than that of a single oscillator strength and, with modern lasers and detectors, is often an easier measurement to make. In particular, the lifetime of a state contains information about radiative transitions not involving the ground state. The more information available for the fitting process, the better the quality of predictions that can be made from the Judd-Ofelt parameters. With the addition of lifetime information to the standard Judd-Ofelt technique, the maximum probability solution is found by minimising

$$\chi^2 = \sum_{r=1..s} \left( \frac{\tau_{m_r} - \tau_{c_r}}{\Delta\tau_{m_r}} \right)^2 + \sum_{p=1..q} \left( \frac{f_{m_p} - f_{c_p}}{\Delta f_{m_p}} \right)^2, \quad (2.8.4.3)$$

where  $\tau$  is the lifetime of the state and  $s$  is the number lines for which lifetime information is included.  $\chi^2$  is still minimised using the same procedure and the uncertainty in the Judd-Ofelt parameters is then

$$\Delta\Omega_i^2 = \sum_{r=1..s} \left( \Delta\tau_{m_r} \frac{\partial\Omega_i}{\partial\tau_{m_r}} \right)^2 + \sum_{p=1..q} \left( \Delta f_{m_p} \frac{\partial\Omega_i}{\partial f_{m_p}} \right)^2. \quad (2.8.4.4)$$

The lifetime information used in this new Judd-Ofelt process is for the  $^1D_2$  state from Medeiros Neto [Medeiros Neto J. A. *et al.*, 1995] and the  $^3P_0$  state from Petreski [Petreski B. P. *et al.*, 1996]. The  $^1G_4$  lifetime information was not included as the

lifetime of this state is mainly dependent on non-radiative (phonon diffusion) processes. Sufficiently good lifetime predictions were made previously for the  $^4F_{3/2}$  state of  $Nd^{3+}$  therefore only the  $Pr^{3+}$  results are presented. The Judd-Ofelt parameters and the lifetimes predicted are presented in table 2.8.4.2 for both the singly doped and codoped samples.

	Nd:Pr:ZBLANP	Pr:ZBLANP
$\Omega_2 \times 10^{-24} \text{ m}^2$	$0.3 \pm 0.6$	$3.0 \pm 0.3$
$\Omega_4 \times 10^{-24} \text{ m}^2$	$2.6 \pm 0.2$	$1.5 \pm 0.2$
$\Omega_6 \times 10^{-24} \text{ m}^2$	$14 \pm 1$	$9.9 \pm 0.5$
$^1G_4 \text{ } \mu\text{s}$	$136 \pm 1$	$113.7 \pm 0.4$
$^1D_2 \text{ } \mu\text{s}$	$390 \pm 40$	$380 \pm 20$
$^3P_0 \text{ } \mu\text{s}$	$48 \pm 3$	$48 \pm 2$

**Table 2.8.4.2** Judd-Ofelt parameters and predicted lifetimes for a singly doped and a codoped ZBLANP glass where lifetime information is included in the Judd-Ofelt process.

It is not surprising that when using lifetimes in the fitting procedure, the Judd-Ofelt parameters predict lifetimes that are similar to the measured lifetimes. To see if any improvement has been made to the technique, it is necessary to compare some other measured parameter to a predicted value.

The branching ratio is the ratio of the radiative decay rate to a lower state to that of the total radiative decay rate of the state, a large number of which have been measured by Remillieux [Remillieux A. *et al.*, 1996]. Judd-Ofelt theory can be used to predict radiative rates so it is a relatively simple process to calculate branching ratios for comparison to Remillieux, table 2.8.4.3. While there are no uncertainties associated with the measurements of Remillieux there does not seem to be any significant

improvement in the Judd-Ofelt technique when it is modified to include lifetime measurements. Improvement is shown for some transitions but a degradation of the prediction of other branching ratios also results.

Transition	Calculated Branching Ratios	Calculated Branching Ratios (including lifetimes)	Measured Branching Ratios [1]
$^1G_4 \rightarrow ^3F_2$	$0.0037 \pm 0.0006$	$0.0025 \pm 0.0001$	0.07
$^3H_6$	$0.32 \pm 0.06$	$0.191 \pm 0.004$	0.26
$^3H_5$	$0.58 \pm 0.05$	$0.709 \pm 0.003$	0.56
$^3H_4$	$0.051 \pm 0.002$	$0.0553 \pm 0.0001$	0.06
$^1D_2 \rightarrow ^3F_2$	$0.06 \pm 0.02$	$0.048 \pm 0.005$	0.15
$^3H_6$	$0.04 \pm 0.02$	$0.053 \pm 0.003$	0.07
$^3H_5$	$0.002 \pm 0.001$	$0.0036 \pm 0.0002$	0.02
$^3H_4$	$0.16 \pm 0.07$	$0.44 \pm 0.02$	0.44
$^3P_0 \rightarrow ^3F_4$	$0.05 \pm 0.02$	$0.051 \pm 0.004$	0.14
$^3F_3$	$0 \pm 0$	$0 \pm 0$	0.14
$^3F_2$	$0.6 \pm 0.1$	$0.37 \pm 0.03$	0.13
$^3H_6$	$0.08 \pm 0.03$	$0.33 \pm 0.02$	0.27
$^3H_5$	$0 \pm 0$	$0 \pm 0$	0.07
$^3H_4$	$0.3 \pm 0.1$	$0.25 \pm 0.02$	0.23
$^3P_1 + ^1I_6 \rightarrow ^3F_3$	$0.3 \pm 0.1$	$0.18 \pm 0.01$	0.28
$^3H_6$	$0.05 \pm 0.02$	$0.16 \pm 0.01$	0.14
$^3H_5$	$0.15 \pm 0.07$	$0.24 \pm 0.01$	0.23
$^3H_4$	$0.10 \pm 0.04$	$0.085 \pm 0.008$	0.17

**Table 2.8.4.3** Branching ratios as calculated from the Judd-Ofelt theory when applied to Pr:ZBLANP. Ratios are calculated just from absorption oscillator strength measurements as well as when lifetimes are included in the Judd-Ofelt process. [1] The predicted ratios are compared to those measured by Remillieux A. *et al.*, 1996.

## 2.9 Temperature dependence of Judd-Ofelt parameters

An original assumption in the formulation of Judd-Ofelt theory was that populations are evenly distributed across sub-states and that this would cause “not too great an error” [Judd B. R., 1962]. As a possible source of error for the Judd-Ofelt theory when applied to Pr<sup>3+</sup> doped materials, this assumption was tested by comparing Judd-Ofelt parameters for Pr:ZBLANP and Nd:ZBLANP at room temperature and at an elevated temperature. Raising the temperature of the glass causes higher energy sub-states to become more populated so the conditions of the Judd-Ofelt theory can be more closely approximated. The maximum temperature to which the glass samples could be heated before damage would occur was considered to be 250°C. The samples in this experiment were only heated to 200°C. From table 2.9.1, it is clear that the  $\Omega_2$  and  $\Omega_6$  parameters for the Pr<sup>3+</sup> doped glass have changed significantly with the elevated temperature while  $\Omega_4$  remains stable. Since the condition of the Judd-Ofelt approximation is more closely satisfied at the elevated temperature, it was postulated that the lifetimes predicted from the new parameters would more closely match the last column of table 2.8.4.1. This is not the case however with predictions of  $5 \pm 1 \mu\text{s}$  for the  $^3\text{P}_0$  state and  $40 \pm 10 \mu\text{s}$  for the  $^1\text{D}_2$  state.

Judd-Ofelt parameters ( $\times 10^{-24} \text{m}^2$ )	Room Temperature	200°C
$\Omega_2$	$20 \pm 10$	$70 \pm 20$
$\Omega_4$	$4.7 \pm 0.4$	$4.2 \pm 0.5$
$\Omega_6$	$7.6 \pm 0.7$	$4 \pm 1$

**Table 2.9.1** Judd-Ofelt parameters for Pr:ZBLANP glass at room temperature and at 200°C.

The  $\Omega_4$  and  $\Omega_6$  parameters for the Nd:ZBLANP glass change significantly when the sample is heated to 200°C while  $\Omega_2$  remains stable, table 2.9.2. The predicted lifetime for the  ${}^4F_{3/2}$  state however does not change significantly ( $430 \pm 50 \mu\text{s}$ ). At this stage it is difficult to conclude that the evenly distributed population approximation is a weakness in the Judd-Ofelt theory when applied to  $\text{Pr}^{3+}$  doped materials as variation in the Judd-Ofelt parameters is also noted when the theory is applied to  $\text{Nd}^{3+}$  at an elevated temperature. However, some justification can be given to the approximation in the case of  $\text{Nd}^{3+}$  as the predicted lifetimes do not show any significant variation. This is not the case with  $\text{Pr}^{3+}$  where the lifetimes predicted by Judd-Ofelt theory vary significantly with temperature.

Judd-Ofelt parameters ( $\times 10^{-24} \text{m}^2$ )	Room Temperature	200°C
$\Omega_2$	$0.9 \pm 0.3$	$1 \pm 1$
$\Omega_4$	$4.4 \pm 0.5$	$2.6 \pm 0.9$
$\Omega_6$	$3.2 \pm 0.2$	$5.6 \pm 0.5$

**Table 2.9.2** Judd-Ofelt parameters for Nd:ZBLANP glass at room temperature and at 200°C.

## 2.10 Spectroscopic parameters

### 2.10.1 Relaxation rates

The total relaxation rate of a state is the sum of all the radiative, all the phonon diffusion and all the concentration dependent energy transfer rates from that state. Depending on the circumstances, the total relaxation rate can be dominated by one or more of these processes. When there is a relatively small energy gap to the next lower state of the ion then the phonon diffusion rate will dominate and when this gap is large then the

radiative and energy transfer rates will dominate the emission rate of the state. If the energy gap to the next lower state of the ion is large then the phonon diffusion rate will be negligible. In this case, the radiative rate will dominate at low concentrations but at high concentrations, if appropriate transfer paths are available, the energy transfer processes dominate.

### 2.10.2 Radiative emission rate $\omega_{N_4}$

One method for predicting the radiative emission rate of an ion is to use the Judd-Ofelt technique. Unfortunately, the technique when applied to Pr:ZBLANP does not produce reasonable results so it will not be used for the prediction of the Pr<sup>3+</sup> spectroscopic parameters required for the rate equation model of the Nd:Pr:ZBLANP glass. There is no such problem with the technique when applied to Nd:ZBLANP and it is used to predict a radiative emission rate for the <sup>4</sup>F<sub>3/2</sub> state of Nd<sup>3+</sup> to be 2000±100 s<sup>-1</sup>. The energy gap to the next lower state is sufficient for the phonon diffusion relaxation rate to be insignificant. The energy transfer rate from the <sup>4</sup>F<sub>3/2</sub> state will be dealt with in the next chapter.

### 2.10.3 Phonon diffusion relaxation rate $\omega_{N_{12}}$

Due to the relatively small energy gaps for the higher energy states of Nd<sup>3+</sup>, the non-radiative (phonon diffusion) relaxation rate will dominate over the other relaxation processes. The phonon diffusion rate between any two states is determined from

$$\omega_{pd} = C[n(T) + 1]^p \exp(-a\Delta E), \quad (2.9.3.1)$$

where C and a are host dependent parameters,  $\Delta E$  is the energy gap between the two

states,  $p$  is the number of phonons required to bridge that gap and  $n(T)$  is the Bose-Einstein occupation number for the effective phonon mode [Digonnet M. J. F., 1993].

The Bose-Einstein occupation number is calculated from

$$n(T) = \frac{1}{\exp\left(\frac{hcE_p}{kT}\right) - 1}, \quad (2.9.3.2)$$

where  $h$  is Planck's constant,  $c$  is the speed of light in vacuum,  $E_p$  is the energy of the phonon,  $k$  is Boltzmann's constant and  $T$  is the temperature in Kelvin. A number of host dependent parameters and phonon energies have been collated by Reisfeld [Reisfeld R. *et al.*, 1987] and from that collection  $C$  is  $1.59 \times 10^{10} \text{ s}^{-1}$ ,  $a$  is  $5.19 \times 10^{-3} \text{ cm}$  and  $E_p$  is  $500 \text{ cm}^{-1}$ . No uncertainties have been provided with these parameters so the uncertainty in the phonon diffusion rate will be determined from the uncertainty in the measured energy gap of the states. It is considered that the population of any of the higher excited states of  $\text{Nd}^{3+}$  will cascade sequentially through the state immediately below it by phonon diffusion. The maximum rate that this cascading can occur is the slowest phonon diffusion rate of the chain of energy states. The slowest phonon diffusion rate is that of the  ${}^2P_{1/2}$  state which is three orders of magnitude slower than the other states. This has a phonon diffusion rate of  $3.5 \pm 0.1 \times 10^6 \text{ s}^{-1}$  and for the purposes of the rate equations, is considered to be the rate at which the  ${}^2G_{9/2}$  state will lose population due to phonon diffusion.

#### 2.10.4 Excited state absorption cross-section $\sigma_{\text{esa}}$

The excited state absorption cross-section is difficult to measure so it is calculated by applying Judd-Ofelt theory. From Hilborn [Hilborn R. C., 1982] the oscillator strength

for a transition from state  $a$  to state  $b$  is related to the cross-section by

$$f_{ab} = \frac{2\varepsilon_0 mc}{\pi e^2} \frac{g_a}{g_b} \sigma_{ab}, \quad (2.9.4.1)$$

where  $f_{13}$  is the absorption oscillator strength for a transition from state  $a$  to state  $b$ ,  $\varepsilon_0$  is the permittivity of free space,  $m$  is the mass of an electron,  $c$  is the speed of light in vacuum,  $e$  is the charge of an electron,  $g_n$  is the degeneracy of the state  $(2J+1)$  and  $\sigma_{ab}$  is the cross-section for a transition from state  $a$  to state  $b$ . Putting this in terms of the ground state and excited state absorptions in  $\text{Nd}^{3+}$  for a 795nm pump source, see figure 1.4.1, the ratio of the absorption oscillator strengths is

$$\frac{f_{05}}{f_{416}} = \frac{\frac{2\varepsilon_0 mc}{\pi e^2} \frac{g_0}{g_5} \sigma_{05}}{\frac{2\varepsilon_0 mc}{\pi e^2} \frac{g_4}{g_{16}} \sigma_{416}}, \quad (2.9.4.2)$$

which can be simplified to

$$\frac{f_{05}}{f_{416}} = \frac{g_0}{g_5} \frac{g_{16}}{g_4} \frac{\sigma_{05}}{\sigma_{416}}. \quad (2.9.4.3)$$

The doubly reduced matrix elements required for such a calculation, see section 2.8.1, have been determined for transitions from the  ${}^4\text{F}_{3/2}$  state to the  ${}^2\text{P}_{1/2}$  state and to the  ${}^2\text{D}_{5/2}$  state of  $\text{Nd}^{3+}$ , table 2.9.4.1. Excited state absorption from the  ${}^4\text{F}_{3/2}$  state is most likely to populate the  ${}^2\text{D}_{5/2}$  state of  $\text{Nd}^{3+}$  for a 795nm pump. Using the predicted oscillator strength for this transition, the ratio of the absorption cross-sections are  $\sigma_{416} = \sigma_{05} \times 0.023 \pm 0.005$ . The cross-sections predicted using the Judd-Ofelt technique are actually the integrated cross-sections. Since the lineshape of the excited state absorption is unknown some reasonable approximations need to be made. If the lineshape of the ground state absorption and the excited state absorption are similar regardless of their

dimensions, then the ratio of the integrated cross-sections is

$$0.023 = \frac{A_{\text{esa}} W_{\text{esa}}}{A_{\text{gsa}} W_{\text{gsa}}}, \quad (2.10.4.3)$$

where  $A_x$  is the peak absorption cross-section,  $W_x$  is the width of the absorption line. If the excited state absorption linewidth is similar to that of the excited state absorption then  $A_{\text{esa}} = A_{\text{gsa}} \times 0.023 \pm 0.005$ . Since  $\sigma_{416}$  is small compared to  $\sigma_{05}$ , if  $W_x$  is assumed to scale with  $A_x$  and that scaling factor is the same for both the excited state absorption and ground state absorption then

$$0.023 = \frac{(A_{\text{esa}})^2}{(A_{\text{gsa}})^2}. \quad (2.10.4.4)$$

From this point on, integrated cross-sections will no longer be discussed so with the risk of possible confusion but for the sake of convention, the peak cross-sections will from here on be denoted with  $\sigma$ . Now it can be stated that  $\sigma_{\text{esa}} = \sigma_{\text{gsa}} \sqrt{0.023 \pm 0.02}$ . The excited state absorption cross-section is required for the determination of energy transfer parameters. From chapter 4, it is seen that the determined energy transfer parameters are relatively insensitive to the difference in excited state absorption cross-sections calculated using the two approximations.

Transition	$U^{(2)}$	$U^{(4)}$	$U^{(6)}$
${}^4F_{3/2} \rightarrow {}^2P_{1/2}$	-0.112261	0	0
${}^4F_{3/2} \rightarrow {}^2D_{5/2}$	-0.0412484	0.0414694	0

**Table 2.9.4.1** Reduced matrix elements for transitions from the  ${}^4F_{3/2}$  state to the  ${}^2P_{1/2}$  and  ${}^2D_{5/2}$  states of  $\text{Nd}^{3+}$ .

### 2.10.5 Ground state absorption cross-section $\sigma_{gsa}$

There are three ground state absorption cross-sections that are required for this thesis. All will be determined from the same set of absorption spectra used in the determination of Judd-Ofelt parameters for the Nd:Pr:ZBLANP sample. By application of equation 2.5.2, the ground state absorption cross-section for a 795nm, 465.8nm and 476.5nm are determined to be  $\sigma_{795} = 2.2 \pm 0.3 \times 10^{-24} \text{ m}^2$ ,  $\sigma_{465.8} = 0.9 \pm 0.1 \times 10^{-24} \text{ m}^2$  and  $\sigma_{476.5} = 0.58 \pm 0.07 \times 10^{-24} \text{ m}^2$ , respectively.

### 2.11 Conclusion

Dopant concentrations for all of the available glass samples have been determined showing that some differed greatly from the nominal values. This highlights the difficulty that glassmakers have when creating their glasses and also reveals the need for a simple, non-destructive system for determining dopant concentrations.

The Judd-Ofelt technique has been applied to the glass samples allowing reasonable predictions for spectroscopic parameters of  $\text{Nd}^{3+}$  to be made. The technique was not so successful with predicting spectroscopic parameters for  $\text{Pr}^{3+}$  although the inclusion of uncertainties in the weighted fit did provide all positive Judd-Ofelt parameters. The introduction of lifetime information to the Judd-Ofelt technique did not improve the accuracy of the predictions of spectroscopic parameters for  $\text{Pr}^{3+}$ . However, this may yet prove to be a useful technique for increasing the precision of Judd-Ofelt parameters for other Rare Earth doped materials.

The effect of codoping  $\text{Nd}^{3+}$  with  $\text{Pr}^{3+}$  appears to have a significant effect on the Judd-Ofelt parameters for  $\text{Pr}^{3+}$ . This would imply that the  $\text{Nd}^{3+}$  has caused some significant change to the structure of the glass host. This does not seem very likely as the  $\text{NdF}_3$  is making a straight substitution for  $\text{LaF}_3$  and it has been concluded elsewhere that this change would not be discernible in the Judd-Ofelt parameters [Binnemans K. *et al.*, 1998]. It is more likely that the Judd-Ofelt theory, when applied to  $\text{Pr}^{3+}$ , still has too many problems associated with it to be a useful analytical tool.

An investigation of the temperature dependence of Judd-Ofelt parameters reveals that there is a variation for both  $\text{Nd}^{3+}$  and  $\text{Pr}^{3+}$  doped glasses. This variation does not translate into a significant change in the predicted lifetime of the  $^4\text{F}_{3/2}$  state of  $\text{Nd}^{3+}$ . Lifetimes predicted for states of  $\text{Pr}^{3+}$  from Judd-Ofelt parameters determined at an elevated temperature do show significant variation from those predicted at room temperature. Due to the unstable nature of Judd-Ofelt theory when applied to  $\text{Pr}^{3+}$ , it is not clear that the evenly distributed population approximation is a significant problem with the theory.

A series of spectroscopic parameters, table 2.10.1, have been determined by measurement and prediction. These parameters will be used in subsequent chapters and in the final rate equation model of a Nd:Pr:ZBLANP glass.

Parameter	Value	Definition
$\omega_{N_4}$	$2,000 \pm 100 \text{ s}^{-1}$	radiative decay rate of the $^4F_{3/2}$ state of $\text{Nd}^{3+}$
$\omega_{N_{12}}$	$3.5 \pm 0.1 \times 10^6 \text{ s}^{-1}$	decay rate assigned to the $^2G_{9/2}$ state of $\text{Nd}^{3+}$
$\sigma_{\text{esa}}$	$0.15 \pm 0.02 \sigma_{795}$	$\text{Nd}^{3+}$ excited state ( $^4F_{3/2}$ ) absorption cross-section for 795nm excitation
$\sigma_{795}$	$2.2 \pm 0.3 \times 10^{-24} \text{ m}^2$	$\text{Nd}^{3+}$ ground state absorption cross-section for 795nm excitation
$\sigma_{465.8}$	$0.9 \pm 0.1 \times 10^{-24} \text{ m}^2$	$\text{Pr}^{3+}$ ground state absorption cross-section for 465.8nm excitation
$\sigma_{476.5}$	$0.58 \pm 0.07 \times 10^{-24} \text{ m}^2$	$\text{Pr}^{3+}$ ground state absorption cross-section for 476.5nm excitation

**Table 2.10.1** Spectroscopic parameters determined in Chapter 2.

### 3. Time dependent fluorescence

Section.....	Page
3.1 Introduction .....	3-2
3.2 The rate equation approach .....	3-2
3.3 Applying the rate equation approach.....	3-7
3.4 Experimental arrangement .....	3-10
3.5 Fitting of decay data .....	3-11
3.6 Energy transfer and concentration.....	3-14
3.7 Applications of $\alpha_1, \alpha_2, \alpha_5, \alpha_6$ .....	3-16
3.8 Conclusion.....	3-17

### 3.1 Introduction

In the chapter 1 a basic model for a codoped system was proposed. In the previous chapter, absorption spectra were used to determine some of the spectroscopic parameters required for the model. In this chapter, fluorescence as a function of time is used to determine further parameters that are required for the model. A technique applied by Petreski [Petreski B. P. *et al.*, 1995] is used to determine energy transfer parameters which allow the quantification of cross relaxation rates for  $\text{Pr}^{3+}$  and  $\text{Nd}^{3+}$  individually. The technique is then modified to allow the determination of energy transfer parameters that describe energy transfer between  $\text{Pr}^{3+}$  and  $\text{Nd}^{3+}$  in a codoped system.

The technique involves pumping ions into a particular excited state, removing the pump source and observing the fluorescence decay. The fluorescence is proportional to the population of the excited state so by solving the population rate equations, population loss mechanisms can be quantified. The population loss mechanisms are comprised of radiative relaxation, phonon diffusion and energy transfer. Radiative relaxation rates and phonon diffusion rates were established in the previous chapter and here, energy transfer parameters will be established that will allow the quantification of energy transfer rates.

### 3.2 The rate equation approach

Energy transfer in a single species ( $\text{Pr}^{3+}$ ) has been investigated by Petreski using rate equations [Petreski B. P. *et al.*, 1995; Petreski B. P. *et al.*, 1996]. This approach can be used and extended to quantify energy transfer parameters, which are useful for

determining energy transfer rates both within and between species of ions. The technique is not specific to the glasses or dopants used in this project but will be described in terms of states of  $\text{Pr}^{3+}$  and  $\text{Nd}^{3+}$ .

The general formulation of the energy transfer parameters is demonstrated by considering two simple species of ions, x and y. A pumping source is used to establish some population in an excited state (state 2) of species x. If the pumping source is removed (at  $t = 0$ ), then the population decay rate from state 2 of species x is given by

$$\frac{\partial x_2(t)}{\partial t} = -\omega_{x_2} x_2(t) - \alpha_1 x_0(t) x_2(t) - \alpha_2 y_0(t) x_2(t) - 2\alpha_3 x_2^2(t) - 2\alpha_4 y_0(t) x_2^2(t), \quad (3.2.1)$$

where  $\omega_{x_n}$  is the concentration independent decay rate of species x in state n,  $x_n$  and  $y_n$  are the population densities of species x and y in state n, respectively and  $\alpha_n$  are the energy transfer parameters. The first term of equation 3.2.1,  $\omega_{x_2} x_2(t)$ , concerns relaxation due to concentration independent processes in species x, this will involve either the radiative emission rate, the phonon diffusion rate or a combination of both. While both will always be present, one rate will usually dominate the other (see section 2.9.1). The next two terms represent energy transfer requiring one ion in an excited state to relax by transferring energy to an ion in some other state, these will be called  $n^1$  processes, figure 3.2.1. The second term of equation 3.2.1,  $\alpha_1 x_0(t) x_2(t)$  represents the relaxation of donor ions by transfer of energy to acceptor ions both of species x, this is often called cross-relaxation. The third term,  $\alpha_2 y_0(t) x_2(t)$  concerns the relaxation of donor ions of species x when energy is transferred to acceptor ions of species y. The final two terms of equation 3.2.1 represent energy transfer requiring the interaction of two ions in the excited state, these will be called  $n^2$  processes,

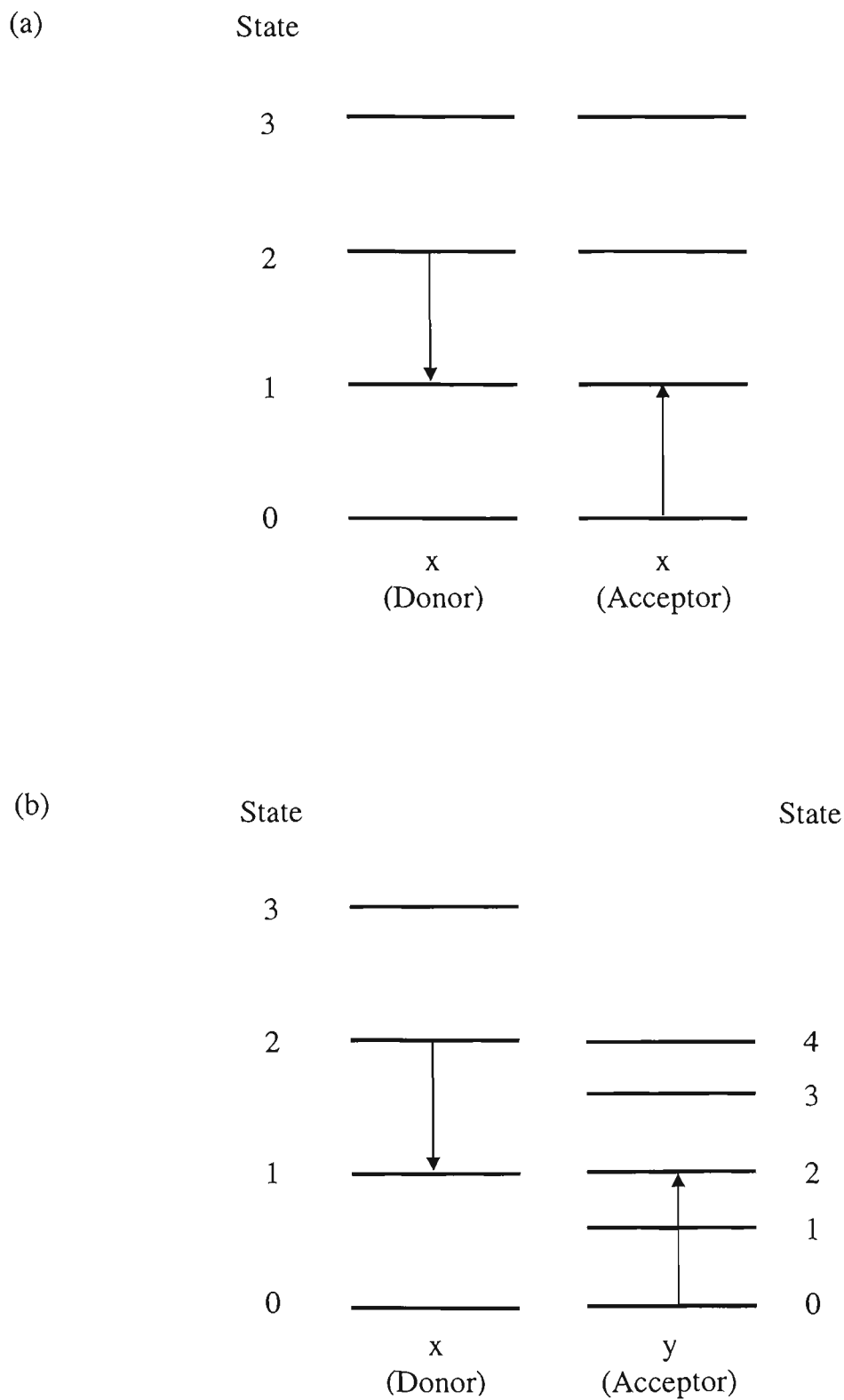


**Figure 3.2.1** Energy level diagram for fictitious ions x and y showing (a) intra-species and (b) inter-species energy transfer of type  $n^1$ .

figure 3.2.2. The fourth term of equation 3.2.1,  $2\alpha_3 x_2^2(t)$  represents a two ion energy transfer process where both ions are of the same species and initially in the same excited state. The relaxation of one ion causes energy to be transferred to the other ion exciting it to a higher state, this is often called cooperative upconversion. The final term of equation 3.2.1,  $2\alpha_4 y_0(t)x_2^2(t)$  represents an inter-species transfer but in this case, two donor ions of species x transfer energy to one acceptor ion of species y. The terms involving the  $\alpha$  parameters represent concentration dependent quenching processes, which depopulate the excited state and can dominate other processes at high concentrations.

If species x is only lightly pumped so that  $x_0 \approx \rho_x$  the concentration of species x, and species y is only excited by energy transfer from species x, such that  $y_0 \approx \rho_y$  the concentration of species y, then the solution for equation 3.2.1 is

$$x_2(t) = \frac{\exp(-at)}{\frac{b}{a}(1 - \exp(-at)) + \frac{1}{x_2(0)}}, \quad (3.2.2)$$

where  $x_2(0)$  is the population of state 2 in species x at  $t = 0$ ,  $a = \omega_{x_2} + \alpha_1 \rho_x + \alpha_2 \rho_y$  and  $b = 2\alpha_3 + 2\alpha_4 \rho_y$ . If  $n^2$  processes are considered to be insignificant ( $b \approx 0$ ) then this solution becomes purely exponential,

$$x_2(t) = x_2(0)\exp(-at). \quad (3.2.3)$$

If the system is not lightly pumped ( $x_0 \ll \rho_x$ ,  $y_0 \ll \rho_y$ ), or if a significant number of  $n^2$  events are occurring then a non-exponential decay will result.

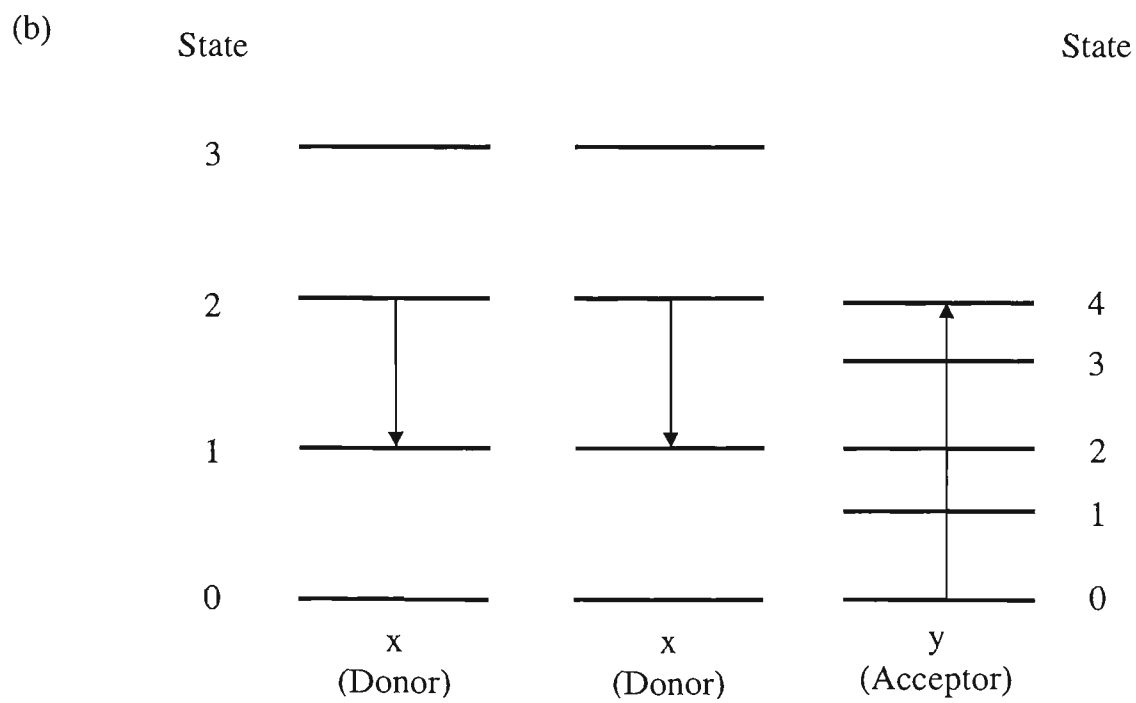
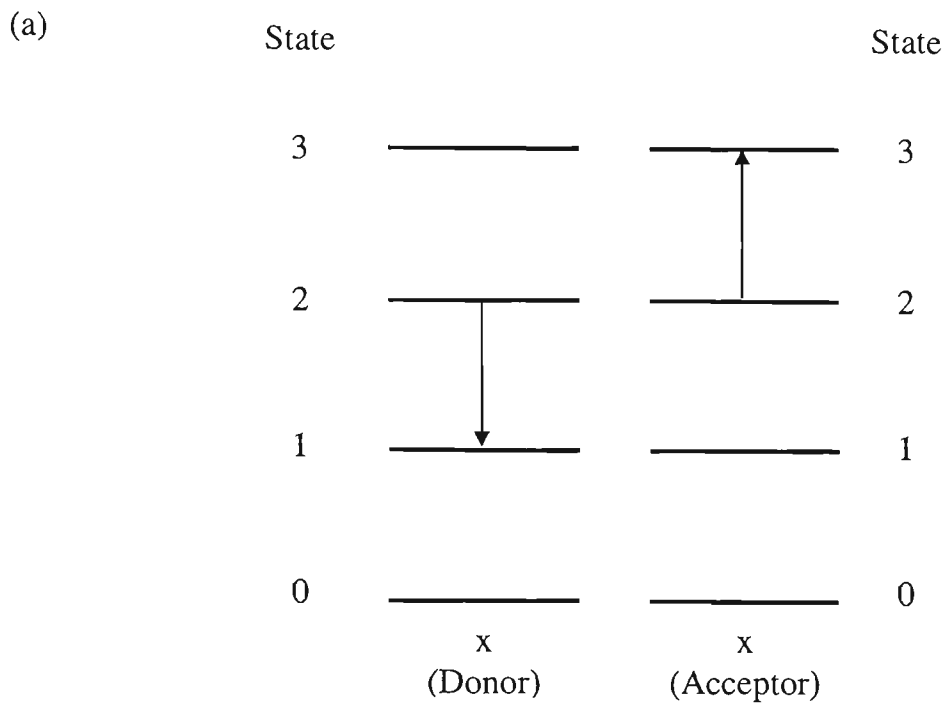


**Figure 3.2.2** Energy level diagram for fictitious ions x and y showing (a) intra-species and (b) inter-species energy transfer of type  $n^2$ .

### 3.3 Applying the rate equation approach.

An energy level diagram of  $\text{Pr}^{3+}$  and  $\text{Nd}^{3+}$ , figure 3.3.1, shows that they are much more complicated than the simple ions x and y. In the work presented here, the states for which the population decay has been observed are  $^3\text{P}_0$  in  $\text{Pr}^{3+}$  and  $^4\text{F}_{3/2}$  in  $\text{Nd}^{3+}$ . Many energy transfer paths are available from these states, both within and between the two ion species. A separate energy transfer parameter ( $\alpha$ ) is required to describe uniquely the decay rate for each individual relaxation path. The purpose of using this particular technique is to establish energy transfer rates for states that have significant steady state populations. The steady state population will be affected by the summation of the individual energy transfer rates from that state. The summed individual energy transfer rates can be divided into the four types of transitions that are represented in ions x and y: (1) cross-relaxation, (2) two ion inter-species, (3) cooperative upconversion and (4) three ion inter-species processes. An energy transfer parameter is then associated with each type of transfer process for each of the species.

By defining  $\alpha_1, \alpha_2, \alpha_3, \alpha_4$  as the energy transfer parameters for relaxation from the  $^3\text{P}_0$  state of  $\text{Pr}^{3+}$  for the cross-relaxation, two ion inter-species, cooperative upconversion and the three ion inter-species transfer respectively, the population decay rate from state 8 of  $\text{Pr}^{3+}$  ( $^3\text{P}_0$ ) is

$$\frac{\partial P_8(t)}{\partial t} = -\omega_{P_8} P_8(t) - \alpha_1 P_0(t) P_8(t) - \alpha_2 N_0(t) P_8(t) - 2\alpha_3 P_8^2(t) - 2\alpha_4 N_0(t) P_8^2(t), \quad (3.3.1)$$

where  $P_n$  and  $N_n$  refer to the population density of  $\text{Pr}^{3+}$  and  $\text{Nd}^{3+}$  ions in state n,

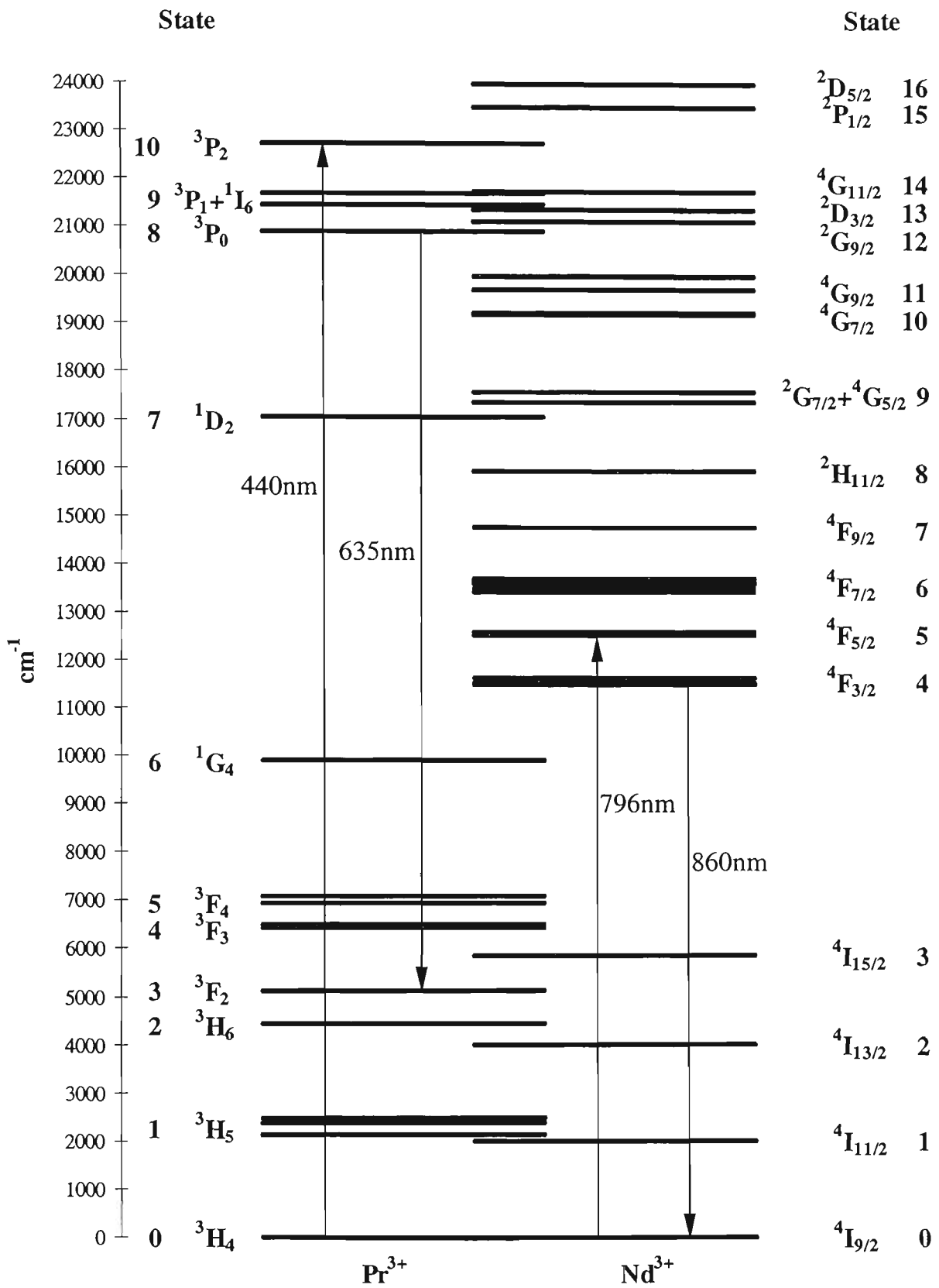


Figure 3.3.1 Energy levels of Pr<sup>3+</sup> and Nd<sup>3+</sup> ions in a ZBLANP host.

respectively. The solution to equation 3.3.1, using the lightly pumped approximation ( $P_0 \approx \rho_P$  and  $N_0 \approx \rho_N$ ), has the form of

$$P_8(t) = \frac{\exp(-at)}{\frac{b}{a}(1 - \exp(-at)) + \frac{1}{P_8(0)}}, \quad (3.3.2)$$

where

$$a = \omega_{p_8} + \alpha_1 \rho_P + \alpha_2 \rho_N \quad (3.3.3)$$

and  $b = 2\alpha_3 + 2\alpha_4 \rho_N$ .

A similar approach for the  ${}^4F_{3/2}$  state of  $Nd^{3+}$  is used where the energy transfer parameters  $\alpha_5, \alpha_6, \alpha_7, \alpha_8$  are defined as describing relaxation by cross-relaxation, two ion inter-species, cooperative upconversion and the three ion inter-species energy transfer processes, respectively. The population decay rate from state 4 of  $Nd^{3+}$  ( ${}^4F_{3/2}$ ) can then be written as

$$\frac{\partial N_4(t)}{\partial t} = -\omega_{N_4} N_4(t) - \alpha_5 N_0(t) N_4(t) - \alpha_6 P_0(t) N_4(t) - 2\alpha_7 N_4^2(t) - 2\alpha_8 P_0(t) N_4^2(t). \quad (3.3.4)$$

The solution to equation 3.3.4, using the lightly pumped approximation ( $P_0 \approx \rho_P$  and  $N_0 \approx \rho_N$ ), takes the form of

$$N_4(t) = \frac{\exp(-ct)}{\frac{d}{c}(1 - \exp(-ct)) + \frac{1}{N_4(0)}}, \quad (3.3.5)$$

where

$$c = \omega_{n_4} + \alpha_5 \rho_N + \alpha_6 \rho_P \quad (3.3.6)$$

and  $d = 2\alpha_7 + 2\alpha_8 \rho_P$ .

### 3.4 Experimental arrangement

The experimental arrangement, figure 3.4.1, was used to record the fluorescence intensity as a function of time. The glass samples were pumped using a Spectra Physics MOPO of pulse length 7ns and a pulse repetition frequency of 10Hz. The pump wavelengths were 440nm and 796nm for the  $\text{Pr}^{3+}$  and  $\text{Nd}^{3+}$ , respectively. At these wavelengths, alternatively  $\text{Nd}^{3+}$  and  $\text{Pr}^{3+}$  have minimal absorption thereby excluding the possibility of exciting the inappropriate species. Some excited state absorption is expected in  $\text{Nd}^{3+}$  when pumped at 796nm but the higher states have large relaxation rates due to phonon diffusion [chapter 2] so any population will relax quickly to the  $^4\text{F}_{3/2}$  state.

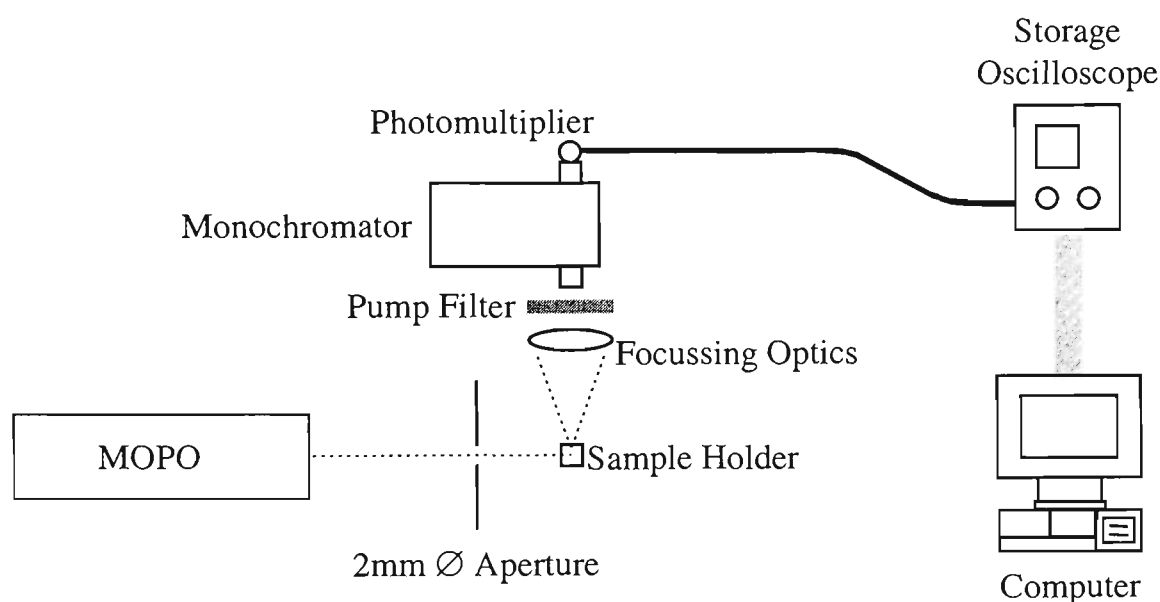


**Figure 3.4.1** Experimental arrangement for fluorescence decay measurements.

Fluorescence at 635nm and at 860nm was used to independently observe the population decay of the  $^3\text{P}_0$  state in  $\text{Pr}^{3+}$  and the  $^4\text{F}_{3/2}$  state in  $\text{Nd}^{3+}$ , respectively. Fluorescence was detected, orthogonally to the direction of the pump, by a monochromator/photomultiplier combination and the data stored on a computer. The

detection system had a response time of  $5\mu\text{s}$  and a spectral resolution of  $1\text{nm}$ , which was sufficient to resolve the  $\text{Pr}^{3+}$   $635\text{nm}$  fluorescence from any possible light from the  ${}^2\text{H}_{11/2} \rightarrow {}^4\text{I}_{9/2}$  transition in  $\text{Nd}^{3+}$ .

### 3.5 Fitting of decay data

The decay data, which is the output voltage from the photomultiplier as a function of time ( $V_{P_8}(t)$ ,  $V_{N_4}(t)$ ), is proportional to the population of the observed state. Due to the various shapes and sizes of the glass samples it was not possible to guarantee the same proportionality constant (transfer function for detector arrangement) for each series of measurements. This then requires that the proportionality constant be included when fitting the data to the decay function ie

$$V_{P_8}(t) = \frac{K \exp(-at)}{\frac{b}{a}(1 - \exp(-at)) + \frac{1}{P_8(0)}} \quad (3.5.1)$$

and

$$V_{N_4}(t) = \frac{K' \exp(-ct)}{\frac{d}{c}(1 - \exp(-ct)) + \frac{1}{N_4(0)}}, \quad (3.5.2)$$

where  $K$  and  $K'$  are the series of proportionality constants for the series of  $\text{Pr}^{3+}$  and  $\text{Nd}^{3+}$  measurements, respectively. A reduction in the number of parameters can be made by incorporating  $K$  and  $K'$  with  $b$ ,  $P_8(0)$ ,  $d$  and  $N_4(0)$  and the decay function can be expressed as

$$V_{P_8}(t) = \frac{\exp(-at)}{\frac{b'}{a}(1 - \exp(-at)) + \frac{1}{V_{P_8}(0)}} \quad (3.5.3)$$

and

$$V_{N_4}(t) = \frac{\exp(-ct)}{\frac{d'}{c}(1 - \exp(-ct)) + \frac{1}{V_{N_4}(0)}}, \quad (3.5.4)$$

where  $b' = \frac{b}{K}$ ,  $V_{P_8}(0) = KP_8(0)$ ,  $d' = \frac{d}{K'}$  and  $V_{N_4}(0) = KN_4(0)$ . Values for a, b',

$V_{P_8}(0)$  and c, d',  $V_{N_4}(0)$  obtained using a least squares fitting method for various

dopant concentrations are presented in Tables 3.5.1 and 3.5.2.

Dopant Concentrations $Nd^{3+}/Pr^{3+} \times 10^{25}$ ions/m <sup>3</sup>	a (s <sup>-1</sup> )	b' (mV <sup>-1</sup> s <sup>-1</sup> )	$V_{P_8}(0)$ (mV)
(i) - /17.15	23,070±60	-	153.2±0.3
(ii) 2.573/2.230	26,550±60	-	66.1±0.1
(iii) 5.317/3.945	30,100±200	3,000±2,000	152.6±0.3
(iv) 14.235/2.401	32,400±300	220,000±5,000	139.8±0.3
(v) 35.158/1.372	47,300±500	1,420,000±20,000	82.8±0.3

**Table 3.5.1** Fitting parameters for the relaxation from the <sup>3</sup>P<sub>0</sub> state of Pr<sup>3+</sup> for various concentration ratios.

Dopant Concentrations $Nd^{3+}/Pr^{3+} \times 10^{25}$ ions/m <sup>3</sup>	c (s <sup>-1</sup> )	$V_{N_4}(0)$ (mV)
(i) 17.15/ -	2,119±6	181.3±0.2
(ii) 2.573/2.230	2,607±6	150.0±0.2
(iii) 5.317/3.945	2,786±7	270.4±0.5
(iv) 14.235/2.401	3,090±10	143.9±0.2
(v) 35.158/1.372	3,390±10	177.0±0.3

**Table 3.5.2** Fitting parameters for the relaxation from the <sup>4</sup>F<sub>3/2</sub> state of Nd<sup>3+</sup> for various concentration ratios.

Plots of log intensity versus time, figures 3.5.1 and 3.5.2, show that for the singly doped samples (plot (i)), a good fit can be obtained using a standard exponential decay, justifying limiting the analysis to two ion processes in a lightly pumped regime. The non-exponential decay of the fluorescence from the <sup>3</sup>P<sub>0</sub> state of Pr<sup>3+</sup> for the codoped

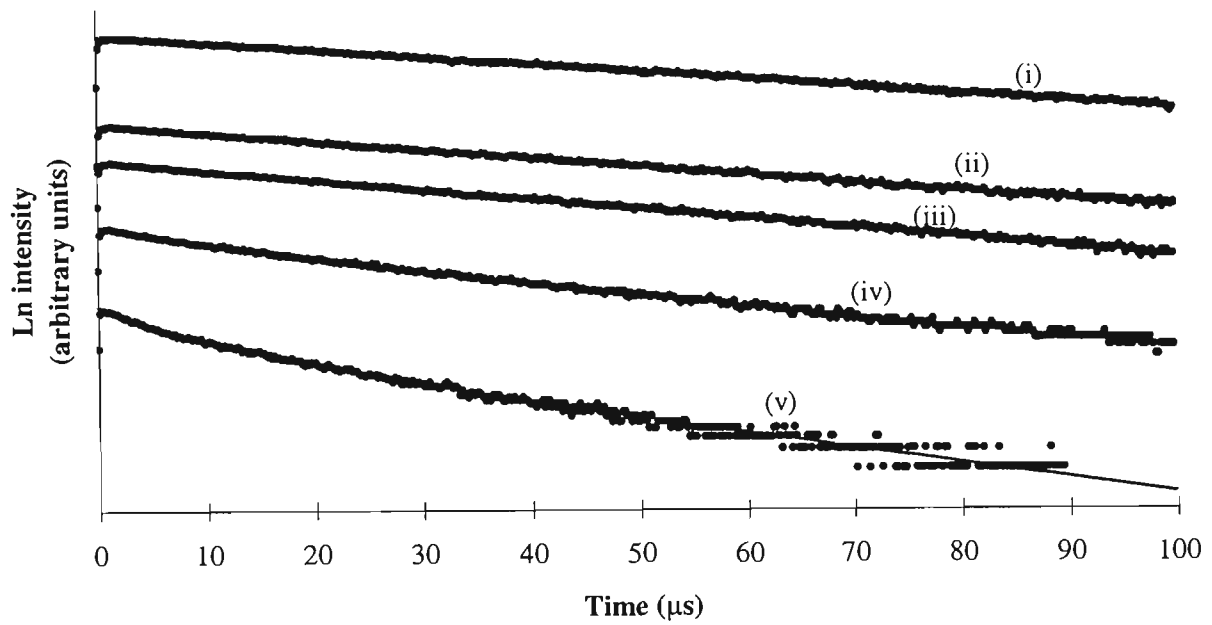


**Figure 3.5.1** Fluorescence decay curves for relaxation from the  $^3P_0$  state of  $\text{Pr}^{3+}$ . Plots (i) to (v) are for the concentration ratios shown in table 3.5.1, fitted with equation 3.5.3. For clarity, the decay curves have been distributed along the “Ln Intensity” axis.

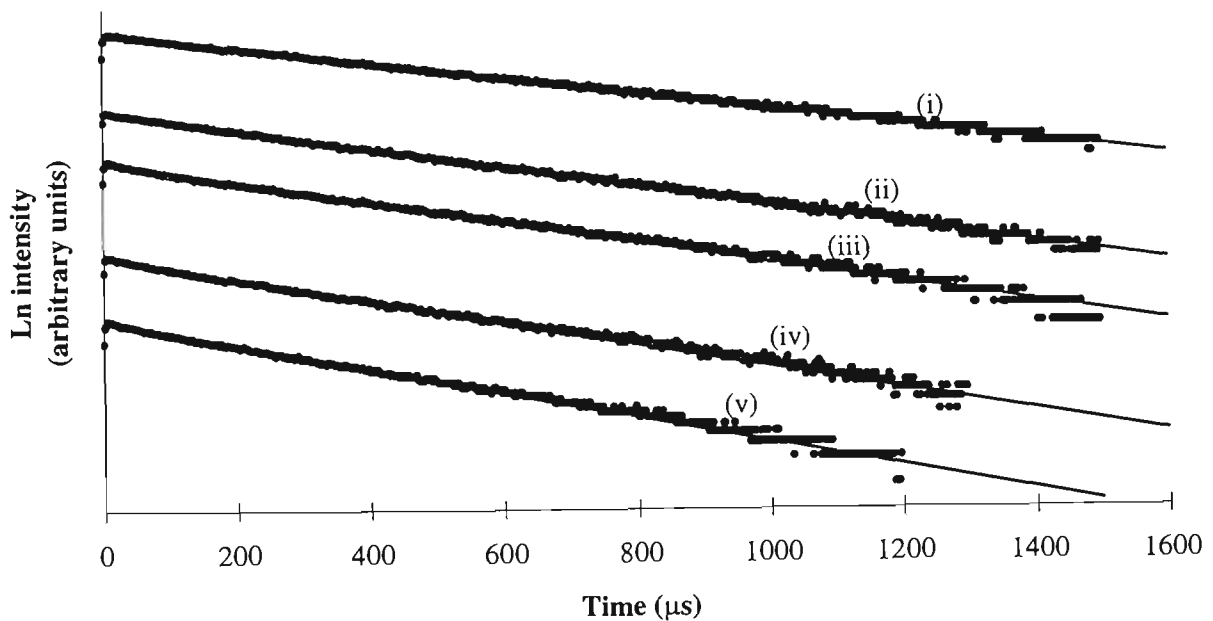


**Figure 3.5.2** Fluorescence decay curves for relaxation from the  $^4F_{3/2}$  state of  $\text{Nd}^{3+}$ . Plots (i) to (v) are for the concentration ratios shown in table 3.5.2, fitted with an exponential decay. For clarity, the decay curves have been distributed along the “Ln Intensity” axis.

samples (plots (ii) to (v)), indicates that  $n^2$  type processes are occurring but since there is no appropriate state of  $\text{Pr}^{3+}$  for cooperative upconversion, it is concluded that three ion processes are occurring. This becomes more apparent with increasing  $\text{Nd}^{3+}$  concentration. The fluorescence decay from the  ${}^4\text{F}_{3/2}$  state of  $\text{Nd}^{3+}$  for the codoped samples would appear not to include a significant number of three ion processes ( $d' \cdot 0$ ).

### 3.6 Energy transfer and concentration

Energy transfer rates for two ion processes can be analysed by subtracting the concentration independent relaxation rates,  $\omega_{p_8} = 20,000 \pm 400\text{s}^{-1}$  [Petreski B. P. *et al.*, 1996] and  $\omega_{n_4} = 2,000 \pm 100\text{s}^{-1}$  [chapter 2] from the fitting parameters “a” and “c” respectively. The remainder of the decay rate is due to both cross-relaxation and two ion inter-species energy transfer. Rearranging equations 3.3.3 and 3.3.6,

$$\frac{a - W_{p_8}}{\rho_n} = \alpha_1 \frac{\rho_p}{\rho_n} + \alpha_2, \frac{c - W_{n_4}}{\rho_n} = \alpha_5 + \alpha_6 \frac{\rho_p}{\rho_n}, \quad (3.6.1)$$

and

$$\frac{a - W_{p_8}}{\rho_p} = \alpha_1 + \alpha_2 \frac{\rho_n}{\rho_p}, \frac{c - W_{n_4}}{\rho_p} = \alpha_5 \frac{\rho_n}{\rho_p} + \alpha_6. \quad (3.6.2)$$

allows the energy transfer rate per ion concentration versus concentration ratio to be plotted. These are linear functions where the intercept on the dependent axis represents one energy transfer parameter and the gradient the other. A least squares fit, weighted by the inverse square of the uncertainties, figures 3.6.1 and 3.6.2 is then used to determine the energy transfer parameters. Values of  $(18 \pm 3) \times 10^{-23} \text{ m}^3/\text{s}$  for  $\alpha_1$ , the

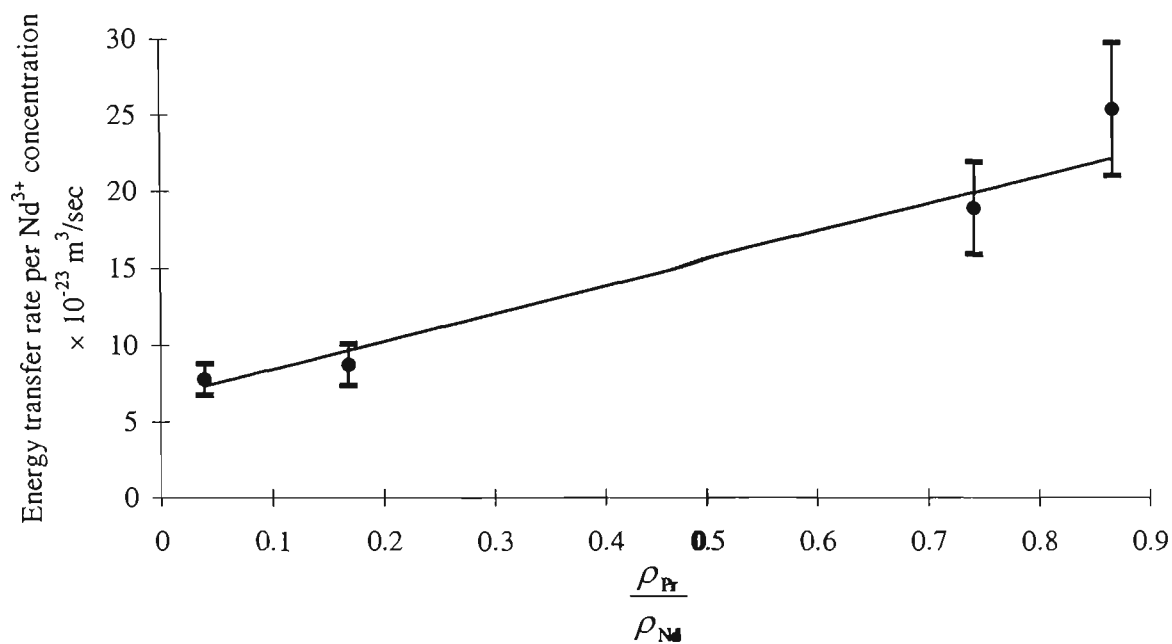


**Figure 3.6.1** Experimentally determined cross relaxation and two ion energy transfer rate per ion concentration for relaxation from the  $^3P_0$  state of  $Pr^{3+}$  as a function of the  $Nd^{3+}$  and  $Pr^{3+}$  concentration ratio.

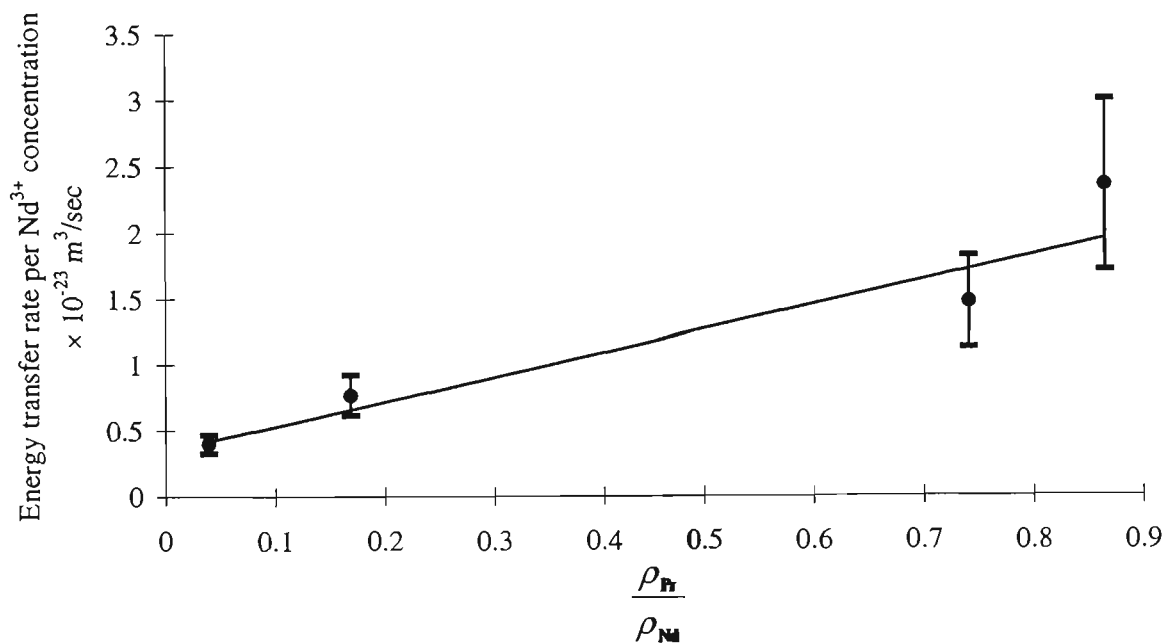


**Figure 3.6.2** Experimentally determined cross relaxation and two ion energy transfer rate per ion concentration for relaxation from the  $^4F_{3/2}$  state of  $Nd^{3+}$  as a function of the  $Nd^{3+}$  and  $Pr^{3+}$  concentration ratio.

energy transfer parameter for cross-relaxation from the  ${}^3P_0$  state of  $\text{Pr}^{3+}$ ;  $(6.6 \pm 0.8) \times 10^{-23} \text{ m}^3/\text{s}$  for  $\alpha_2$ , the energy transfer parameter for energy transfer from the  ${}^3P_0$  state of  $\text{Pr}^{3+}$  to  $\text{Nd}^{3+}$ ;  $(0.34 \pm 0.06) \times 10^{-23} \text{ m}^3/\text{s}$  for  $\alpha_5$ , the energy transfer parameter for cross-relaxation from the  ${}^4F_{3/2}$  state of  $\text{Nd}^{3+}$  and;  $(1.9 \pm 0.4) \times 10^{-23} \text{ m}^3/\text{s}$  for  $\alpha_6$ , the energy transfer parameter for energy transfer from the  ${}^4F_{3/2}$  state of  $\text{Nd}^{3+}$  to  $\text{Pr}^{3+}$ .

Transfer rates for the  $n^2$  processes are difficult to separate from the “b” fitting parameters due to the inconsistent proportionality constant. The evaluation of  $\alpha_4$  is not possible using the data from this section of the work, however it will be quantified using a different approach in chapter 4.

### 3.7 Applications of $\alpha_1$ , $\alpha_2$ , $\alpha_5$ , $\alpha_6$

A particularly useful application for the energy transfer parameters ( $\alpha_1$ ,  $\alpha_2$ ,  $\alpha_5$  and  $\alpha_6$ ) is the determination of absolute concentrations of  $\text{Pr}^{3+}$  and  $\text{Nd}^{3+}$  in a ZBLANP host. As can be seen from the rate equations, the fluorescence decay rate depends on the energy transfer parameters and the ion concentration densities. The energy transfer parameters were determined from a knowledge of the ion concentration densities. Now that the energy transfer parameters are known, concentration densities can be determined for an unknown sample of  $\text{Pr}^{3+}$ ,  $\text{Nd}^{3+}$  or a combination of both, doped ZBLANP. Fluorescence from the appropriate state ( ${}^3P_0$  and  ${}^4F_{3/2}$ ) is least squares fitted to equations 3.5.3 and 3.5.4, resulting in numerical values for “a” and “c” which, when substituted along with the energy transfer parameters into equations 3.3.3 and 3.3.6, form a pair of simultaneous equations. Solving these equations provides absolute concentration densities for  $\text{Pr}^{3+}$  ( $\rho_p$ ) and  $\text{Nd}^{3+}$  ( $\rho_n$ ).

The distribution of dopants in a fibre can greatly effect the performance of a fibre laser or amplifier. Utilising confocal microscopy techniques and the energy transfer parameters,  $\alpha_1$ ,  $\alpha_2$ ,  $\alpha_5$  and  $\alpha_6$ , can be used to map concentration densities across the distribution of dopants in a fibre can be determined.

### 3.8 Conclusion

By analysing the fluorescence decay of codoped Nd:Pr:ZBLANP glasses, energy transfer parameters have been determined, table 3.8.1. The  $\alpha_1$  and  $\alpha_5$  parameters are useful for predicting self-quenching from the commonly used metastable states in  $\text{Pr}^{3+}$  and  $\text{Nd}^{3+}$ , respectively. Energy transfer parameters ( $\alpha_2$ ,  $\alpha_6$ ) have also been determined that will aid with the prediction of quenching due to codoping. Together these parameters can be used to image  $\text{Nd}^{3+}$  and  $\text{Pr}^{3+}$  dopant concentrations in a ZBLANP host using the fluorescence lifetime technique.

At this stage it has not been possible to quantify the  $n^2$  processes that are occurring between the  $^3\text{P}_0$  state of  $\text{Pr}^{3+}$  and  $\text{Nd}^{3+}$ . Techniques for determining the parameter that describe these processes will be discussed in the next chapter.

Parameter	Value ( $\times 10^{-23} \text{ m}^3/\text{s}$ )	Definition
$\alpha_1$	$18 \pm 3$	Parameter for cross-relaxation from the $^3\text{P}_0$ state of $\text{Pr}^{3+}$
$\alpha_2$	$6.6 \pm 0.8$	Parameter for two ion energy transfer from the $^3\text{P}_0$ state of $\text{Pr}^{3+}$ to $\text{Nd}^{3+}$ ,
$\alpha_5$	$0.34 \pm 0.06$	Parameter for cross-relaxation from the $^4\text{F}_{3/2}$ state of $\text{Nd}^{3+}$
$\alpha_6$	$1.9 \pm 0.4$	Parameter for two ion energy transfer from the $^4\text{F}_{3/2}$ state of $\text{Nd}^{3+}$ to $\text{Pr}^{3+}$

**Table 3.8.1** Energy transfer parameters for the  $^3\text{P}_0$  state of  $\text{Pr}^{3+}$  and the  $^4\text{F}_{3/2}$  state of  $\text{Nd}^{3+}$  in Nd:Pr:ZBLANP.

## 4. Steady state fluorescence

Section.....	Page
4.1 Introduction.....	4-2
4.2 Spot size determination.....	4-3
4.3 Power in the spot.....	4-3
4.4 Pumping rate ( $\overline{\omega}_p$ ).....	4-4
4.5 Measurement of fluorescence.....	4-5
4.6 $\alpha_4$ .....	4-5
4.7 465.8nm pump experiment.....	4-6
4.8 $\alpha_7$ and $\alpha_9$ . ....	4-9
4.9 795nm pump experiment.....	4-16
4.10 Other processes .....	4-19
4.11 Pumping approximations .....	4-23
4.12 Conclusion.....	4-24

## 4.1 Introduction

In previous chapters, parameters for the model have been established from both absorption and lifetime measurements. In this chapter, steady state fluorescence measurements have been used to establish further parameters necessary to complete the model. Parameters established so far do not provide information regarding the energy transfer from  $\text{Nd}^{3+}$  to  $\text{Pr}^{3+}$  that leads to the visible emissions from the  $^3\text{P}_0$  state of  $\text{Pr}^{3+}$ . Also, while the existence of a  $n^2$  energy transfer process from the  $^3\text{P}_0$  state of  $\text{Pr}^{3+}$  has been established, the magnitude of the associated parameter ( $\alpha_4$ ) has yet to be determined.

The measurements made in this part of the work are based on the premise that the optical power from fluorescence is proportional to the excited state population of the emitting ions. The excited state population can be determined by the use of rate equations that are solved for the steady state. Using a monochromator/photomultiplier combination for a detection system, the fluorescence detected is proportional to the excited state population. With a consistent detection system, normalised fluorescence can be analysed as a function of pump power and compared to the solution for the steady state rate equations.

The sample chosen for the work in this chapter was the preform (0.31% $\text{NdF}_3$ -0.24% $\text{PrF}_3$ ) which has two advantages, the first being that, by eye, it produces the brightest fluorescence for the 795nm pump source. The second advantage is that the core region made a consistent target for pump beams ensuring that the detected fluorescence was from the same region of the sample for different pump wavelengths.

In order to calculate the power entering the sample it was necessary to determine the spot size of the pump beam as it entered the glass. The eventual spot size is dependent on the pumping geometry, the pump wavelength and the focussing optics. A relationship is developed allowing the calculation of pumping rates from input powers for use in the rate equations.

## **4.2 Spot size determination**

The spot size of the pump beam at the initial surface of the sample is determined from the ABCD law for gaussian beams [Laufer G., 1996]. Confirmation of the calculated spot size is provided by a measurement utilising a Melles Griot Super Beam Analyser 13 SKP 003. During the course of the steady state fluorescence measurements, it was not possible to use the beam analyser, as this would have required the glass sample and detection system to be moved. However, the beam analyser was used later to measure a pump beam spot size of  $160\pm 20\mu\text{m}$  for the same configuration, within the tolerance of the sample placement, as the 465.8nm pumping experiment. The calculated spot size for this configuration ( $140\pm 20\mu\text{m}$ ) was considered to provide confirmation that the calculated spot sizes were of reasonable accuracy to be used in the determination of the energy transfer parameters.

## **4.3 Power in the spot**

If the beam diameter of a pump source is larger than the sample then not all of the pump power will be coupled in to the sample. In the case of a fibre or pre-form, the size of the sample can be considered to be the size of the core region. The beam of a laser has a

Gaussian intensity profile, the power of which can be found by integrating across the beam from  $-\infty$  to  $+\infty$  in the  $x$ - $y$  plane. The power in a beam entering a sample of limited size can be found by integrating across the beam over the diameter of the sample. The ratio of these two integrals produces a scaling factor for the measured power, which provides an estimate of the actual power entering the sample. Centring of the pump beam in the core region is realised by aligning for peak fluorescence.

#### 4.4 Pumping rate ( $\bar{\omega}_p$ )

If  $P_{in}$  is the input power to a system of ions then the maximum possible number of ions that can be excited per second is  $P_{in} \frac{\lambda}{hc}$ , where  $h$  is Planck's constant,  $c$  is the speed of light and  $\lambda$  is the wavelength of the input photons. The probability of a single photon being absorbed by a single ion is  $\sigma_{abs}/A_{spot}$ , where  $\sigma_{abs}$  is the absorption cross-section of the transition and  $A_{spot}$  is the cross-sectional area of the pump beam. Combining these terms gives the probability of absorbing pump photons per second or the pump rate,

$$\bar{\omega}_p = P_{in} \frac{\lambda}{hc} \frac{\sigma_{abs}}{A_{spot}}. \quad (4.4.1)$$

The power of a pump beam at any point along the length ( $l$ ) of an absorbing medium  $P(l) = P_{in} e^{-\alpha l}$ , where  $\alpha$  is the absorption coefficient of the medium. The pump rate along the length of the absorbing medium  $\omega_p(l)$  changes as

$$\omega_p(l) = P(l) \frac{\lambda}{hc} \frac{\sigma_{abs}}{A_{spot}}. \quad (4.4.2)$$

The detection system used in the experiments measures the average fluorescence along

the length the sample. The average fluorescence is proportional to the average excited state population which is a result of the average pump rate,

$$\bar{\omega}_p = \frac{1}{l} \int_0^l \omega_p(l) dl, \quad (4.4.3)$$

where  $\bar{\omega}_p$  is the average pump rate.

#### 4.5 Measurement of fluorescence

Spontaneous emission (fluorescence) of a particular wavelength is directly proportional to the population of ions in the excited state, the proportionality constant being the spontaneous emission rate for the transition involved. The measurement of fluorescence introduces a further proportionality constant that describes the response of the detection system. In chapter 3, the detection system was varied to cater for the variety of samples used with the result that  $\alpha_4$  could not be determined from the data. By using the same detection configuration for all measurements, normalised fluorescence can be related to the average population densities calculated from the rate equations as the normalising process eliminates the proportionality constants. In order to keep the detection system as consistent as possible, only the pre-form was used. It was mounted directly on to the entrance slit of the monochromator, which was in turn mounted directly to the bench.

#### 4.6 $\alpha_4$

By pumping ions from the ground state of  $\text{Pr}^{3+}$  to the  ${}^3\text{P}_1+{}^1\text{I}_6$  state and assuming that the population of that state relaxes quickly to  ${}^3\text{P}_0$ , then the steady state rate equation for the population of the  ${}^3\text{P}_0$  state of  $\text{Pr}^{3+}$  is

$$\bar{\omega}_p N_{P_0} = \omega_{P_8} N_{P_8} + \alpha_1 N_{P_0} N_{P_8} + \alpha_2 N_{N_0} N_{P_8} + 2\alpha_3 N_{P_8}^2 + 2\alpha_4 N_{N_0} N_{P_8}^2, \quad (4.6.1)$$

where  $\omega_{P_n}$  is the radiative relaxation rate from state  $n$  of  $\text{Pr}^{3+}$ ,  $N_{P_n}$  is the average population density of state  $n$  of  $\text{Pr}^{3+}$ ,  $N_{N_n}$  is the average population density of state  $n$  of  $\text{Nd}^{3+}$  and  $\alpha_m$  are the energy transfer parameters. There is no appropriate state for cooperative upconversion from the  $^3P_0$  state of  $\text{Pr}^{3+}$  to occur therefore  $\alpha_3=0$ . If there are no other significant population reservoirs, then  $N_{P_0} = \rho_P - N_{P_8}$ , where  $\rho_P$  is the  $\text{Pr}^{3+}$  concentration and if the system is lightly pumped then the ground state population of  $\text{Nd}^{3+}$ ,  $N_{N_0}$ , can be approximated to the ion concentration  $\rho_N$ . Equation 4.6.1 is a quadratic, the solution to which can be written in the form of

$$N_{P_8} = \frac{\left( b - \sqrt{(b)^2 - 4ac} \right)}{2a}, \quad (4.6.2)$$

where  $a = \alpha_1 - 2\alpha_4\rho_N$ ,  $b = \bar{\omega}_p + \omega_{P_8} + \alpha_1\rho_P + \alpha_2\rho_N$  and  $c = \rho_P\bar{\omega}_p$ . The measured fluorescence is proportional to the average population density  $N_{P_8}$ . All of the parameters in equation 4.6.2 are known with the exception of  $\alpha_4$ . If the fluorescence normalised to the peak emission is measured over a range of input powers then  $\alpha_4$  can be determined.

#### 4.7 465.8nm pump experiment.

The preform was positioned directly along the 20mm long entrance slit of the monochromator with the face where the pump beam enters the sample adjacent to the bottom of the entrance slit. The experimental length for this sample is therefore considered to be 20mm. A Spectra Physics Stabilite<sup>®</sup> 2017 argon ion laser with a beam

diameter ( $1/e^2$ ) of 1.37mm and a full angle divergence of 0.476mrad [Anonymous, 1994] was used for pumping the preform at a wavelength of 465.8nm. This wavelength does not correspond to any significant absorption in  $\text{Nd}^{3+}$  so it was assumed that only the  $\text{Pr}^{3+}$  was pumped. An  $f=500\text{mm}$  plano-convex lens, placed  $2720\pm 10\text{mm}$  after the pump laser and  $550\pm 5\text{mm}$  before the preform, was used to focus the pump beam into the sample, figure 4.7.1. This produced a calculated spot size of  $174\pm 8\mu\text{m}$  which was used in the determination of  $A_{\text{spot}}$ . Saturation of the detector occurs with the pump laser just above threshold so that in order to keep it lasing in a more stable region, the power was increased and neutral density (ND) filters were placed after the plano-convex lens. Densities of 1.51 and 0.98 were used concurrently which, allowing for 4% reflections from each surface, produced a reduction in the pump power by a factor of  $2.75\times 10^{-3}$ . The fluorescence was detected by a monochromator set to pass a wavelength of 635nm, with  $150\mu\text{m}$  entrance and exit slits, coupled to a Hamamatsu R629 photomultiplier (PMT), the combination providing a 1nm resolution.  $P_{\text{in}}$  was measured on a LabMaster power meter with a silicon head. All measurements were made with the laboratory lights off to minimise the amount of stray light detected. Table 4.7.1 shows the voltage measured across the PMT ( $V_{\text{out}}$ ) for various  $P_{\text{in}}$  and the input power calculated after the ND filters ( $P_{\text{in}}'$ ). Input powers were selected to produce the conveniently stepped output voltages.

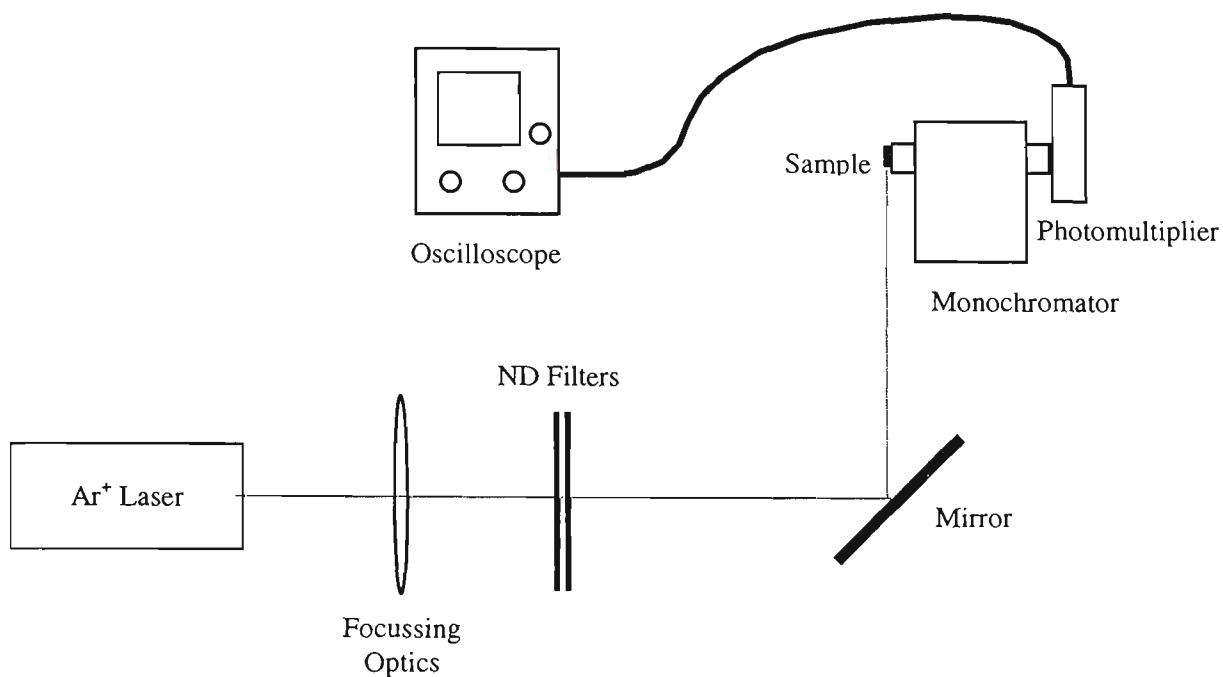


**Figure 4.7.1** Experimental arrangement used in the determination of  $\alpha_4$ .

A plot of  $P_{in}'$  versus  $V_{out}$  normalised to the peak output voltage, figure 4.7.2, shows an almost linear response that is fitted using the normalised version of equation 4.6.2. Using the known parameters and normalising equation 4.6.2 for fluorescence at a  $P_{in}'$  of  $363\mu\text{W}$ , a least squares fit was used to determine  $\alpha_4 = 1.6 \pm 0.2 \times 10^{-43} \text{ m}^6/\text{s}$ .

$P_{in}$ (mW)	$P_{in}'$ ( $\mu\text{W}$ )	$V_{out}$ (mV)
$132 \pm 1$	363	$80 \pm 2$
$100 \pm 1$	275	$60 \pm 2$
$66 \pm 1$	181	$40 \pm 2$
$33 \pm 1$	91	$20 \pm 2$
$16 \pm 1$	44	$10 \pm 2$

**Table 4.7.1** Measured output voltage for various input powers of a 465.8nm pump source.

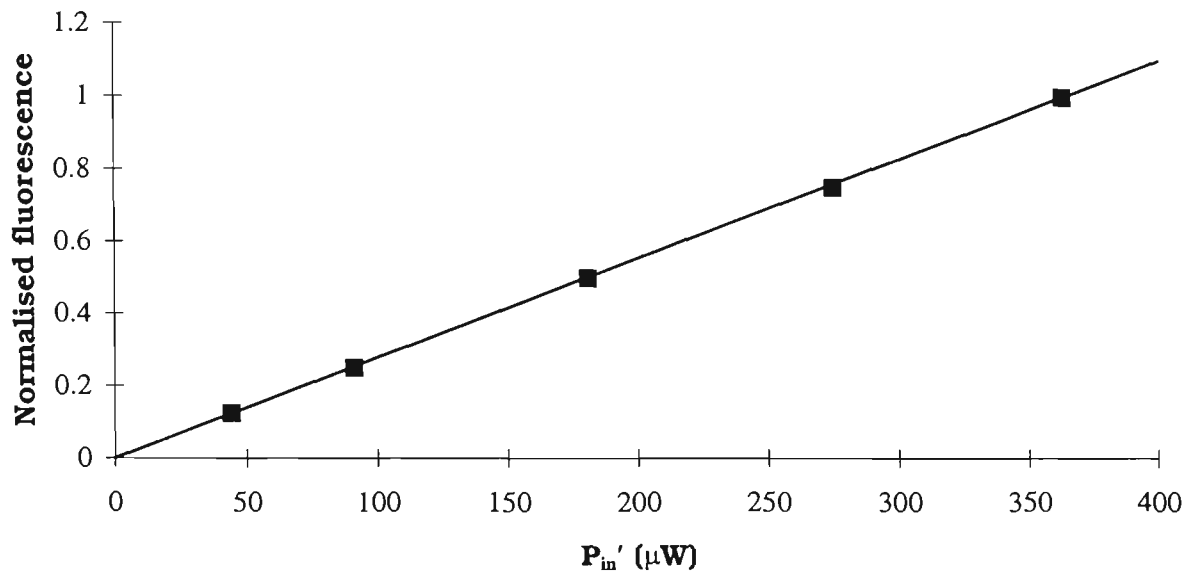


**Figure 4.7.2** Input power versus normalised fluorescence from the  $^3P_0$  state of  $\text{Pr}^{3+}$  fitted by the normalised version of equation 4.6.2.

The process described by  $\alpha_4$  involves three ions, two  $\text{Pr}^{3+}$  donors transferring energy to one  $\text{Nd}^{3+}$  acceptor. Branching ratios from the  $^3P_0$  state of  $\text{Pr}^{3+}$  (chapter 2) would imply that the energy transferred would be large enough to excite the  $\text{Nd}^{3+}$  into some state higher than  $^2G_{9/2}$ . It is assumed that ions in this higher state relax quickly by phonon diffusion to the  $^2G_{9/2}$  state. The steady state rate equation describing the population density of the  $^2G_{9/2}$  state of  $\text{Nd}^{3+}$  is then

$$\bar{\omega}_{\text{esa}} N_{N_4} + \alpha_4 \rho_N N_{P_8}^2 = \omega_{N_{12}} N_{N_{12}} + \omega_{\text{et}} N_{N_{12}}, \quad (4.7.1)$$

where  $\bar{\omega}_{\text{esa}}$  is the average excited state absorption rate.

#### 4.8 $\alpha_7$ and $\alpha_9$ .

The energy transfer parameters established so far do not directly contribute to populating of the  $^3P_0$  state of  $\text{Pr}^{3+}$ . At least one parameter  $\alpha_9$  is required to describe the energy transfer rate from  $\text{Nd}^{3+}$  in the  $^2G_{9/2}$  state to excite  $\text{Pr}^{3+}$  to the  $^3P_0$  state. As a first

order approximation, it is assumed to be a two ion process much the same as those involving  $\alpha_2$ , and  $\alpha_6$ , figure 4.8.1. It is also assumed that all energy transfer from ions in the  ${}^2G_{9/2}$  state of  $Nd^{3+}$  will excite  $Pr^{3+}$  to the  ${}^3P_0$  state giving a steady state rate equation of

$$N_{P_8} \left( \omega_{P_8} + \alpha_1 N_{P_0} + \alpha_2 N_{N_0} + 2\alpha_4 N_{N_0} N_{P_8} \right) = \alpha_9 N_{P_0} N_{N_{12}}, \quad (4.8.1)$$

where  $\alpha_9$  is the energy transfer parameter describing the two ion energy transfer from the  ${}^2G_{9/2}$  state of  $Nd^{3+}$  to  $Pr^{3+}$ .

A further new parameter  $\alpha_7$ , is required to describe the cooperative upconversion energy transfer process for the  ${}^4F_{3/2}$  state of  $Nd^{3+}$ , figure 4.8.2. Cooperative upconversion from the  ${}^4F_{3/2}$  state of  $Nd^{3+}$  was not observed in the experiments of chapter 3 as they were performed in a light-pumping regime. However, cooperative upconversion has been observed from this state of  $Nd^{3+}$  in a ZBLAN host and will be included in the rate equations of this chapter [Stanley A. T. *et al.*, 1993]. While the three ion process as described by  $\alpha_4$  are considered to be a significant loss mechanism for the  ${}^3P_0$  state of  $Pr^{3+}$ , it is assumed that it is not a major pumping source for exciting  $Nd^{3+}$  to the  ${}^2G_{9/2}$  state when compared to optical pumping and so it is neglected from the  ${}^2G_{9/2}$  equation, figure 4.8.3. The steady state rate equation describing the population of the  ${}^2G_{9/2}$  state of  $Nd^{3+}$  is then

$$N_{N_{12}} \left( \alpha_9 N_{P_0} + \omega_{N_{12}} \right) = N_{N_4} \left( \bar{\omega}_{esa} + \alpha_7 N_{N_4} \right), \quad (4.8.2)$$

where  $\omega_{N_{12}}$  is the phonon diffusion rate of state 12 of  $Nd^{3+}$  and  $\alpha_7$  is the energy transfer parameter describing the cooperative upconversion of ions in the  ${}^4F_{3/2}$  state of  $Nd^{3+}$ .

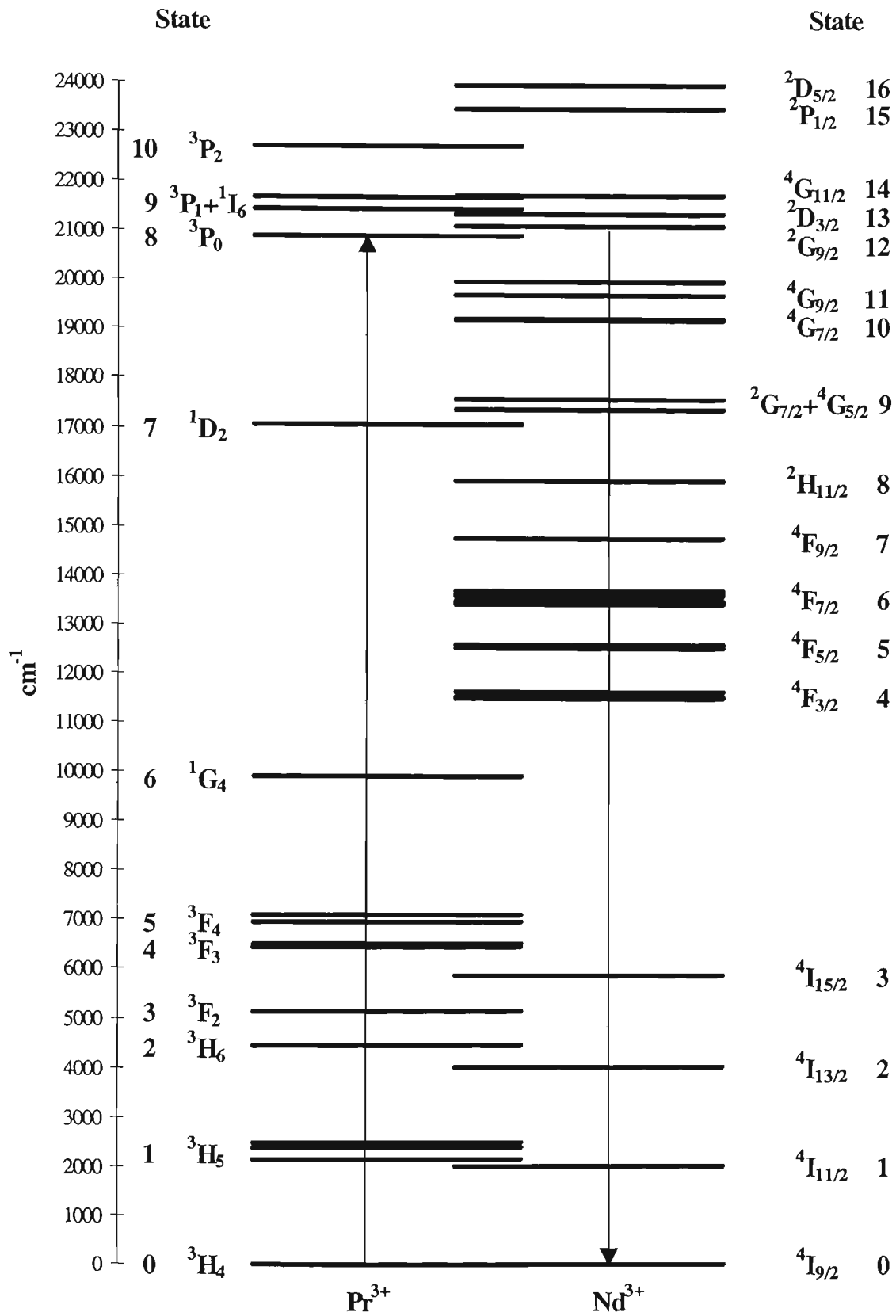


Figure 4.8.1 Energy levels of Pr<sup>3+</sup> and Nd<sup>3+</sup> ions in a ZBLANP host showing Nd<sup>3+</sup>-Pr<sup>3+</sup>, 2 ion energy transfer process from the <sup>2</sup>G<sub>9/2</sub> state of Nd<sup>3+</sup> to the <sup>3</sup>P<sub>0</sub> state of Pr<sup>3+</sup> as described by α<sub>9</sub>.

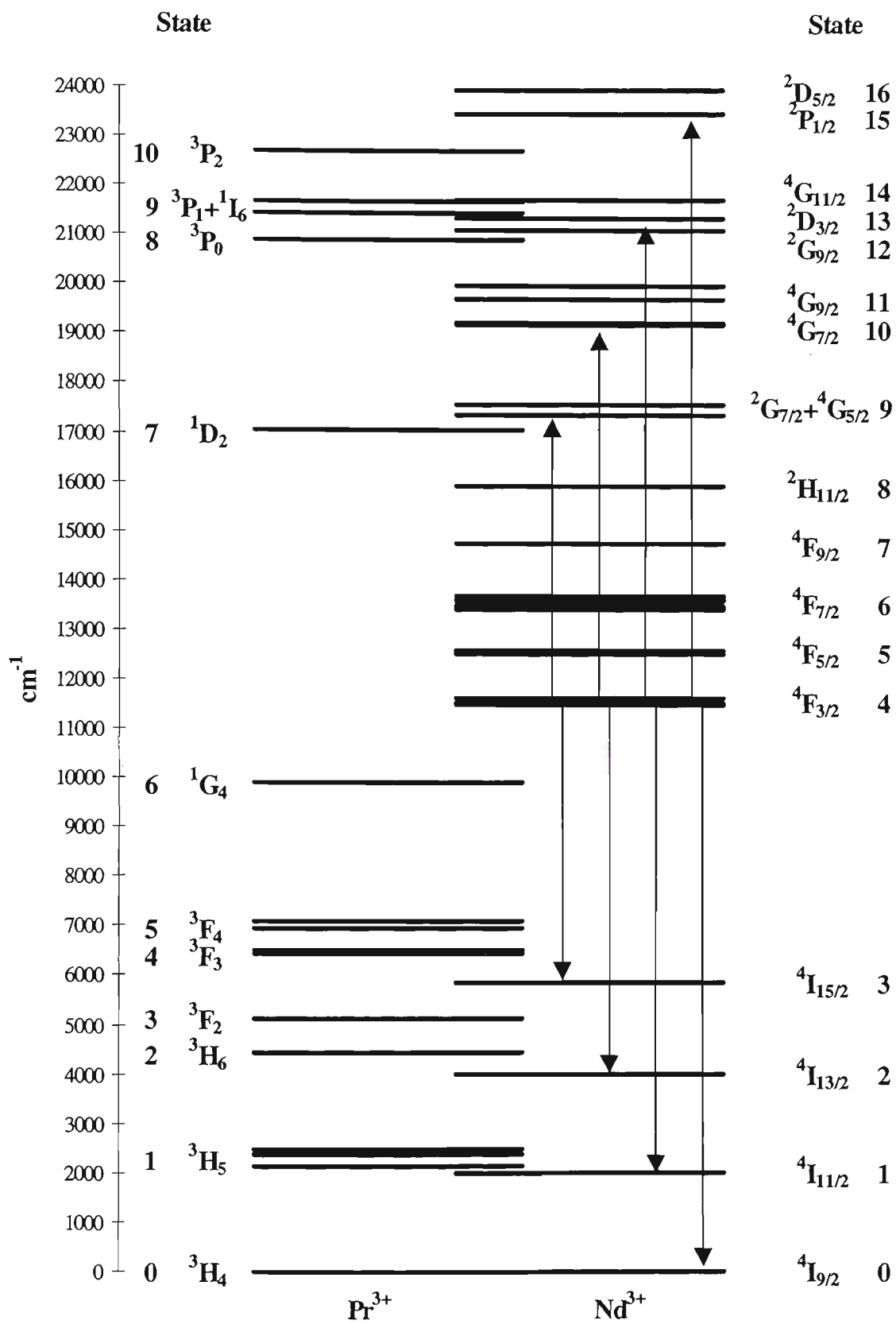


Figure 4.8.2 Energy levels of Pr<sup>3+</sup> and Nd<sup>3+</sup> ions in a ZBLANP host showing possible dipole-dipole interactions of Nd<sup>3+</sup> in the <sup>4</sup>F<sub>3/2</sub> state as described in the rate equations by  $\alpha_7$ .

To determine parameters  $\alpha_7$  and  $\alpha_9$ , fluorescence from the  ${}^3P_0$  state of  $\text{Pr}^{3+}$  is observed while varying the pump intensity. 795nm-pump radiation is used to excite the  $\text{Nd}^{3+}$  in the ground state to the  ${}^4F_{5/2}$  state, quickly relaxing to the  ${}^4F_{3/2}$  state, figure 1.4.1. The  ${}^4F_{3/2}$  state is relatively long lived and becomes a population reservoir from which excited state absorption can occur, exciting ions to the  ${}^2P_{1/2}$  state. Relaxation from the higher states of  $\text{Nd}^{3+}$  is mainly by phonon diffusion and is rapid. Ions in the  ${}^2P_{1/2}$  state will relax rapidly through the  ${}^4G_{11/2}$ ,  ${}^2D_{3/2}$  and  ${}^2G_{9/2}$  states of  $\text{Nd}^{3+}$ . From these states, it is possible that relaxation can occur by transferring energy to the  ${}^3P_0$  state of  $\text{Pr}^{3+}$  and it is relaxation from this state that produces the fluorescence observed in this part of the experiment.

Branching ratios for the  ${}^3P_0$  state of  $\text{Pr}^{3+}$  indicate that most energy transferred to  $\text{Nd}^{3+}$  by two ion processes would excite the  $\text{Nd}^{3+}$  to a state at least higher than  ${}^4F_{3/2}$  but not as high as  ${}^2G_{9/2}$ , figure 4.8.2. However, it is also assumed this will not be a major pumping mechanism for ions populating this state when compared to optical pumping and so it is neglected, giving a steady state rate equation for the  ${}^4F_{3/2}$  state of  $\text{Nd}^{3+}$  of

$$N_{N_4} \left( \omega_{N_4} + \alpha_5 N_{N_0} + \alpha_6 N_{P_0} + \bar{\omega}_{\text{esa}} + 2\alpha_7 N_{N_4} \right) = \bar{\omega}_{\text{gsa}} N_{N_0} + \omega_{N_{12}} N_{N_{12}}, \quad (4.8.3)$$

where  $\bar{\omega}_{\text{gsa}}$  is the average ground state absorption rate. If the system is lightly pumped such that  $N_{N_0} \approx \rho_N$  and  $N_{P_0} \approx \rho_P$  equations 4.8.1-4.8.3 become

$$N_{P_8} \left( \omega_{P_8} + \alpha_1 \rho_P + \alpha_2 \rho_N + 2\alpha_4 \rho_N N_{P_8} \right) = \alpha_9 \rho_P N_{N_{12}}, \quad (4.8.1a)$$

$$N_{N_{12}} \left( \alpha_9 \rho_P + \omega_{N_{12}} \right) = N_{N_4} \left( \bar{\omega}_{\text{esa}} + \alpha_7 N_{N_4} \right), \quad (4.8.2a)$$

$$N_{N_4} \left( \omega_{N_4} + \alpha_5 \rho_N + \alpha_6 \rho_P + \bar{\omega}_{\text{esa}} + 2\alpha_7 N_{N_4} \right) = \bar{\omega}_{\text{gsa}} \rho_N + \omega_{N_{12}} N_{N_{12}}. \quad (4.8.3a)$$

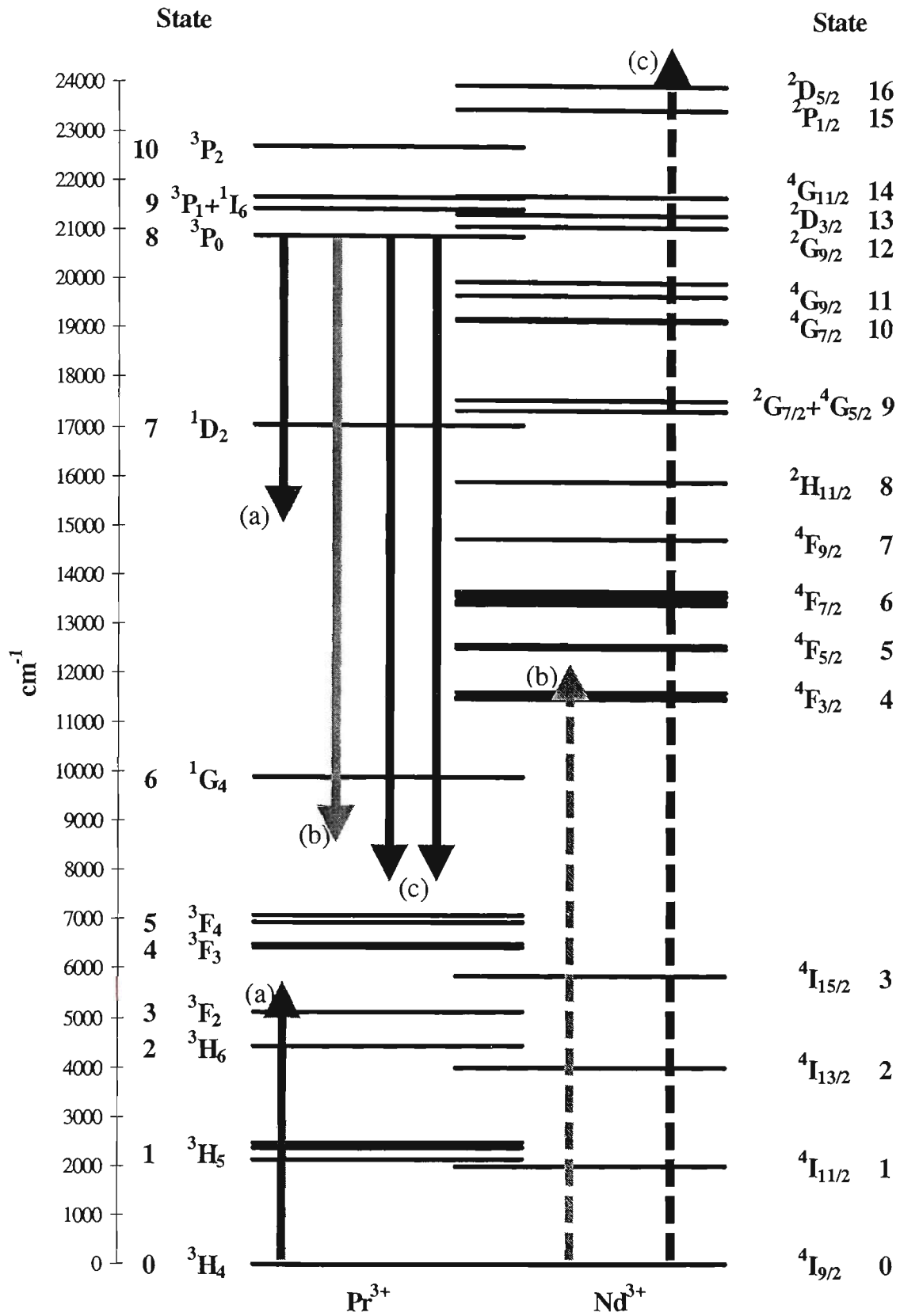


Figure 4.8.3 Energy levels of Pr<sup>3+</sup> and Nd<sup>3+</sup> ions in a ZBLANP host showing (a) Pr<sup>3+</sup>-Pr<sup>3+</sup> energy transfer as described by  $\alpha_1$ , (b) Pr<sup>3+</sup>-Nd<sup>3+</sup> 2 ion energy transfer as described by  $\alpha_2$  and (c) Pr<sup>3+</sup>-Nd<sup>3+</sup> 3 ion energy transfer as described by  $\alpha_4$  process. The dashed lines indicate energy transfer pumping processes that are considered negligible compared to the optical pumping processes.

The solution of these equations is extensive and therefore not particularly instructive so it will not be displayed here.

Since there is no change to the detection system between the previous 465.8nm and the current 795nm pumping experiment, it is assumed that the population of  $^3P_0$  is the same when  $V_{out}$  is the same for both pump wavelengths. Over the full range of  $P_{in}'$  for 465.8nm, the loss mechanism involving  $\alpha_4$  is an order of magnitude smaller than the other loss mechanisms for the  $^3P_0$  state of  $Pr^{3+}$ , table 4.8.1. Based on this, it is assumed that at the dopant concentrations being used in these experiments, the three ion process involving  $\alpha_4$  does not contribute greatly to the depletion of the  $^3P_0$  state of  $Pr^{3+}$  and so it is neglected from the rate equations. The modified rate equations, neglecting the pumping processes caused by energy transfer from  $Pr^{3+}$ , are

$$N_{P_8} (\omega_{P_8} + \alpha_1 \rho_P + \alpha_2 \rho_N) = \alpha_9 \rho_P N_{N_{12}}, \quad (4.8.4)$$

$$N_{N_{12}} (\alpha_9 \rho_P + \omega_{N_{12}}) = N_{N_4} (\bar{\omega}_{esa} + \alpha_7 N_{N_4}), \quad (4.8.5)$$

$$N_{N_4} (\omega_{N_4} + \alpha_5 \rho_N + \alpha_6 \rho_P + 2\alpha_7 N_{N_4} + \bar{\omega}_{esa}) = \bar{\omega}_{gsa} \rho_N + \omega_{N_{12}} N_{N_{12}}. \quad (4.8.6)$$

465.8nm Pump power ( $\mu W$ )	Loss mechanism (ions/m <sup>3</sup> s)			
	$\omega_{P_8} N_{P_8}$	$\alpha_1 \rho_P N_{P_8}$	$\alpha_2 \rho_N N_{P_8}$	$2\alpha_4 \rho_N N_{P_8}^2$
44	$7.04 \times 10^{22}$	$2.60 \times 10^{22}$	$1.23 \times 10^{22}$	$0.02 \times 10^{22}$
363	$5.73 \times 10^{23}$	$2.12 \times 10^{23}$	$1.00 \times 10^{23}$	$0.14 \times 10^{23}$

**Table 4.8.1** Magnitude of loss mechanisms for the  $^3P_0$  state of  $Pr^{3+}$  for extreme values of  $P_{in}'$  at 465.8nm.

The solution to equations 4.8.4-4.8.6, normalised for a peak fluorescence (population), does not depend on  $\alpha_9$ . A least squares fit can then be used to determine  $\alpha_7$  from the

normalised  $V_{\text{out}}$  data. By knowing the parameters for the 465.8nm experiment, the population of the  $^3P_0$  state of  $\text{Pr}^{3+}$  required to produce a particular voltage across the PMT is known. If the absolute (not normalised) solutions to the rate equations are used, then by knowing the required population to produce a particular  $V_{\text{out}}$ ,  $\alpha_9$  can be determined. The simplification provided by neglecting the three ion process when determining  $\alpha_7$  is no longer required and so the loss mechanism involving  $\alpha_4$  is reinserted into the equations giving

$$N_{P_8} \left( \omega_{P_8} + \alpha_1 \rho_P + \alpha_2 \rho_N + 2\alpha_4 \rho_N N_{P_8} \right) = \alpha_9 \rho_P N_{N_{12}}, \quad (4.8.7)$$

$$N_{N_{12}} \left( \alpha_9 \rho_P + \omega_{N_{12}} \right) = N_{N_4} \left( \bar{\omega}_{\text{esa}} + \alpha_7 N_{N_4} \right), \quad (4.8.8)$$

$$N_{N_4} \left( \omega_{N_4} + \alpha_5 \rho_N + \alpha_6 \rho_P + 2\alpha_7 N_{N_4} + \bar{\omega}_{\text{esa}} \right) = \bar{\omega}_{\text{gsa}} \rho_N + \omega_{N_{12}} N_{N_{12}}. \quad (4.8.9)$$

#### 4.9 795nm pump experiment

Using the same detection system as was used for the 465.8nm pump experiment ie. preform placed directly along the entrance slit of the monochromator, a Spectra Physics 3900S Ti:sapphire laser with a beam diameter ( $1/e^2$ ) of 0.95mm and a full angle divergence of 1.0mrad was used for pumping the preform at a wavelength of 795nm [Anonymous, 1990]. The pump spot was located such that maximum fluorescence was observed therefore providing an indication that the beam path was similar to that of the 465.8nm pump experiment. The 795nm pump wavelength does not correspond to any significant absorptions in  $\text{Pr}^{3+}$  so it was assumed that only the  $\text{Nd}^{3+}$  were pumped. An  $f=300\text{mm}$  plano-convex lens, placed  $1370 \pm 10\text{mm}$  after the pump laser and  $430 \pm 5\text{mm}$  before the preform, was used to focus the pump beam into the sample, figure 4.9.1.

This produced a calculated spot size ( $530 \pm 30 \mu\text{m}$ ) that was larger than the core size of the preform ( $400 \mu\text{m}$ ) and so the actual power entering the preform ( $P_{in}'$ ) was scaled accordingly (see section 4.3).  $P_{in}$  was measured using a LabMaster power meter with a silicon head and all measurements were made with the laboratory lights off to minimise the amount of stray light detected. Table 4.9.1 shows the voltage measured across the PMT ( $V_{out}$ ) for various  $P_{in}$  and the calculated  $P_{in}'$ . The input powers were selected to produce the conveniently stepped output voltages.

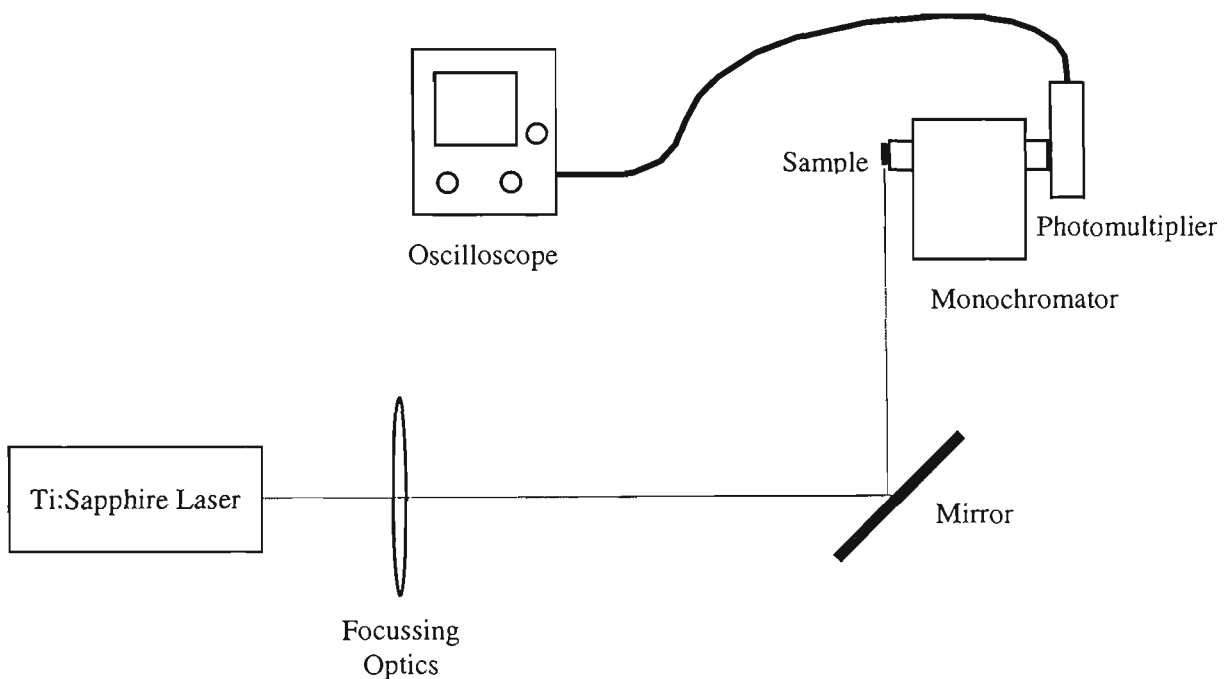


**Figure 4.9.1** Experimental arrangement used in the determination of  $\alpha_7$  and  $\alpha_9$ .

A plot of the normalised  $V_{out}$  versus  $P_{in}'$ , figure 4.9.2, shows a quadratic response that is fitted by the normalised solutions to equations 4.8.4-4.8.6 producing  $\alpha_7 = 500 \pm 100 \times 10^{-23} \text{ m}^3/\text{s}$ . Similarly, a plot of the non-normalised  $V_{out}$  versus  $P_{in}'$ , figure 4.9.3, which is least squares fitted by the solution to equations 4.8.7-4.8.9 produces  $\alpha_9 = 17 \pm 5 \times 10^{-23} \text{ m}^3/\text{s}$ .

$P_{in}$ (mW)	$P_{in}'$ (mW)	$V_{out}$ (mV)
470±2	355	13.5±0.5
425±2	321	12.0±0.5
370±2	279	10.0±0.5
321±2	242	8.0±0.2
273±2	206	6.0±0.2
210±2	159	4.0±0.2
130±2	98	2.0±0.2

**Table 4.9.1** Measured output voltage for various input powers of a 795nm-pump source.

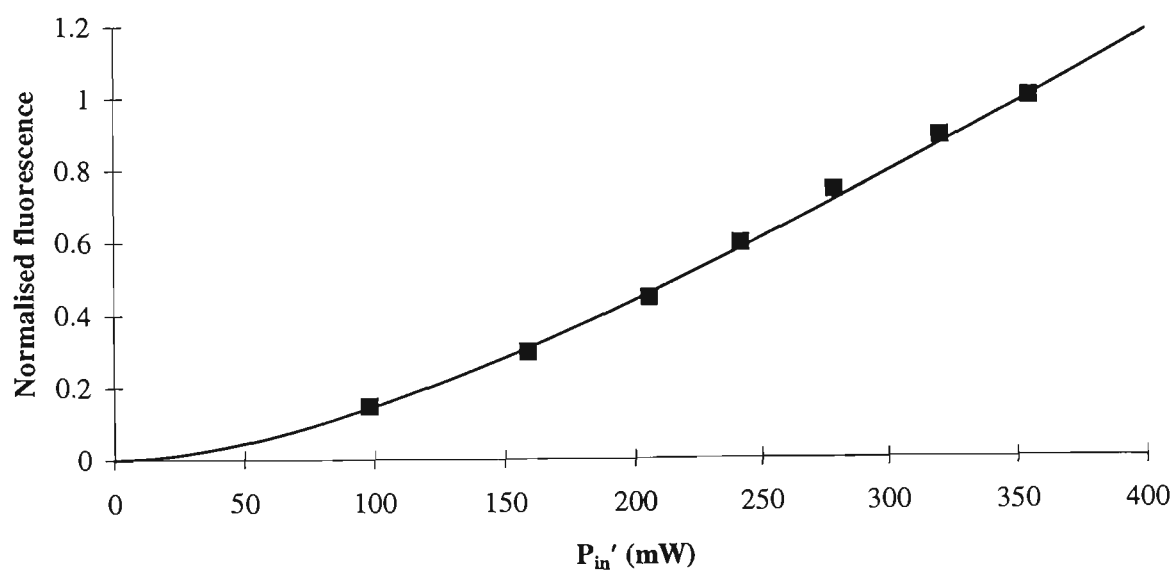


**Figure 4.9.2** Input power versus normalised fluorescence from the  $^3P_0$  state of  $Pr^{3+}$  fitted by the normalised solution to equations 4.8.4-4.8.6.

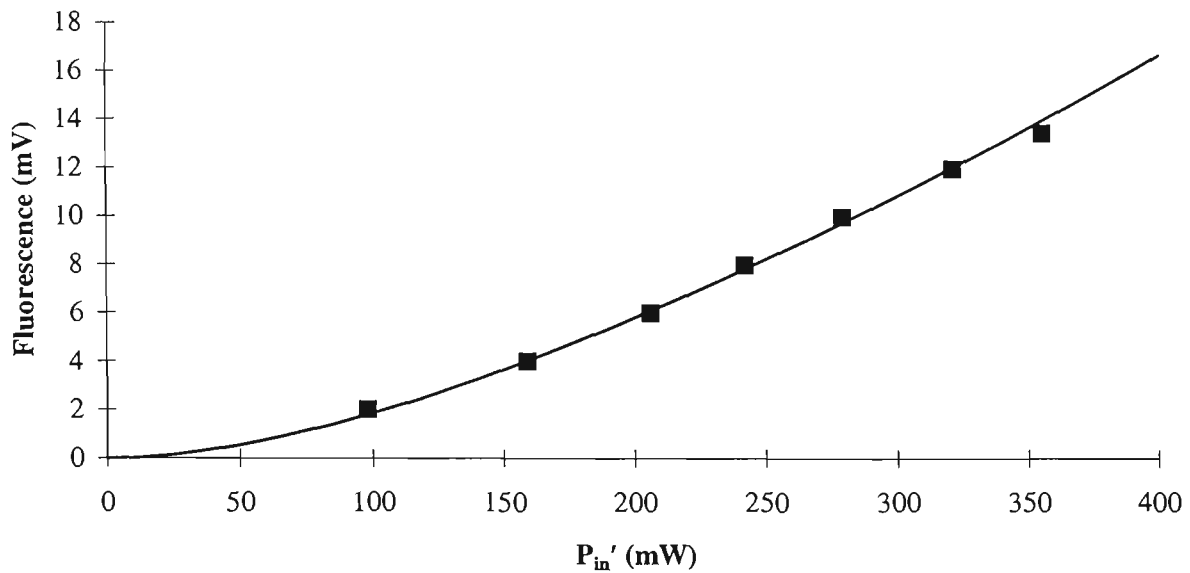


**Figure 4.9.3** Input power versus fluorescence from the  $^3P_0$  state of  $Pr^{3+}$  fitted by the solution to equations 4.8.7-4.8.9.

#### 4.10 Other processes

The processes for which energy transfer parameters have been determined thus far are not the only interactions in and between  $Pr^{3+}$  and  $Nd^{3+}$ . Other processes that should reasonably exist are three ion energy transfer from the  $^4F_{3/2}$  and  $^2G_{9/2}$  states of  $Nd^{3+}$  to  $Pr^{3+}$  in the same vein as  $\alpha_4$ , figure 4.10.1, two ion energy transfer from the  $^2G_{9/2}$  state to other states of  $Nd^{3+}$  in the same vein as  $\alpha_5$ , figure 4.10.2, and two ion energy transfer from the  $^2G_{9/2}$  state to states of  $Pr^{3+}$  other than the  $^3P_0$  state in the same vein as  $\alpha_9$ , figure 4.10.3. The majority of the proposed applications for Nd:Pr:ZBLANP glasses involve transitions from the  $^3P_0$  state of  $Pr^{3+}$ . It is thought that the other processes mentioned here do not contribute significantly to the population of the  $^3P_0$  state. By far, the greatest loss mechanism for the  $^2G_{9/2}$  state is phonon diffusion and it seems unlikely that the additional two and three ion loss mechanisms will significantly affect the population of this state. The three ion loss mechanism from the  $^4F_{3/2}$  state of  $Nd^{3+}$  has not been considered as being significant as only samples with low  $Pr^{3+}$  concentrations

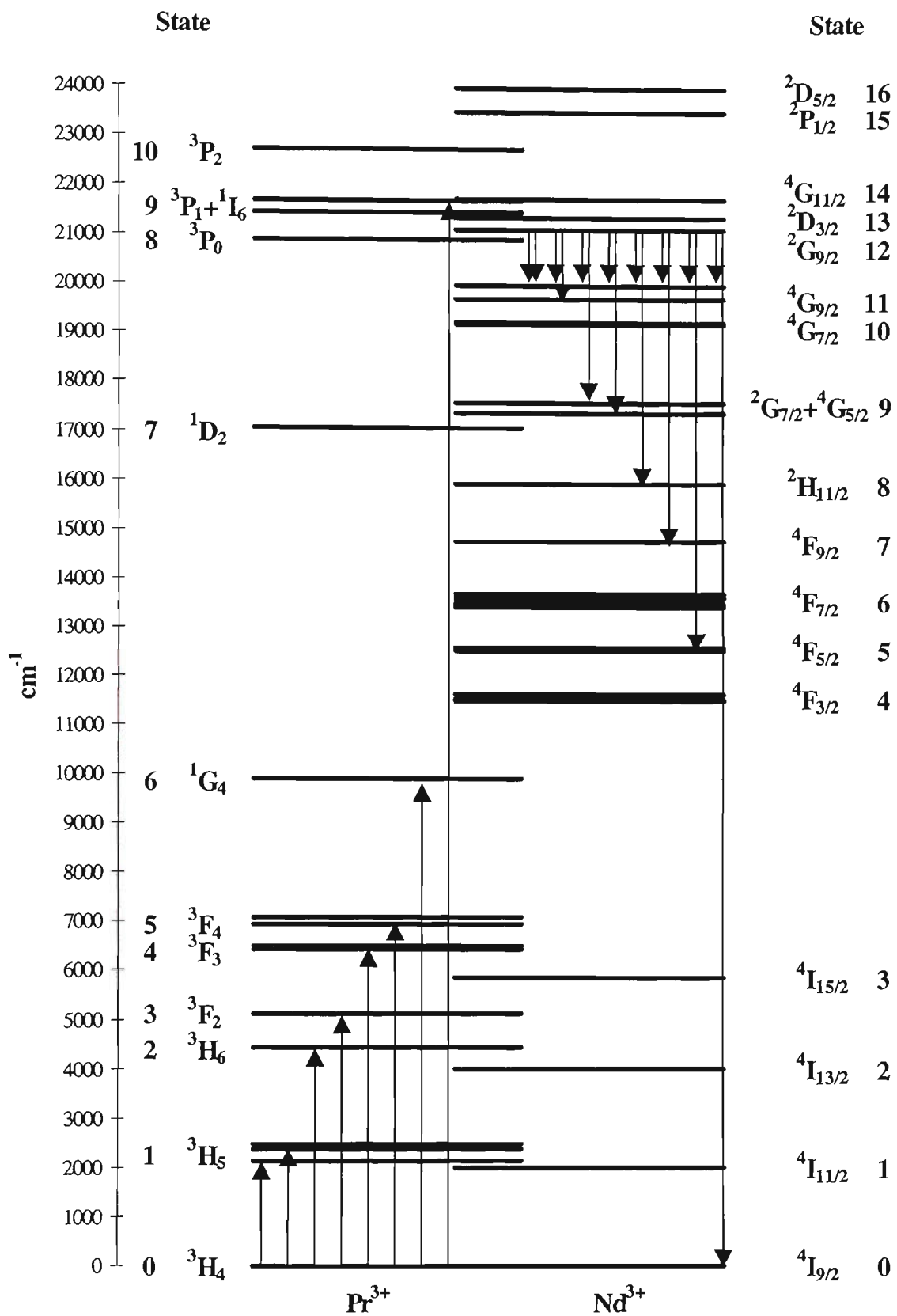


Figure 4.10.1 Energy levels of  $\text{Pr}^{3+}$  and  $\text{Nd}^{3+}$  ions in a ZBLANP host showing some of the possible 3 ion energy transfer processes from the  ${}^2G_{9/2}$  state of  $\text{Nd}^{3+}$ .

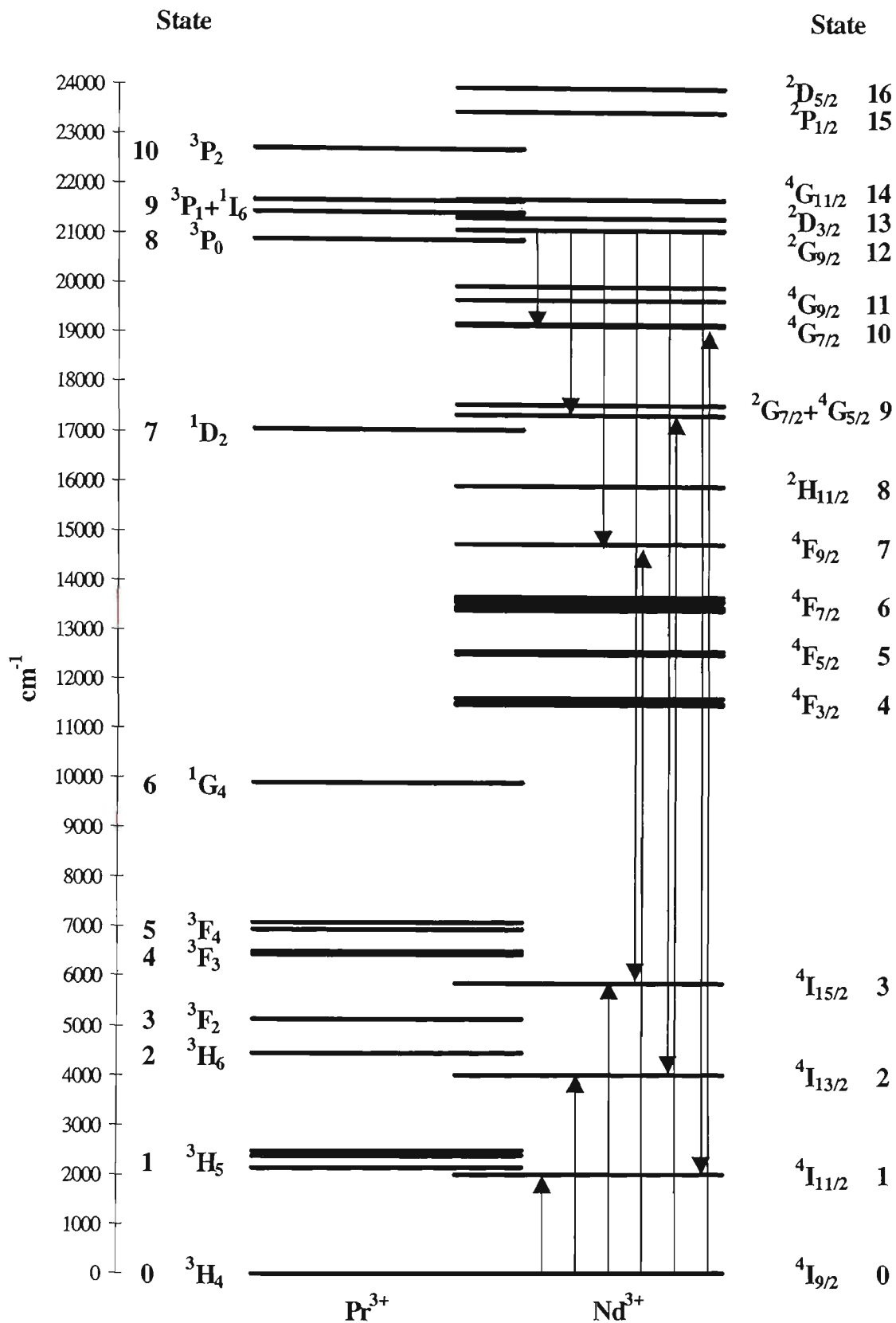


Figure 4.10.2 Energy levels of  $\text{Pr}^{3+}$  and  $\text{Nd}^{3+}$  ions in a ZBLANP host showing possible  $\text{Nd}^{3+}$ - $\text{Nd}^{3+}$ , 2 ion energy transfer processes from the  ${}^2G_{9/2}$  state of  $\text{Nd}^{3+}$ .

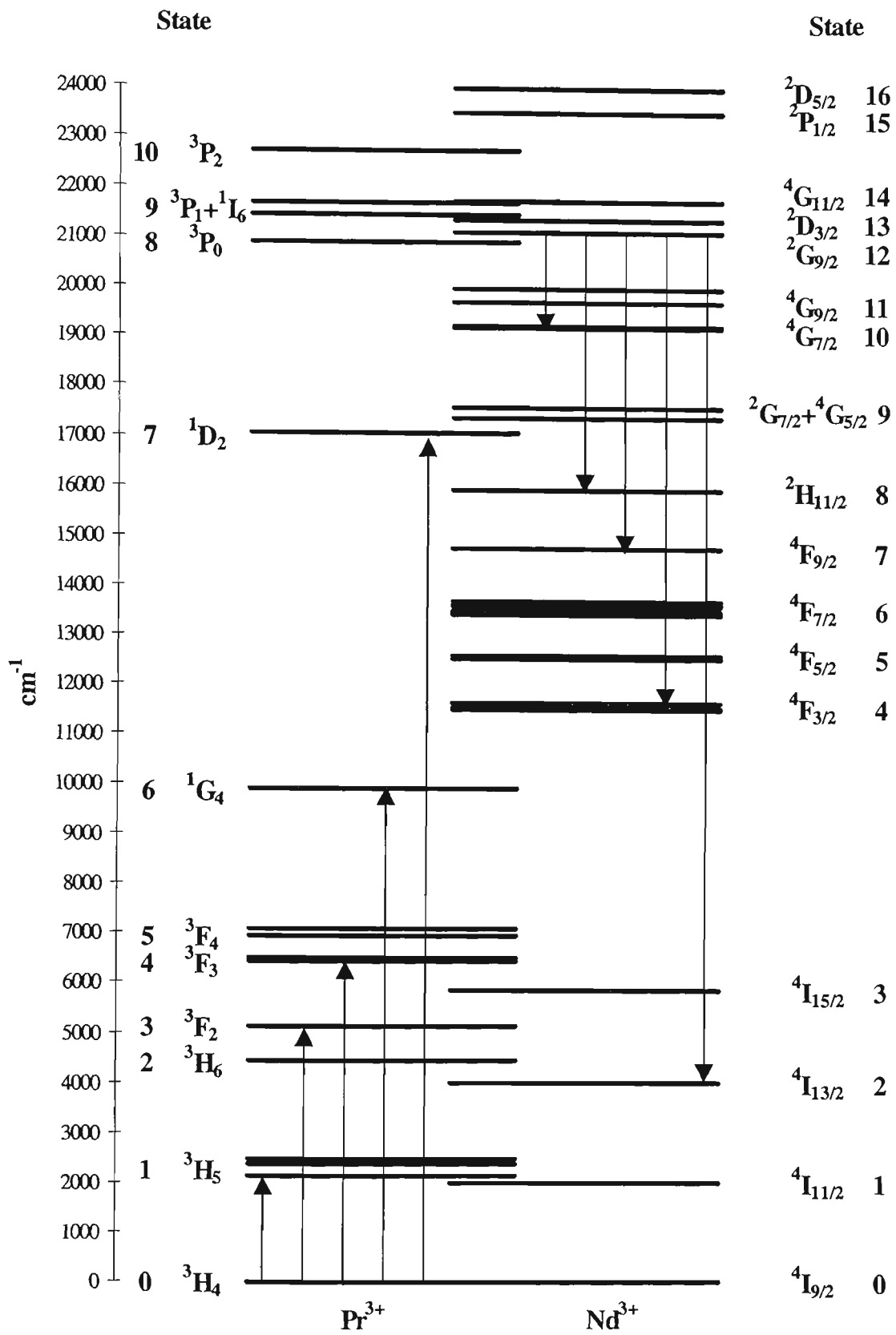


Figure 4.10.3 Energy levels of  $\text{Pr}^{3+}$  and  $\text{Nd}^{3+}$  ions in a ZBLANP host showing other possible  $\text{Nd}^{3+}$ - $\text{Pr}^{3+}$ , 2 ion energy transfer processes from the  ${}^2G_{9/2}$  state of  $\text{Nd}^{3+}$ .

have been available for analysis. This process may become significant at high  $\text{Pr}^{3+}$  concentrations. With no other processes to be accounted for, the final steady state rate equations are

$$N_{P_8} \left( \omega_{P_8} + \alpha_1 \rho_P + \alpha_2 \rho_N + 2\alpha_4 N_{P_8} \right) = \alpha_9 \rho_P N_{N_{12}}, \quad (4.10.1)$$

$$N_{N_{12}} \left( \alpha_9 \rho_P + \omega_{N_{12}} \right) = N_{N_4} \left( \bar{\omega}_{\text{esa}} + \alpha_7 N_{N_4} \right), \quad (4.10.2)$$

$$N_{N_4} \left( \omega_{N_4} + \alpha_5 \rho_N + \alpha_6 \rho_P + 2\alpha_7 N_{N_4} + \bar{\omega}_{\text{esa}} \right) = \bar{\omega}_{\text{gsa}} N_{N_0} + \omega_{N_{12}} N_{N_{12}}, \quad (4.10.3)$$

$$\rho_N = N_{N_0} + N_{N_4} + N_{N_{12}} \quad (4.10.4)$$

which can be solved to provide estimations of population density for the various states of the system.

#### 4.11 Pumping approximations

During the development of this model some approximations have been made which are yet to be justified, namely that the pumping of  $\text{Nd}^{3+}$  by energy transfer from  $\text{Pr}^{3+}$  is insignificant compared to the optical pumping. It is easier to see the justification for such approximations if they are expressed numerically. From Table 4.11.1 it is clear that the evaluations in the second column, optical pumping of  $\text{Nd}^{3+}$ , are larger than those in the third, pumping of  $\text{Nd}^{3+}$  by energy transfer from  $\text{Pr}^{3+}$  in the  $^3\text{P}_0$  state, by many orders of magnitude. This indicates that neglecting the pumping processes as a result of energy transfer is a reasonable approximation.

$P_{in}'$ (mW)	Optical pumping $\left(\frac{\text{ions}}{\text{m}^3\text{s}}\right)$ $\bar{\omega}_p N_{N_0}$	Energy transfer $\left(\frac{\text{ions}}{\text{m}^3\text{s}}\right)$ $\alpha_2 N_{P_8} N_{N_0}$
98	$20 \times 10^{19}$	$54 \times 10^9$
355	$73 \times 10^{19}$	$71 \times 10^{10}$
$P_{in}'$ (mW)	$\bar{\omega}_{csa} N_{N_4}$	$\alpha_4 N_{P_8}^2 N_{N_0}$
98	$14 \times 10^9$	$62 \times 10^{-13}$
355	$19 \times 10^{10}$	$82 \times 10^{-12}$

**Table 4.11.1** Evaluation of loss mechanisms as justification for approximations made in the derivation of the model.

## 4.12 Conclusion

Steady state fluorescence has been used to determine energy transfer parameters that describe  $n^2$  type transfer processes from the  $^3P_0$  state of  $\text{Pr}^{3+}$  and the  $^4F_{3/2}$  state of  $\text{Nd}^{3+}$ , table 4.12.1. The value determined for  $\alpha_7$  is an order of magnitude larger than that of other two ion processes. This may indicate that a further process for populating the  $^3P_0$  state of  $\text{Pr}^{3+}$  exists, the rate of that process being attributed to  $\alpha_7$ . One such possible process is excited state absorption from the  $^1G_4$  state of  $\text{Pr}^{3+}$  but further investigation will be needed to determine this.

The parameter describing the energy transfer from the  $^2G_{9/2}$  state of  $\text{Nd}^{3+}$  to the excited state of  $\text{Pr}^{3+}$ ,  $\alpha_9$  has also been determined, table 4.12.1. By using the rate equations 4.10.1-4 and the energy transfer parameters, it is now possible to determine excited state

populations of the  $^3P_0$  state of  $Pr^{3+}$  and the  $^4F_{3/2}$  state of  $Nd^{3+}$  for any 795nm input power.

Parameter	Value	Definition
$\alpha_4$	$(1.6 \pm 0.2) \times 10^{-43} \text{ m}^6/\text{s}$	Parameter for three ion energy transfer from the $^3P_0$ state of $Pr^{3+}$ to $Nd^{3+}$
$\alpha_7$	$(500 \pm 100) \times 10^{-23} \text{ m}^3/\text{s}$	Parameter for two ion cooperative upconversion from the $^4F_{3/2}$ state of $Nd^{3+}$
$\alpha_9$	$(17 \pm 5) \times 10^{-23} \text{ m}^3/\text{s}$	Parameter for two ion energy transfer from the $^2G_{9/2}$ state of $Nd^{3+}$ to $Pr^{3+}$

**Table 4.12.1** Energy transfer parameters for the  $n^2$  processes and the transfer of energy that leads to the visible fluorescence from  $Pr^{3+}$ .

# 5. Applications

Section.....	Page
5.1 Introduction .....	5-2
5.2 Gain .....	5-4
5.2.1 Determination of loss in the system for 635nm light. ....	5-5
5.2.2 Prediction of gain .....	5-5
5.3 Optimal concentrations .....	5-7
5.4 Concentration determination .....	5-10
5.5 Imaging.....	5-11
5.6 1300nm amplifiers .....	5-17
5.7 Temperature sensors.....	5-19
5.8 The future for Nd:Pr codoping .....	5-25
5.9 Conclusion.....	5-27

## 5.1 Introduction

In the preceding chapters, spectroscopic parameters have been determined for use in the rate equation model, table 5.1.1. In this chapter, the steady state rate equations, 5.1.1-4, are used to determine the performance of Nd:Pr:ZBLANP glasses.

$$N_{P_8} \left( \omega_{P_8} + \alpha_1 \rho_P + \alpha_2 \rho_N + 2\alpha_4 N_{P_8} \right) = \alpha_9 \rho_P N_{N_{12}}, \quad (5.1.1)$$

$$N_{N_{12}} \left( \alpha_9 \rho_P + \omega_{N_{12}} \right) = N_{N_4} \left( \bar{\omega}_{esa} + \alpha_7 N_{N_4} \right), \quad (5.1.2)$$

$$N_{N_4} \left( \omega_{N_4} + \alpha_5 \rho_N + \alpha_6 \rho_P + 2\alpha_7 N_{N_4} + \bar{\omega}_{esa} \right) = \bar{\omega}_{gsa} N_{N_0} + \omega_{N_{12}} N_{N_{12}}, \quad (5.1.3)$$

$$\rho_N = N_{N_0} + N_{N_4} + N_{N_{12}}. \quad (5.1.4)$$

Many of the applications discussed in chapter 1 involve the lasing of visible transitions from the  $^3P_0$  state of  $Pr^{3+}$ . In order for lasing to take place, the gain of the transition must exceed the overall loss in the system. Gain is related to the excited state population, the emission cross-section for the transition and the length of the active medium. The emission cross-section is available from literature and the excited state population is determined by solving the rate equations thereby allowing the calculation of gains. These are then compared to experimental results. Solving the rate equations also facilitates the prediction of optimal concentrations for the two dopants as well as providing some insight into the operation of a Nd:Pr:ZBLANP amplifier or laser.

In addition to the above, a new technique for imaging dopant concentration of fibres is demonstrated. The new technique utilises the rate equations to determine dopant concentration from steady state fluorescence measurements. The fluorescence measurements are made in the steady state with a currently available, commercial,

scanning confocal microscope making it more convenient than the fluorescence lifetime technique of Petreski [Petreski B. P. *et al.*, 1997].

The development of potential temperature sensors and a 1300nm amplifier are also discussed.

Parameter	Value	Source
$\omega_{P_8}$	$20,000 \pm 400s^{-1}$	[1]
$\omega_{N_{12}}$	$(35 \pm 0.1) \times 10^6 s^{-1}$	Chapter 2
$\omega_{N_4}$	$2,000 \pm 100s^{-1}$	Chapter 2
$\alpha_1$	$(18 \pm 3) \times 10^{-23} m^3/s$	Chapter 3
$\alpha_2$	$(6.6 \pm 0.8) \times 10^{-23} m^3/s$	Chapter 3
$\alpha_4$	$(1.6 \pm 0.2) \times 10^{-43} m^6/s$	Chapter 4
$\alpha_5$	$(0.34 \pm 0.06) \times 10^{-23} m^3/s$	Chapter 3
$\alpha_6$	$(1.9 \pm 0.4) \times 10^{-23} m^3/s$	Chapter 3
$\alpha_7$	$(500 \pm 100) \times 10^{-23} m^3/s$	Chapter 4
$\alpha_9$	$(17 \pm 5) \times 10^{-23} m^3/s$	Chapter 4
$\sigma_{795}$	$(2.2 \pm 0.3) \times 10^{-24} m^2$	Chapter 2
$\sigma_{465.8}$	$(0.9 \pm 0.1) \times 10^{-24} m^2$	Chapter 2
$\sigma_{476.5}$	$(0.58 \pm 0.07) \times 10^{-24} m^2$	Chapter 2
$\sigma_{esa}$	$\sigma_{gsa} 0.15 \pm 0.02$	Chapter 2

**Table 5.1.1** Spectroscopic parameters for the rate equation model. [1] Petreski *et al.*, 1996

## 5.2 Gain

In order to establish a laser or amplifier, the active medium needs to have a gain greater than one. The overall gain, including losses in the system, can be directly measured by taking the ratio of output power to input power of a signal. The absolute gain, not including losses in the system, can also be calculated from

$$G = \exp(\sigma_{ba}(N_b - N_a)L), \quad (5.2.1)$$

where  $\sigma_{ba}$  is the emission cross-section from state  $b$  to state  $a$ ,  $N_b$  is the population density of state  $b$ ,  $N_a$  is the population density of state  $a$  and  $L$  is the length of the active medium [Svelto O., 1989]. In a four level system, it is reasonable and convenient to assume that the lower state has negligible population compared to the upper state such that  $N_a \approx 0$ . The gain of the active medium will then depend on the population of the upper state. For the system presented in this thesis, the upper state population of  $\text{Pr}^{3+}$  is established by pumping  $\text{Nd}^{3+}$  with 795nm Ti:Sapphire laser or by pumping  $\text{Pr}^{3+}$  with a 465.8nm Argon ion laser. Since the system is end pumped, the upper state population density will decrease with distance into the active medium. As the population density of the excited state reduces, so to does the gain coefficient  $\sigma_{ba}N_b$ . An average gain coefficient, which is determined from the gain coefficients calculated at regular intervals along the length of the active medium, is used to determine the overall gain of the system.

The transition to be investigated is  ${}^3\text{P}_0$  to  ${}^3\text{F}_2$  in  $\text{Pr}^{3+}$ , producing a 635nm emission. This is a quasi-four level system, allowing the assumption of negligible lower state population to be made.

### 5.2.1 Determination of loss in the system for 635nm light.

To determine the scattering loss in the system for 635nm light a HeNe laser was used for which no significant absorption in the  $\text{Nd}^{3+}$  or  $\text{Pr}^{3+}$  is expected. The beam of the HeNe was aimed through the centre and along the 20mm length of the preform. The input power, allowing for a 4% reflection as the beam enters the sample, was determined to be  $41.2\mu\text{W}$ . The transmitted power, again allowing for a 4% reflection as the beam exits the sample, was determined to be  $25.2\mu\text{W}$ , giving a transmittance of 0.61 for the preform. This indicates the exponential loss factor is  $25\text{ m}^{-1}$ . The signal beam was not focussed tightly enough for all of it to enter the core region of the sample but the cladding material is considered to be similar to that of the core and consequently has similar scattering properties. The loss in the system is then one minus the transmittance.

### 5.2.2 Prediction of gain

From observation of the fluorescence experiments, it is clear that the quantum efficiency of the system is far greater when a 465.8nm pump is used as compared to a 795nm pump source. The 465.8nm pump source can produce far greater excited state populations even though less power is available from the pump laser. The greater excited state population produces a greater probability of the system having some gain. An experiment to measure the gain where the entire core region was pumped with a 465.8nm source showed that there was no perceivable gain. Under such conditions, the model, which assumes direct pumping of the  $\text{Pr}^{3+} {}^3\text{P}_1$  state (equation 4.6.2), predicts pump powers in the order of 100's of kilowatts before a gain greater than one can be attained. Using the minimum diffraction limited spot size for the pump beam ( $30\mu\text{m}$ )

the pump power required to produce a gain greater than one is in the order of 100's of Watts. For gains greater than one with reasonable pump powers, the model predicts that it is necessary to confine the pump volume to less than  $10\mu\text{m}$ . This implies that the use of fibre as opposed to bulk glass is required to produce a laser or amplifier.

In the paper by Goh [Goh S. C. *et. al.*, 1995], a 600mm length,  $6\mu\text{m}$  core fibre, of the same composition as the preform, was pumped with a 795nm source. The experiment shows that the normalised output of all spectral lines from 450nm to 750nm increase simultaneously relative to the 717nm spectral line when laser mirrors are placed on the end of the fibre. The magnitude of the power used to pump this system would suggest that bleaching of the ground state of  $\text{Nd}^{3+}$  has occurred. The current model, equations 5.1.1-4, does not allow for bleaching but the effect would be to increase the active length of the fibre, producing more gain. For this experiment, the model predicts a required pump power in the order of kW before a gain greater than one can be achieved. This is mainly due to an excessive length of fibre that has been used with 99% of the pump power being absorbed in the first 44mm of fibre. In the regime where bleaching is not a factor, a more appropriate length of fibre, 44mm, the model predicts that a pump power of around 10mW is required before a gain greater than one can be attained. Even at this relatively low pump power, 93% of the population is in the ground state of  $\text{Nd}^{3+}$  due to the relatively high pump intensity entering the  $6\mu\text{m}$  core. This still only produces a gain marginally greater than one and this does not change significantly with large increases of pump power. The model predicts populations of the  $^3\text{P}_0$  state to  $\pm 10\%$  as calculated from the square root of the sum of the squares of the uncertainties of the spectroscopic parameters. This is the dominant factor in limiting the uncertainty of the

predicted gains to  $\pm 10\%$ . When this is coupled with the shallow gradient of the potential gain curves the thresholds for gains greater than one could be much higher, figure 5.2.2.1. In systems that do not have the  $\text{NdF}_3$  co-dopant, the gain is sufficient for lasing on the  ${}^3\text{P}_0 \rightarrow {}^3\text{H}_4$ ,  ${}^3\text{P}_0 \rightarrow {}^3\text{H}_5$  and  ${}^3\text{P}_0 \rightarrow {}^3\text{F}_2$  transitions [Zhao Y. *et al.*, 1997]. This indicates that in spite of the benefit of utilising a single pump wavelength (the Zhao paper uses two) the use of  $\text{NdF}_3$  makes the present pumping scheme is highly inefficient as can be seen by the virtually flat gradient of figure 5.2.2.1.

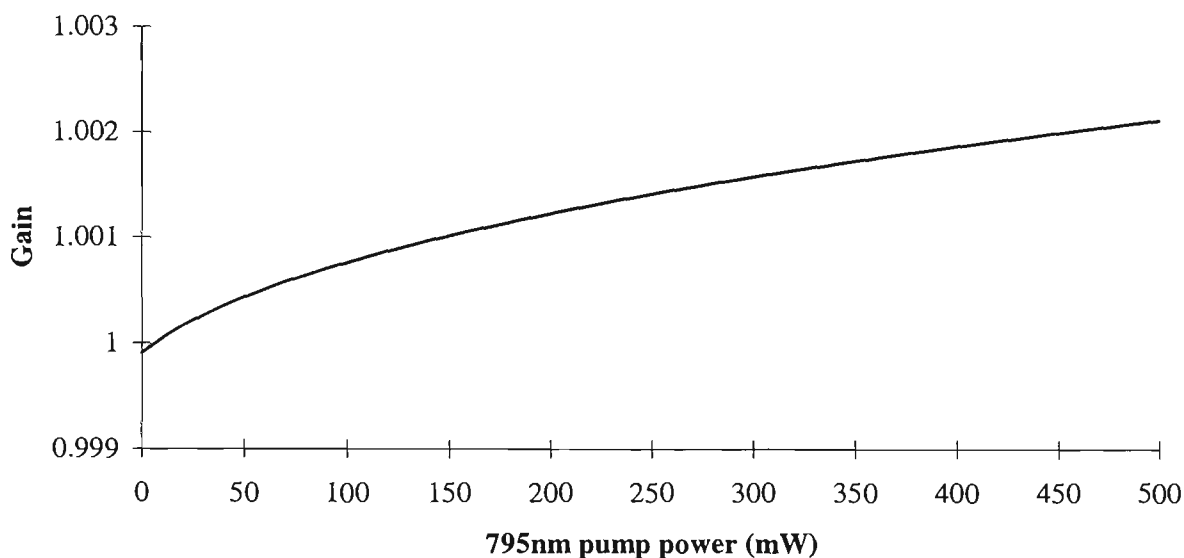


**Figure 5.2.2.1** Predicted gain curve for a 44mm length of codoped fibre similar to that used by Goh *et al.*

### 5.3 Optimal concentrations

As a method for determining optimal concentrations of  $\text{Pr}^{3+}$  and  $\text{Nd}^{3+}$ , the rate equation model can be used to maximise the population of the  ${}^3\text{P}_0$  state of  $\text{Pr}^{3+}$ . The uncertainty of the predicted population is  $\pm 10\%$  for a preform type sample with a length of 28mm and a core diameter of  $400\mu\text{m}$ . The  $\text{Pr}^{3+}$  dopant concentration at which the predicted peak population occurs depends on the  $\text{Nd}^{3+}$  dopant concentration. For  $\text{Nd}^{3+}$

concentrations less than 0.1%, the peak population occurs with 0.3% Pr<sup>3+</sup> but with 2% of Nd<sup>3+</sup> the peak population occurs with 0.8% of Pr<sup>3+</sup>, figure 5.3.1. A significant amount of quenching of the <sup>3</sup>P<sub>0</sub> state of Pr<sup>3+</sup> occurs once the Pr<sup>3+</sup> concentration increases above 0.8%. A 2%Nd<sup>3+</sup>-2%Pr<sup>3+</sup> codoped glass has been produced but the fluorescence observed from this sample was minimal. In early experiments, the other glass samples were all observed to produce more fluorescence than the 2%Nd<sup>3+</sup>-2%Pr<sup>3+</sup> codoped glass. This can be partially explained by the fact that the 2%Nd<sup>3+</sup>-2%Pr<sup>3+</sup> codoped glass sample has a very much larger absorption coefficient and so fluorescence is observed from only a very small region. Another problem is that the 2%Nd<sup>3+</sup>-2%Pr<sup>3+</sup> codoped glass sample was damaged with pump powers greater than 200mW and so was never pumped as hard, therefore producing less fluorescence. The other samples were all observed at pump powers of 800mW. It is also highly probable that clustering has occurred while making the 2%Nd<sup>3+</sup>-2%Pr<sup>3+</sup> sample. The formation of dopant clusters makes the occurrence of higher order ion processes (3, 4, 5 etc ion processes) more likely. It is these higher order processes that lead to the depletion of the excited state population of Pr<sup>3+</sup>, which would lead to greater phonon diffusion and therefore greater heat in the sample, making it more susceptible to optical damage. The current model predicts populations for evenly distributed dopants and further work is required to extend that to glasses that exhibit the formation of dopant clusters. Other workers in rare-earth doped fluoride glasses have achieved much higher concentrations without evidence of clustering [Bogdanov V. *et al.*, 1996] so the possibility of making highly doped Nd:Pr:ZBLANP glasses remains.

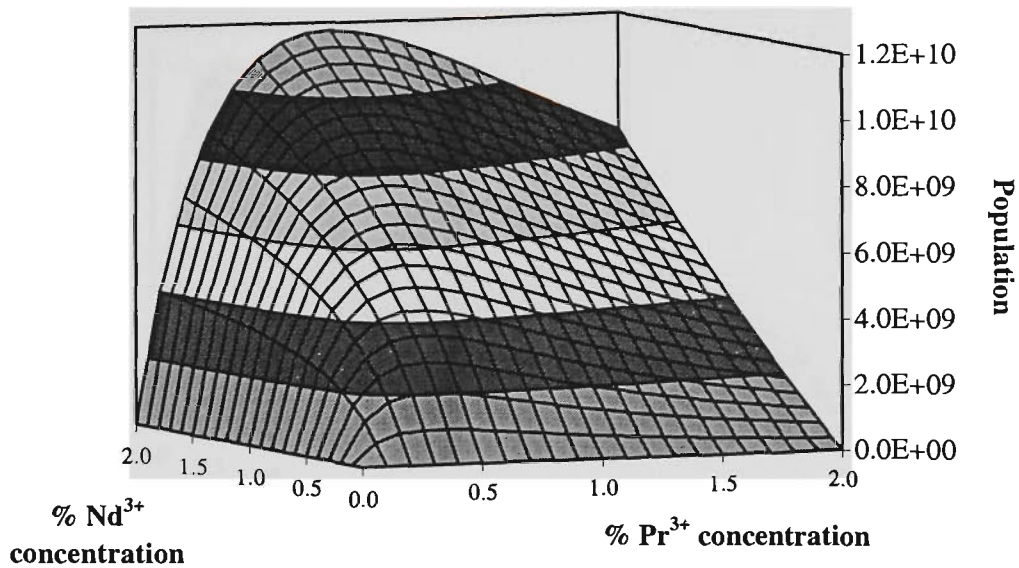


**Figure 5.3.1** Population of the  $^3P_0$  state of  $Pr^{3+}$  for varying concentrations of  $Pr^{3+}$  and  $Nd^{3+}$  pumped by a 100mW, 795nm source.

Observation of fluorescence from all the samples, excluding the 2% $Nd^{3+}$  -2% $Pr^{3+}$  sample, would seem to indicate that around 0.3%  $Nd^{3+}$  and 0.2%  $Pr^{3+}$  dopant concentrations would produce the highest excited state population. This is not shown in figure 5.3.1 as the model is only being pumped with 100mW of 795nm radiation. Figure 5.3.2 shows that when the pump power is increased to 800mW and the pump spot size decreased to 40 $\mu m$ , the 0.3%  $Nd^{3+}$ -0.2%  $Pr^{3+}$  should produce greater fluorescence than the other samples. The model is based on a lightly pumped regime and figure 5.3.2 is only included as an indication as to what may occur.

The highest excited state population will produce the greatest gain and the lowest threshold for lasing. This is predicted to occur with a 2% $Nd^{3+}$ -0.8% $Pr^{3+}$  co-doped sample. Even in this optimised state, the model still predicts gains that are marginally greater than one.

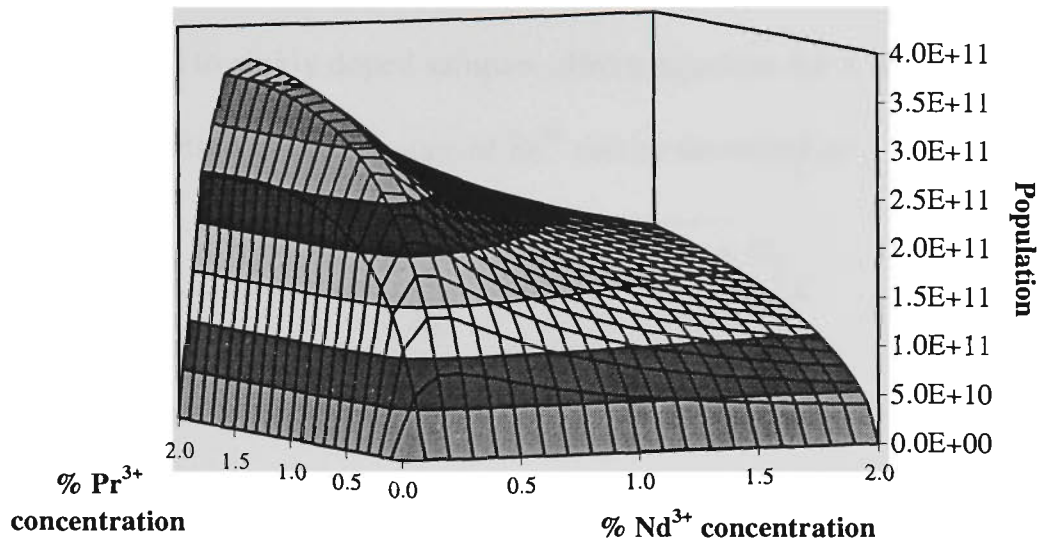


**Figure 5.3.2** Population of the  $^3P_0$  state of  $Pr^{3+}$  for varying concentrations of  $Pr^{3+}$  and  $Nd^{3+}$  pumped by a 800mW, 795nm source.

#### 5.4 Concentration determination

In chapter 4 the steady state rate equation describing the population of the  $^3P_0$  state of  $Pr^{3+}$  was solved to produce equation 4.6.2, which described how the population varied with pump rate. A similar process can be used to produce an equation that describes the population variation of the  $^4F_{3/2}$  state of  $Nd^{3+}$  from equation 4.8.3. Assuming the sample will be lightly pumped such that  $N_{N_{12}} \approx 0$ , the population variation for the  $^4F_{3/2}$  will vary with pump rate as

$$N_{N_4} = \frac{\bar{\omega}_{gsa} + \bar{\omega}_{esa} + b - \sqrt{(\bar{\omega}_{gsa} + \bar{\omega}_{esa} + b)^2 - 4a\bar{\omega}_{gsa}\rho_N}}{2a}, \quad (5.4.1)$$

where  $a = \alpha_5 - 2\alpha_7$  and  $b = \omega_{N_4} + \alpha_5\rho_N + \alpha_6\rho_P$ . Since all parameters have been determined, if the population of these states ( $^3P_0$  and  $^4F_{3/2}$ ) is observed experimentally for varying pump rates, then the unknown concentrations can be determined. Unfortunately, the only glass samples available have been used in the determination of the parameters that would be used to determine the concentration. To determine the

concentration of such glasses would be meaningless. However, the process can be just as easily applied to singly doped samples. From equation 4.6.2, without the presence of  $\text{Nd}^{3+}$ , the population of the  ${}^3\text{P}_0$  state of  $\text{Pr}^{3+}$  can be described by

$$\bar{N}_{P_8} = \frac{\left( \bar{\omega}_p + \omega_{P_8} + \alpha_1 \rho_P - \sqrt{(\bar{\omega}_p + \omega_{P_8} + \alpha_1 \rho_P)^2 + 4\alpha_1 \rho_P \bar{\omega}_p} \right)}{2\alpha_1}. \quad (5.4.2)$$

As previously discussed, the population of the excited state is related to the output fluorescence by a proportionality constant that depends on the measurement system. By normalising to the population at the peak pumping rate, the proportionality constant is eliminated giving a direct correlation between pump power and normalised fluorescence. Utilising the parameters determined in the previous chapters, it is now possible to determine concentration of  $\text{Pr}^{3+}$  and  $\text{Nd}^{3+}$  from fluorescence measurements. For low concentrations of a single dopant, normalisation may not be appropriate as the noise in the measurement may exceed the effect caused by concentration variation. In this case, the fluorescence should not be normalised and alternative strategies for determining the proportionality constant should be sought. One possible method is to have a calibrating signal from a sample of known concentration.

## 5.5 Imaging

A confocal microscope is one where a small spot of light is used to illuminate the object, the image of which is collected by a small, ideally a point source, detector. By scanning the illuminating spot across the object, an image map can be built up providing an overall image that is of a higher resolution than that which can be formed from a conventional microscope [Gu M., 1996].

The image in the  $x, y$  plane is defined as being in “image space” and the 2D Fourier transform of this image is defined as being in the “spatial frequency domain” [Hecht E., 1990].

An OLYMPUS Fluoview 1X70 is used to observe fluorescence from a Pr:ZBLANP fibre for varying input powers, the images from which are used to determine the dopant concentration distribution across the fibre. Due to the dimensions of the fibre, the instrument function associated with the microscope becomes a significant modifying factor to the image [Gu M., 1996]. To determine the true image of the concentration profile it is necessary to remove the instrument function from the measured image. The measured image is in terms of intensity units as determined by the microscope, 0 represents the lowest intensity and 4096 the brightest. In order to convert between the units of the instrument to those of concentration (ions/m<sup>3</sup>), it is necessary to include a modifying factor. The measured image also contains extraneous noise from the pump laser and detection system, so that

$$\text{Im}(t_x, t_y) = \text{Inst}(t_x, t_y) \otimes (k \times \rho(t_x, t_y)) + n(t_x, t_y), \quad (5.5.1)$$

where  $\text{Im}$  is the recorded image,  $\text{Inst}$  is the instrument function,  $\rho$  is the concentration profile and  $n$  is the noise, all defined in image space and  $k$  is the modifying factor. The instrument function is assumed to be the convolution of the two Airy disks formed by the pump and signal beams passing through the microscope objective. By taking the two-dimensional Fourier transform of both sides of this equation, the concentration profile can be determined from

$$\left( K \otimes \rho(f_x, f_y) \right) = \frac{\text{Im}(f_x, f_y)}{\text{Inst}(f_x, f_y)} + \frac{N(f_x, f_y)}{\text{Inst}(f_x, f_y)}, \quad (5.5.2)$$

where  $K$  is the modifying factor in the spatial frequency domain. For large regions of the spatial frequency domain the instrument function is small which causes the noise signal to be amplified excessively, figure 5.5.1. The vertical scale of figure 5.5.1 has been limited to accommodate the viewing of the image signal which appears at the corners and not the excessively amplified noise which appears as the saturated structure in the centre. By judiciously choosing a maximum amplitude that the noise in the central region of figure 5.5.1 can attain, image information can be retrieved without removing any possible high frequency contributions, figures 5.5.2 and 5.5.3. The validity of the resulting image can be tested by convolving it with the instrument function and comparing that result to the original image, figure 5.5.4. The difference between these two images, figure 5.5.5, reveals that the noise has been reduced with little or no structural change to the original image.

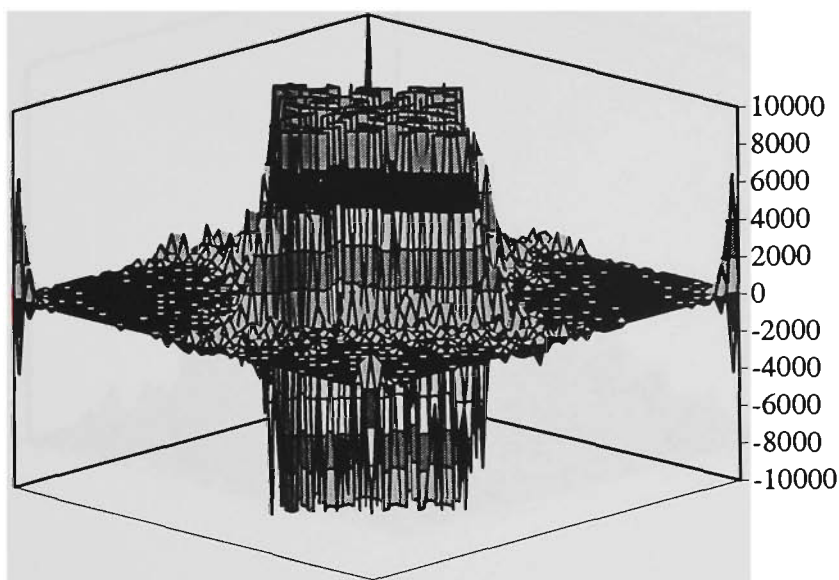


**Figure 5.5.1** Deconvolution in the spatial frequency domain. The example shown is for the worst case.

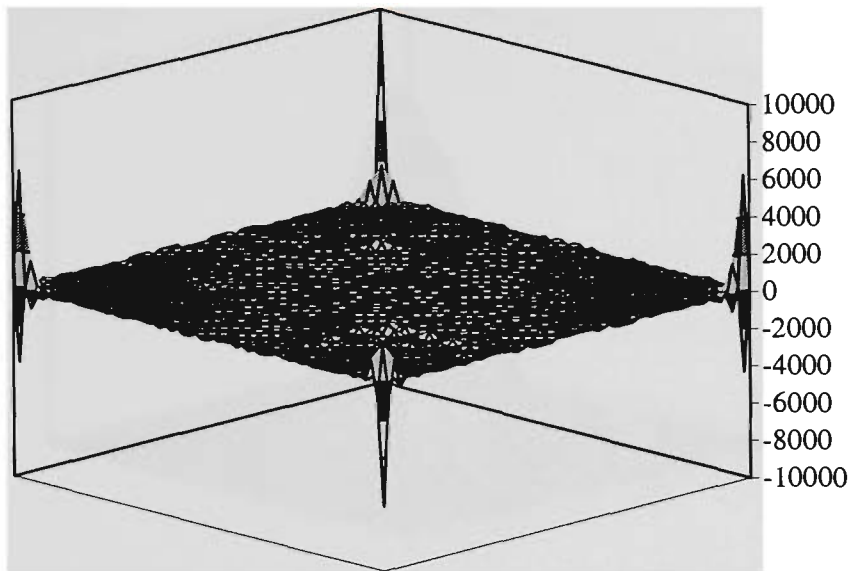


**Figure 5.5.2** Deconvolution in the spatial frequency domain with noise reduced.

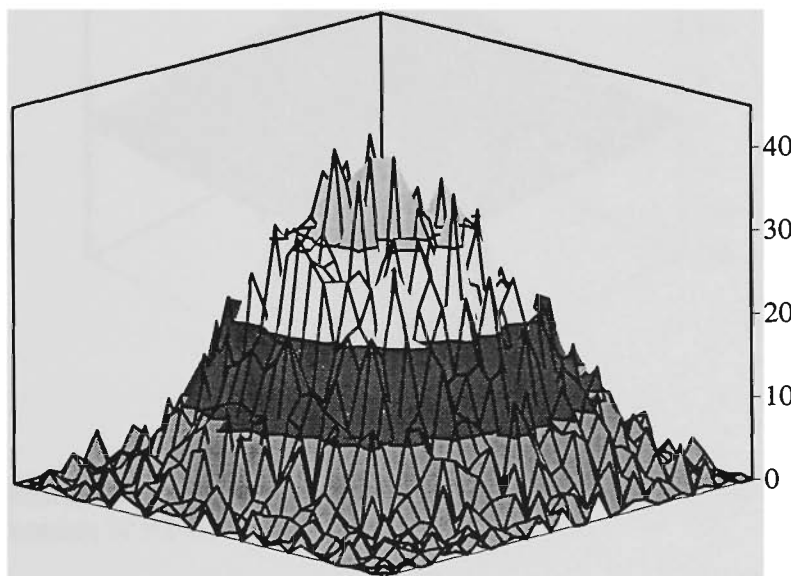


**Figure 5.5.3** Modified image with noise reduction.

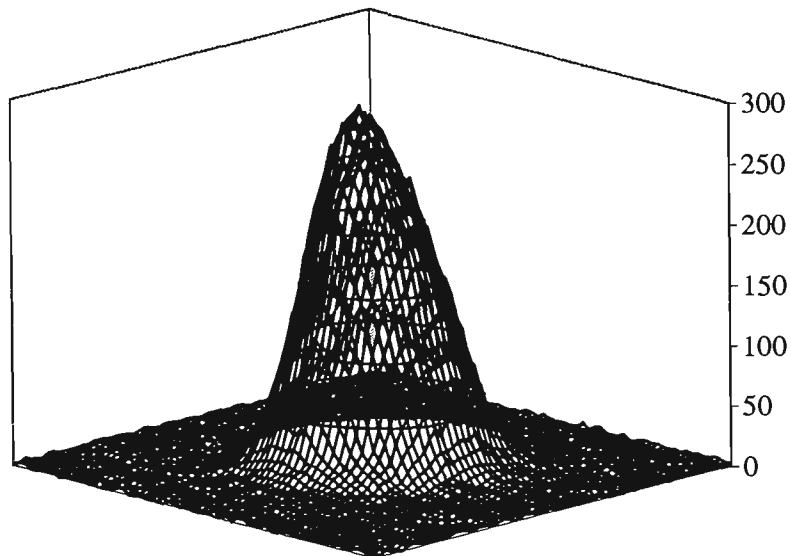


**Figure 5.5.4** Convolution of reduced noise modified image with instrument function overlaid with the original image.

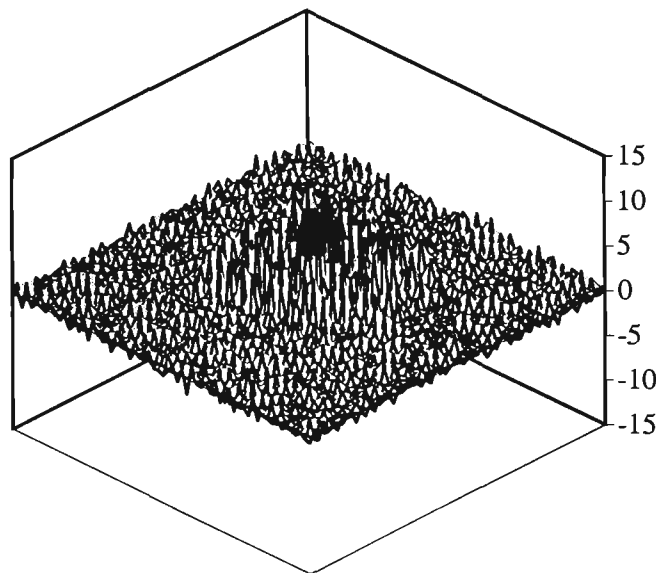


**Figure 5.5.5** Difference between the original image and the re-convolved image. No structure is evident with maximum differences of 5% at the peak of the image.

The ZBLANP fibre chosen for this imaging experiment, according to the manufacturer's specification, is 1,000ppm  $\text{Pr}^{3+}$  dopant concentration in a  $2.5\mu\text{m}$  diameter core. The fibre was mounted as vertical as possible on the adjustable table of the scanning confocal microscope. The 476.5nm line from an  $\text{Ar}^+$  laser was used to pump the system

at an input power of 7mW as measured at the input to the microscope. Neutral density filters were placed in the beam path to vary the input power to the system. Varying the input attenuator on the microscope unit varies the beam paths through the microscope causing the images to be offset from one another. The highest numerical aperture, 1.25, microscope objective was used to create the largest possible image. This was further enhanced by the use of the  $\times 10$  zoom control on the instrument. A  $100 \times 100$  region of interest was created and a  $\times 32$  Kalman filter used to provide the clearest images at the slowest scan speed. Reflected pump signal was removed by use of the BA590 filter which is incorporated within the microscope and passes wavelengths greater than 590nm. Input powers of  $73 \pm 3 \mu\text{W}$ ,  $63 \pm 3 \mu\text{W}$ ,  $55 \pm 2 \mu\text{W}$ ,  $43 \pm 3 \mu\text{W}$  and  $5.8 \pm 0.2 \mu\text{W}$  to the fibre on test were measured by placing the power meter directly on to the end of the microscope objective.

The modifying factor  $k$ , is determined by assuming that the volume of the noise reduced image is proportional to that of an “ideal” concentration profile. This profile, created from the manufacturer’s specifications, is that of a radially symmetric “top hat” function, the height of which is determined from the rate equations and the diameter is that specified for the fibre core. The ratio of the volume of the ideal image to that of the modified image is determined to be the modifying factor.

A least squares fit of the concentration profiles for the five different input powers to the rate equation model is used to determine the ultimate image concentration profile, figure 5.5.6. The square root of the sum of the squares is used to determine that the uncertainty in this image profile is  $\pm 9\%$ .

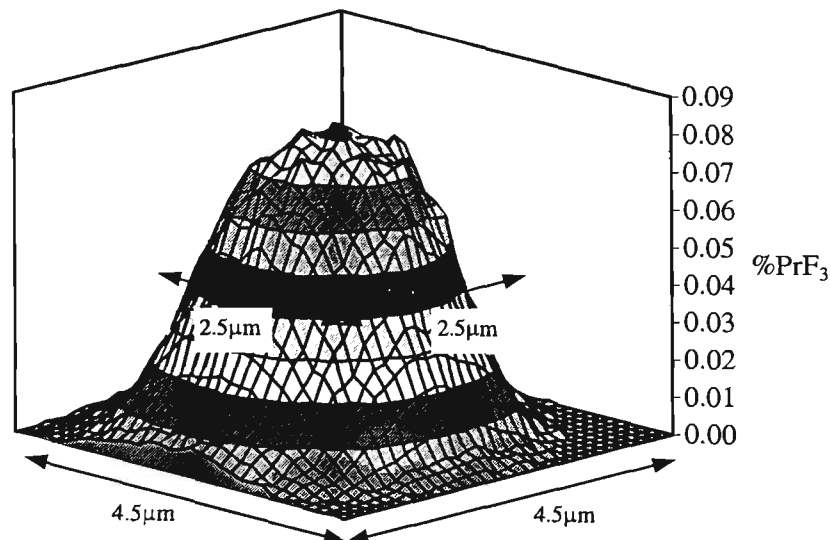


**Figure 5.5.6** Dopant concentration profile of a Pr:ZBLANP fibre.

As mentioned previously, an ideal concentration profile for the fibre would be a radially symmetric top hat function with the dopant material coinciding with the core of the fibre. From figure 5.5.6, it can be seen that the dopant has diffused into the cladding of the fibre, probably during the drawing process.

In the modeling of fibre amplifiers and lasers it is assumed that the concentration profile is a radially symmetric “top hat” function which, from figure 5.5.6 is clearly not the case. The peak concentration of the core region is not as great as would be assumed with the “top hat” profile and the average concentration is even less. With this imaging technique, actual concentration profiles can be determined which will allow more accurate modeling of fibre amplifiers and lasers.

## 5.6 1300nm amplifiers

Another very useful transition in  $\text{Pr}^{3+}$ ,  $^1\text{G}_4$  to  $^3\text{H}_5$ , is used to produce 1300nm amplifiers and lasers which are of particular interest to the communications industry [Nishida Y. *et al.*, 1998]. Current commercial systems utilise Nd:YLF lasers to directly populate the

$^1G_4$  state of  $Pr^{3+}$  [NTT Electronics, Fibercore]. The absorption oscillator strength to this state is an order of magnitude smaller than those of other absorptions in  $Pr^{3+}$  [chapter 2] as this transition requires a change of spin state for the ion. This change of state is forbidden under the selection rules, therefore ground state absorption to the  $^1G_4$  state is weak.

In chapter 3, it was established that there was energy transfer from  $Nd^{3+}$  in the  $^4F_{3/2}$  state to  $Pr^{3+}$ . One of the three possible mechanisms by which that energy could be transferred is relaxation of  $Nd^{3+}$  in the  $^4F_{3/2}$  state to the  $^4I_{11/2}$  state, exciting  $Pr^{3+}$  to the  $^1G_4$  state. A further energy transfer path that could populate the  $^1G_4$  state of  $Pr^{3+}$  is the cross-relaxation of  $Pr^{3+}$  in the  $^3P_0$  state. Some  $Pr^{3+}$  in the  $^3P_0$  state will relax directly to the  $^1G_4$  state by transferring energy to other  $Pr^{3+}$  in the ground state,  $^3H_4$ , causing ions in the ground state to excite also to the  $^1G_4$  state. Another path that could lead to the further population of the  $^1G_4$  state of  $Pr^{3+}$  is by energy transfer from  $Pr^{3+}$  in the  $^3P_0$  state of  $Pr^{3+}$  to  $Nd^{3+}$ . All three of these processes have been identified in chapter 3. The energy transfer parameters that are determined in chapter 3 do not uniquely quantify these three pumping paths for the  $^1G_4$  state of  $Pr^{3+}$ , thus making it difficult to discuss the efficiencies of these processes. However, all of these processes still require ground state absorption of the  $Pr^{3+}$  to the  $^1G_4$  state, which as discussed earlier, is a weak transition.

One particular benefit of utilising these energy transfer schemes is that  $Pr^{3+}$  in the  $^1G_4$  state will not relax by the stimulated emission caused by pump photons as can happen with direct pumping of this state. However, there are at least two competing processes when using this energy transfer scheme for pumping. Excited state absorption of 795nm pump photons will lead to a further excitation of  $Pr^{3+}$  in the  $^1G_4$  state to the  $^3P_0$  state.

This is not so much of a problem as part of the population of the  $^3P_0$  state relaxes to populate the  $^1G_4$  state of  $Pr^{3+}$ . If the dominant relaxation path for the  $^3P_0$  state is cross-relaxation then excited state absorption from the  $^1G_4$  state will actually be beneficial. One  $Pr^{3+}$  in the  $^1G_4$  state becomes one  $Pr^{3+}$  in the  $^3P_0$  state through excited state absorption but this then, through cross-relaxation, results in two  $Pr^{3+}$  in the  $^1G_4$  state. The second competing process is perhaps more detrimental to the performance of an amplifier or laser.  $Pr^{3+}$  in the  $^1G_4$  state is likely to relax by transfer of energy to  $Nd^{3+}$  in the  $^4F_{3/2}$  state, which leads to quenching of the  $^1G_4$  state population. Further work is required to quantify the energy transfer parameter that is used to describe this quenching process.

## 5.7 Temperature sensors

There are at least three potential temperature sensor configurations that can be constructed from a Pr:ZBLANP fibre. A fluorescence intensity ratio (FIR) sensor is possible utilising transitions from the  $^3P_0$  and  $^3P_1+^1I_6$  states of  $Pr^{3+}$ . These states are thermally linked therefore the ratio of the intensities of the fluorescence caused by transitions from the  $^3P_0$  and  $^3P_1+^1I_6$  states will be temperature dependent [Collins S. F. *et al.*, 1999]. The lifetime of the  $^3P_1+^1I_6$  state is different to that of the  $^3P_0$  state, however since these states are thermally linked, they can be considered to be a single state, the lifetime of which is thermally dependent on the lifetimes of the two constituent states. This aspect can be exploited to produce a fluorescence lifetime (FL) temperature sensor [Sun T. *et al.*, 1997]. By codoping with  $Nd^{3+}$ , it is possible to create both FIR and FL based temperature sensors which would operate with inexpensive laser diodes as the pump source.

The third scheme for a possible FL based temperature sensor has become apparent during the course of this work. As mentioned in chapter 2, the  $^1G_4$  state of  $Pr^{3+}$  is relatively highly temperature dependent. Using Judd-Ofelt theory, the radiative lifetime of this state is of the order of milliseconds. Experimental measurements show lifetimes of the order of  $100\mu s$  [Sugawa T. *et al.*, 1991]. This discrepancy is not due to the poor performance of Judd-Ofelt theory with regard to  $Pr^{3+}$  but due to phonon diffusion from this state. Inclusion of the phonon diffusion rate from the  $^1G_4$  state show predicted lifetimes similar to those measured by other workers, see chapter 2. The phonon diffusion rate is a temperature dependent process so by observing the fluorescence decay from the  $^1G_4$  state of  $Pr^{3+}$ , the temperature can be determined, figure 5.7.1.

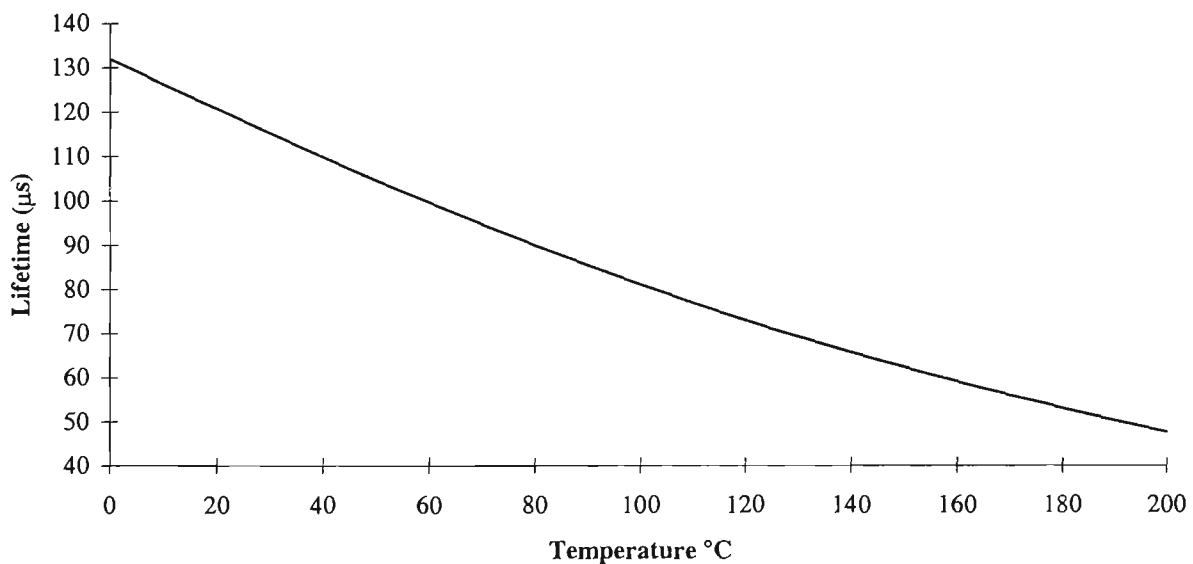


**Figure 5.7.1** Temperature dependence of the predicted lifetime of the  $^1G_4$  state of  $Pr^{3+}$ .

Ground state absorption to the  $^1G_4$  state of  $Pr^{3+}$  has a relatively small oscillator strength [chapter 2] therefore larger pump rates are required to establish significant excited state populations. The addition of  $Nd^{3+}$  allows an alternative pumping scheme at 795nm, which may be more efficient than pumping the ground state of  $Pr^{3+}$ . More work is

required to develop this sensor, including an investigation into more appropriate pumping schemes. The sensitivity for the proposed sensor is approximately 400ns/°C.

The host of this proposed temperature sensor, ZBLANP, is hygroscopic, delicate and has a melting point around 250°C. Some sort of sealed jacket would be required to provide mechanical support and to prevent moisture getting in. Other host materials may prove to be a better option. A silicate host is not appropriate as the large phonon energies reduce the lifetime of the  $^1G_4$  state to the order of hundreds of nano-seconds, requiring faster pump rates and detection systems.

One particular aspect of FL based temperature sensors that is of interest is the effect of concentration dependent process on lifetime. An initial investigation can be made by extracting results for the  $^3P_0$  state of  $Pr^{3+}$  from a paper by Sun [Sun T. *et al.*, 1997], figure 5.7.2. The previous simplified analysis of this data set had been carried out ignoring any concentration-dependent effects but clearly this is something of an approximation. It is important to determine the degree to which this approximation limits the performance of a sensor system and to provide a better calibration. The relaxation rate of the  $^3P_0$  state is a linear function of the concentration, as shown in the theoretical analysis presented in chapter 3. This allows the concentration independent decay rate and the energy transfer parameter,  $\alpha_1(T)$ , to be determined for each temperature, T, from

$$\omega = \omega_{P_8} + \alpha_1(T)\rho_P, \quad (5.7.1)$$

where  $\omega$  is the fluorescence decay rate,  $\omega_{P_8}$  is the concentration independent decay rate,  $\rho_P$  is the  $Pr^{3+}$  concentration and  $\alpha_1(T)$  is the energy transfer parameter. The linear least

squares fitting of equation 5.7.1 to the raw data is represented by the solid curves in figure 5.7.3 for a series of temperatures in the region of interest, 300 to 500 K.

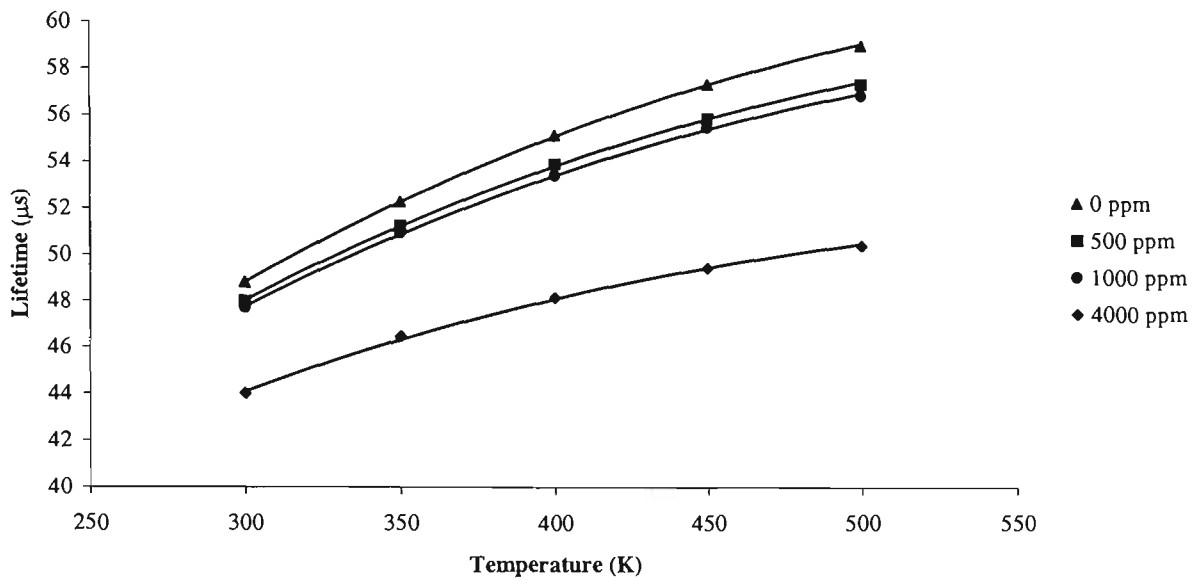


**Figure 5.7.2** Measured lifetimes of the  $^3P_0$  state as a function of temperature for various  $Pr^{3+}$  concentrations. This plot has been derived from data extracted from the work of [Sun T. *et al.*, 1997] and includes data derived for the lifetimes in the limit of zero dopant concentration.

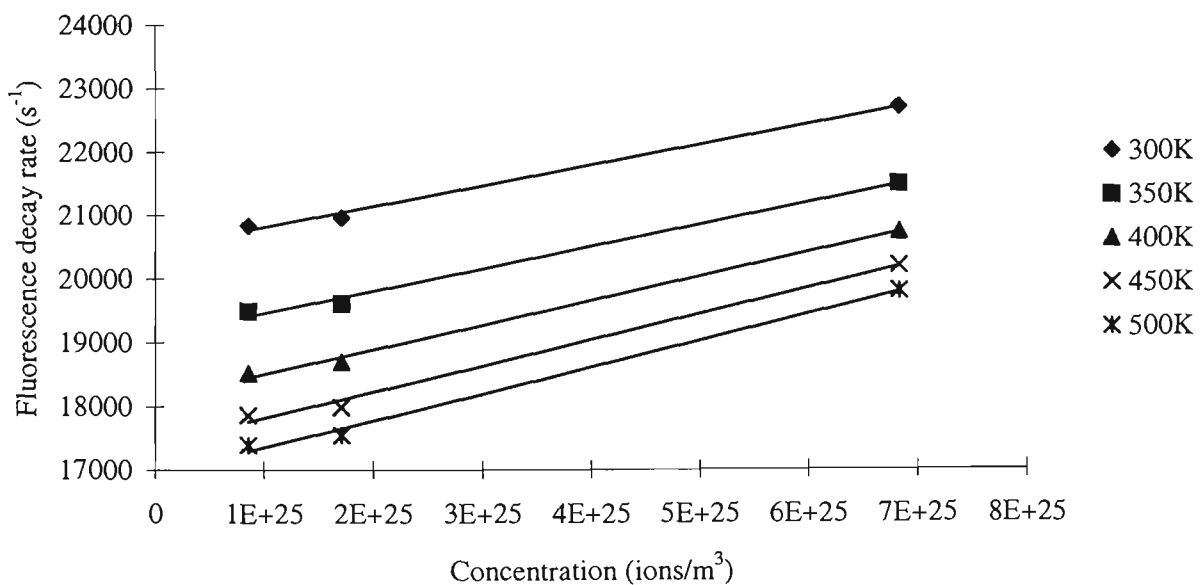


**Figure 5.7.3** Fluorescence decay rates as a function of  $Pr^{3+}$  concentration for various temperatures. This data has been extracted from the work of [Sun T. *et al.*, 1997].

The analysis of the data shows that the temperature responsivity decreases with increasing concentration over the range studied. It is therefore preferable to use a low concentration praseodymium sample as the sensing element. While there is a trade off between smaller signal levels at low concentration and increased temperature sensitivity, practical sensor systems can be constructed using low concentrations of  $\text{Pr}^{3+}$ , thereby avoiding deleterious concentration effects.

Figure 5.7.4 shows the energy transfer parameter,  $\alpha_1$ , again for the same range of temperatures. While this illustrates an approximately linear change with temperature over the range studied, it is expected that a saturation of this effect could be shown at sufficiently high temperatures. For completeness, the parameters of the linear least squares fit shown in figure 5.7.4 are  $1.9 \pm 0.2 \times 10^{-23} \text{ m}^3/\text{s}$  for the intercept and  $0.0048 \pm 0.0004 \times 10^{-23} \text{ m}^3/\text{s/K}$  for the slope.

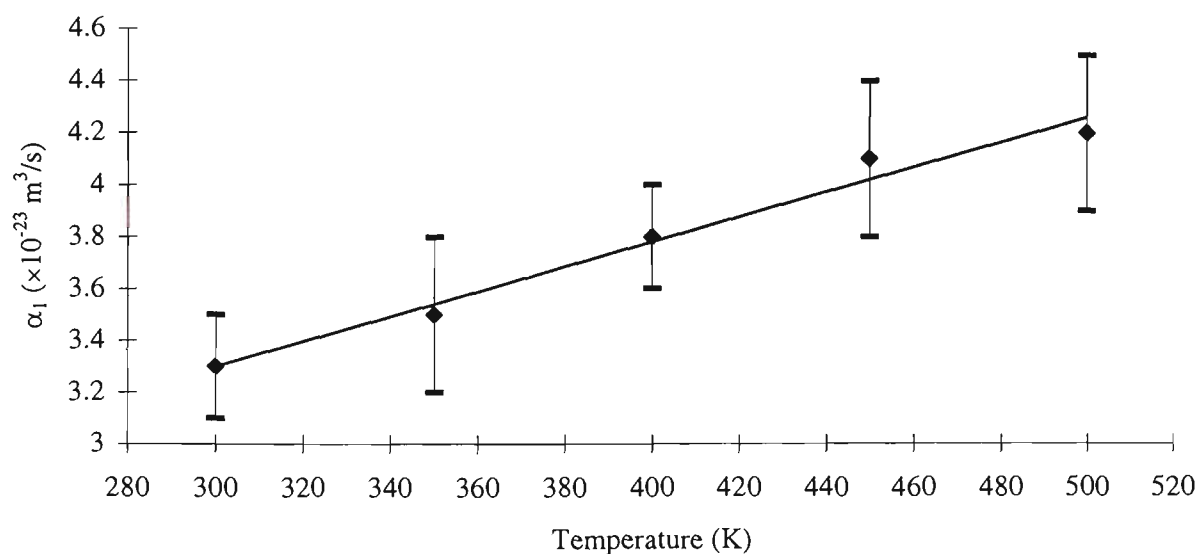


**Figure 5.7.4** Energy transfer parameter  $\alpha_1$  as a function of temperature.

Previous investigations by Sun [Sun T. *et al.*, 1999] of the similar  $\text{Nd}^{3+}$  ion in both silica glass and in yttrium aluminium garnet (YAG) showed very different behaviour of the

fluorescence decay time of that ion in these different hosts with temperature. An ambiguous response (for temperature sensor calibration) was seen over the range from 300 to 1000 K for the Nd<sup>3+</sup>:YAG but not for the Nd<sup>3+</sup>:glass. The explanation given by Sun [Sun T. *et al.*, 1999] appeared consistent with the ratio of the multiphonon cross section to the total radiative cross section of the <sup>4</sup>F<sub>3/2</sub> state being  $\cong 0.25$ , and a significant level of multiphonon quenching being present. The situation in this material has been analysed by a number of authors, as discussed in the paper by Sun [Sun T. *et al.*, 1999, and references therein], reaching the general conclusion that the complex nature of the system made the interpretation of the results difficult – the likelihood is that a similar complexity prevails in the Pr<sup>3+</sup> ion in the ZBLAN host. As a result, the development of an effective quasi-empirical calibration that may be used is a useful achievement of this type of analysis.

The analysis that has been carried out has shown that there is a concentration dependence on the lifetime against temperature data, which has an effect upon the calibration of any optical sensor constructed using this material. It is important to be able to appeal to a calibration that is soundly based upon the fundamental physical principles which underpin the characteristics of the material involved, so that any systematic errors may be more easily determined and corrections applied. In particular, in cases where the material may be produced in different batches, with the same *nominal* but a different *actual* dopant concentrations, the calibration data can therefore be corrected and the precision of the resulting sensor improved, thus easing constraints on material manufacture and supply. This makes it easier to source material for these sensors from different suppliers, without the major concerns of different calibration

sensitivities resulting from the sensors produced. Further, this sort of analysis could be applied to other species similarly doped, or co-doped in these hosts, e.g.  $\text{Nd}^{3+}$ ,  $\text{Nd}^{3+}/\text{Pr}^{3+}$  and  $\text{Er}^{3+}/\text{Yb}^{3+}$ , all of which are important in both temperature and strain sensors [Sun T. *et al.*, 1999]. The fact that increasing concentration decreases the temperature responsivity for  $\text{Pr}^{3+}$  doped ZBLAN cannot be used as evidence that this behaviour is the same for other transitions in the rare earths, due to the complicated temperature dependence of the emission and absorption cross sections. This is the subject of continuing work by the authors.

It was expected that the energy transfer parameter,  $\alpha_1$ , should be similar in magnitude to the  $\alpha_1$  calculated in chapter 3. A plot of  $\alpha_1$  as a function of temperature, figure 5.7.4, shows that this is not the case. A speculative reason for this is that when  $\text{NdF}_3$  and  $\text{PrF}_3$  are codoped into a ZBLANP host, the  $\text{NdF}_3$  tends to occupy sites collectively as does the  $\text{PrF}_3$ . This causes an apparent increase of the dopant concentrations and therefore changes the magnitude of the determined energy transfer parameters. More work is required to test the validity of this speculation.

## 5.8 The future for Nd:Pr codoping

By parameterising Nd:Pr:ZBLANP it has become clear that the proposed pumping scheme to establish population in the  $^3\text{P}_0$  state of  $\text{Pr}^{3+}$  is too inefficient to produce a laser or amplifier. The weakness in the scheme is the large relaxation rate from phonon diffusion of the  $^2\text{G}_{9/2}$  state when compared to the energy transfer rate from this state to  $\text{Pr}^{3+}$ . For a 2%  $\text{PrF}_3$  doped glass, the efficiency of the transfer is approximately 2% which, when considering the 2% efficiency of the excited state absorption pumping

scheme, provides an insufficient overall pumping scheme. A further problem is the large level of quenching caused by energy transfer back to  $\text{Nd}^{3+}$  from the  ${}^3\text{P}_0$  state as quantified by  $\alpha_2$ . For a 1% $\text{NdF}_3$  doped glass, this energy transfer rate,  $11,286\text{s}^{-1}$ , is over half of the normal radiative rate of the  ${}^3\text{P}_0$  state,  $20,000\text{s}^{-1}$ .

One possible method for improving the pumping efficiency is to add a further codopant, ytterbium ( $\text{Yb}^{3+}$ ).  $\text{Yb}^{3+}$  has only one broad absorption band from 900nm to  $1\mu\text{m}$  [France P.W., 1990]. The pump wavelength (795nm) would remain the same and the pump process would also essentially remain the same. The extra efficiency would come as a result of energy transferring to the excited state of  $\text{Yb}^{3+}$ , which is relatively long lived. Relaxation of  $\text{Yb}^{3+}$  by transfer of energy to  $\text{Nd}^{3+}$  in the ground state is unlikely due to the energy mismatch. However, relaxation of the  $\text{Yb}^{3+}$  by transfer of energy to  $\text{Nd}^{3+}$  in the  ${}^4\text{F}_{3/2}$  state will excite the  $\text{Nd}^{3+}$  directly to the excited states which are in resonance with the higher energy states of  $\text{Pr}^{3+}$ . As outlined previously, these higher excited states of  $\text{Nd}^{3+}$  are short lived so this is not expected to greatly improve the pumping process. As mentioned in chapter 3, one of the transfer processes from the  ${}^4\text{F}_{3/2}$  state of  $\text{Nd}^{3+}$  is by excitation of the  $\text{Pr}^{3+}$  to the  ${}^1\text{G}_4$  state. The addition of  $\text{Yb}^{3+}$  will contribute to this situation as the excited state overlaps those of  $\text{Pr}^{3+}$  and  $\text{Nd}^{3+}$  providing an intermediate state through which energy can cascade leading to greater population of the  ${}^1\text{G}_4$  state of  $\text{Pr}^{3+}$ . If a 795nm pump photon was to interact with  $\text{Pr}^{3+}$  in the  ${}^1\text{G}_4$  state then it would excite the ion to the  ${}^3\text{P}_2$  state from which it would quickly relax to the  ${}^3\text{P}_0$  state. This process becomes more common with greater population of the  ${}^1\text{G}_4$  state. A further path for populating the  ${}^3\text{P}_0$  state occurs when  $\text{Nd}^{3+}$  in the  ${}^4\text{F}_{3/2}$  state relaxes simultaneously with an excited  $\text{Yb}^{3+}$ , transferring energy to a  $\text{Pr}^{3+}$ . This is a three ion

process but as has been discussed in chapter 3, these do occur and are more likely to occur with higher dopant concentrations. Predictions for dopant concentrations will require further work and appropriate modeling. However, even then this new scheme may not work due to unforeseen relaxation paths and it does not reduce the loss associated with the  $\alpha_2$  parameter to  $\text{Nd}^{3+}$ .

## 5.9 Conclusion

A new, non-destructive technique has been developed for the imaging of fibre dopant concentration profiles. The new technique involves fluorescence measurements utilising a commercial scanning confocal microscope. Manufacturer specifications are required for low concentrations of singly doped fibre to determine the modifying proportionality constant of the image. Normalising the fluorescence is a simple technique but can only be performed with higher concentrations or if there are codopants. The threshold at which normalising can be used is dependent on the magnitude of the energy transfer parameters and the concentration products. This new technique combines ease of use with currently available equipment.

From the gain experiments it is clear that the current pumping scheme is inadequate. The potential for creating a multi-line laser remains but a more efficient pumping scheme is required. The addition of  $\text{Yb}^{3+}$  as a further codopant creates several new paths by which the  $^3\text{P}_0$  state of  $\text{Pr}^{3+}$  can be populated and will be of benefit to the current pumping scheme. Should a more efficient pumping scheme be discovered then the potential laser or amplifier medium would need to be in the form of a fibre. This is shown when directly pumping the  $\text{Pr}^{3+}$ , it is only possible to attain gains greater than one

if the pump spot size is small. A further possibility for pumping this material would be to use a pulsed light source however, these sources tend to be expensive and not particularly compact. As well, cw operation is a requirement of the original motivation for this work.

A new fluorescence lifetime temperature sensor has been proposed involving the  $^1G_4$  state of  $Pr^{3+}$ . Nd:Pr:ZBLANP glass facilitates the use of the use of inexpensive laser diodes as a pumping source. The most efficient pumping scheme is yet to be determined and the addition of  $Yb^{3+}$  as a further codopant may improve the efficiency of a potential fluorescence lifetime temperature sensor.

Further to the work of chapter 3, it has been observed from data presented by Sun [Sun T. *et al.*, 1997] that the energy transfer parameters are temperature dependent. Analysis of the work with regard to concentration dependent processes will facilitate the better design of optical sensors. Concentration of dopant species can be optimised to achieve high levels of fluorescence emission leading to improved signal-to-noise ratio in the system and can provide high sensitivity to the parameter of interest. Knowledge of the concentration dependent processes allows workers to be able to deal better with cross-sensitivities, such as those to strain or pressure and temperature, by selection of the best material for any particular application. In addition, the use of co-dopants greatly facilitates the pumping efficiency of sensor systems of this type, but this must not be at the expense of deleterious effects on the ion-ion interactions involved due to the presence of these additional, and usually helpful species present. Further experimental investigation of such co-doped materials is continuing.

The data from Sun [Sun T. *et al.*, 1997] also revealed a significant difference between the two ion intra-species energy transfer parameters  $\alpha_1$  for the Pr:ZBLANP and the Nd:Pr:ZBLANP glass. A speculative reason for this difference has been proposed but further work is required to establish its validity.

Due to excited state absorptions in  $\text{Nd}^{3+}$ , Nd:Pr:ZBLANP will not produce an efficient fibre amplifier for the 1300nm communications window. The addition of  $\text{Yb}^{3+}$  will increase the excited state population but it seems unlikely that this will be sufficient to produce large gains.

# 6. Conclusions

Section.....	Page
6.1 Conclusion.....	6-2

## 6.1 Conclusion

This is the concluding chapter of a study on Nd:Pr:ZBLANP glasses in which a model has been developed including terms for concentration dependent energy transfer processes. Seven energy transfer parameters are required for the model and all have been determined during the course of this study. The techniques that have been employed are equally applicable to all the rare-earth doped amplifiers and lasers. It is hoped that workers in the field will continue to determine such parameters so that similar modelling can be applied to a wide variety of rare earth doped amplifiers and lasers. The cataloguing of these energy transfer parameters would be of great benefit to glass makers, researchers and manufacturers of such devices.

The model produced in this study has been used to predict the performance of a Pr<sup>3+</sup> based laser or amplifier system as well as to image the dopant concentration profile of a fibre. Unfortunately, it would seem that the intended pumping scheme is too inefficient to fulfil many of the applications mentioned in the first chapter. The inefficient pumping scheme produces populations in the <sup>3</sup>P<sub>0</sub> state of Pr<sup>3+</sup> that are too small to produce sufficient gain to overcome the losses of the system. The addition of a third dopant, Yb<sup>3+</sup>, should be investigated as a possible enhancement to the current pumping scheme.

The possibility of producing an amplifier for applications in the 1300nm communications window is unlikely. The addition of Nd<sup>3+</sup> marginally aids the pumping process of the <sup>1</sup>G<sub>4</sub> state of Pr<sup>3+</sup> but energy transfer from this state of Pr<sup>3+</sup> back to Nd<sup>3+</sup> and excited state absorption of 1300nm in Nd<sup>3+</sup> will contribute significant losses to the system.

The problems of Judd-Ofelt theory when applied to  $\text{Pr}^{3+}$  have not been fully solved. It is certainly true that some sort of expanded theory is required for this ion but this must be coupled with the inclusion of uncertainties in the least squares fitting process. It seems that the initial obsession with workers in this field has been to produce non-negative Judd-Ofelt parameters. This is clearly achievable by the weighting of the fitting process. While temperature dependence of Judd-Ofelt parameters have been observed for both  $\text{Nd}^{3+}$  and  $\text{Pr}^{3+}$ , predictions of spectroscopic parameters for  $\text{Nd}^{3+}$  do not show significant temperature dependence. The predictions for  $\text{Pr}^{3+}$  spectroscopic parameters show significant temperature dependence but the Judd-Ofelt theory is too unstable when applied to  $\text{Pr}^{3+}$  to draw any conclusions from this. The incorporation of lifetime data into the fitting process does not improve the reliability of the theory when applied to  $\text{Pr}^{3+}$ , however this may still be a useful technique to improve the precision and accuracy of predictions of spectroscopic parameters for other rare earth doped materials. Perhaps the next attempt to establish a reliable technique for  $\text{Pr}^{3+}$  should be to apply a weighted fit to the modified theory as proposed by Kornienko [Kornienko A. A. *et al.*, 1990].

A fluorescence intensity ratio based temperature sensor that can be pumped with inexpensive 795nm laser diodes is realisable. A further temperature sensor based on the fluorescence lifetime of the  $^1\text{G}_4$  state that would also be pumped with a 795nm laser diode is also realisable. Both of these sensors have medical applications and could be operated simultaneously in the same device. Further research is required in to the performance of the sensors with consideration given to packaging for commercial use.

The technique of describing energy transfer with the energy transfer parameters is simple, applicable to all rare-earths and with the advent of variable wavelength pulsed

lasers, accessible to many researchers. The parameters define energy transfers between ions of the same species and between ions of different species. They provide quantitative information on energy transfer rates making them extremely useful in the design of optical amplifiers and lasers.

Not only are the energy transfer parameters essential for modelling of amplifiers and lasers, they are central to two techniques for dopant concentration determination. The first technique involves a single measurement of lifetime of an appropriate transition. Many currently available scanning confocal microscopes do not have the necessary timing functions required to image concentration profiles with this technique. For this reason, a second involving simple fluorescence measurements for a number of different input powers has been developed. This second technique depends on the knowledge of an average dopant concentration. This can be easily determined by application of the first technique to a large area of the sample.

The possibility of producing a  $\text{Pr}^{3+}$  based multi-line fibre laser for the many applications that are mentioned in chapter one, is still good if the appropriate pumping scheme can be found. Desired transitions can be made to lase ahead of competing transitions with inclusion of in-fibre bragg gratings. An appropriate photonic device may include several fibres, each tuned by an appropriate pair of bragg reflectors and pumped by the same source.

## References

Anonymous, Model 3900S CW Ti:sapphire laser instruction manual, Spectra-Physics, 1990.

Anonymous, Stabilite<sup>®</sup> 2017 ion laser user's manual, Spectra-Physics, 1994.

Arons I. J. "The outlook for diode lasers in medicine," Proceedings SPIE Biomedical Fiber Optic Instrumentation, vol 2131, pp 24, Jan. 1994.

Balda R., Fernández J., Mendioroz A., Adam J. L. and Boulard B. "Temperature-dependent concentration quenching of Nd<sup>3+</sup> fluorescence in fluoride glasses," Journal of Condensed Matter, vol 6, pp 913, 1994.

Berthou H. and Jørgensen C. K. "Optical fiber temperature sensor based on upconversion excited state fluorescence," Optical Letters, vol 15, no 19, pp 1100, 1990.

Binnemans K. and Görller-Walrand C. "Are the Judd-Ofelt intensity parameters sensitive enough to reflect small compositional changes in lanthanide-doped glasses?" Journal of Physics: Condensed Matter, vol 10, pp L167, 1998.

Bogdanov V., Gibbs W. E. K., Booth D. J., Javorniczky J., Newman P. J. and MacFarlane D. R., "Fluorescence from highly doped erbium fluorozirconate glasses pumped at 800nm," Optics Communications, Vol 132, pp 73, 1996.

Bucholtz C. "Blue lasers increase disc storage space," Computer, vol 28, no 6, pp 9, 1995.

Carnall W. T., Fields P. R. and Rajnak K. "Electronic energy levels in the trivalent lanthanide aquo ions. I. Pr<sup>3+</sup>, Nd<sup>3+</sup>, Pm<sup>3+</sup>, Sm<sup>3+</sup>, Dy<sup>3+</sup>, Ho<sup>3+</sup>, Er<sup>3+</sup>, and Tm<sup>3+</sup>," Journal of Chemical Physics, vol 49, no 10, pp 4424, 1968.

Collins S. F., Baxter G. W., Wade S. A., Sun T., Grattan K. T. V., Zhang Z. Y. and Palmer A. W. "Comparison of fluorescence-based temperature sensor schemes: Theoretical analysis and experimental validation," *Journal of Applied Physics*, vol 84, no 9, pp 1, 1999.

Culshaw B. and J. Dakin (editors) "Optical fiber sensors: systems and applications," Artech House Inc., 1988.

Digonnet M. J. F. (editor) "Rare earth doped fiber lasers and amplifiers," Marcel Dekker, Inc., 1993.

Fasol G. "Longer life for the blue laser," *Science*, vol 278, pp 1902, 1997.

Fibercore. "1.3-AMPU, Series 20," <http://www.fibercore.com/products/1300amp.html>.

France P. W. "Fluoride glass optical fibers," CRC Press, Inc., 1990.

Goh S. C., Pattie R., Byrne C. and Coulson D. "Blue and red laser action in Nd<sup>3+</sup>:Pr<sup>3+</sup> co-doped fluorozirconate glass," *Applied Physics Letters*, vol 67, no 6, pp 768, 1995.

Goldner P. and Auzel F. "Comparison between standard and modified Judd-Ofelt theories in a Pr<sup>3+</sup>-doped fluoride glass," *Acta Physica Polonica A*, vol 90, no 1, pp 191, 1996.

Grattan K. T. V. and Meggitt B. T. (editors) "Optical fiber sensor technology, vol 2," Chapman & Hall, 1998.

Gu M. "Principles of three-dimensional imaging in confocal microscopes," World Scientific, 1996.

Hecht E. "Optics, 2<sup>nd</sup> edition," Addison-Wesley Publishing Company, 1990.

Hecht J. "Galium nitride heats up blue-green laser race," Laser Focus World, vol 32, pp 53, 1996.

Hemmerlich A., Zimmermann C. and Hansch T. W. "Compact source of coherent blue light," Applied Optics, vol 33, no 6, pp 988, 1994.

Hilborn R. C. "Einstein coefficients, cross sections,  $f$  values, dipole moments, and all that," American Journal of Physics. Vol 50, no 11, pp 982, 1982.

Huang Z., Chia T., Zheng W., Xie S., Diong C. and Seow-Choen F. "Fluorescence spectroscopy of human colon tissues," Proceedings SPIE Biomedical Optics and Lasers: Diagnostics and Treatments, vol 3548, pp 234, Sept 1998.

Jacquier B., Remillieux A. and Joubert M. F. "Upconversion and relaxation of high lying states in rare-earth-doped ZBLAN bulk and fibers," Journal of Non-Crystalline Solids, vol 161, pp 241, 1993.

Judd B. R. "Optical absorption intensities of rare-earth ions," Physical Review, vol 127, no 3, pp 750, 1962.

Kornienko A. A., Kaminski A. A. and Dunina E. B. "Dependence of the line strength of  $f$ - $f$  transitions on the manifold energy," Physica Status Solidi B, vol 157, pp 267, 1990

Laufer G. "Introduction to Optics and Lasers in Engineering," Cambridge University Press, 1996.

Li J. and Harrington J. A. (chairs and editors) "Biomedical optics and lasers: diagnostics and treatments," Proceedings SPIE Beijing, China, September 1998.

Maurice E., Monnom G., Baxter G. W., Wade S. A., Petreski B. P. and Collins S. F. "Blue light-emitting-diode-pumped point temperature sensor based on a fluorescence intensity ratio in Pr<sup>3+</sup>:ZBLAN glass," *Optical Review*, vol 4, no 1A, pp 89, 1997.

Maurice E., Wade S. A., Collins S. F., Monnom G. and Baxter G. W. "Self-referenced point temperature sensor based on a fluorescence intensity ration in Yb<sup>3+</sup>-doped silica fiber," *Applied Optics*, vol 36, pp 8264, 1997.

Medeiros Neto J. A., Hewak D. W. and Tate H. "Application of a modified Judd-Ofelt theory to praseodymium-doped fluoride glasses," *Journal of Non-Crystalline Solids*, vol 183, pp 201, 1995.

Mitchell I. R., Bogdanov V. K. and Farrell P. M. "Energy transfer in praseodymium and neodymium co-doped fluorozirconate glass," *Optics Communications*, vol 155, pp 275, 1998.

Nakamura S. "Blue lasers meet tough commercial requirements," *Photonics Spectra*, vol 32, no 5, pp 130, 1998.

Nishida Y., Yamada M., Kanamori T., Kobayashi K., Temmyo J., Sudo S. and Ohishi Y. "Development of an efficient praseodymium-doped fiber amplifier," *IEEE Journal of Quantum Electronics*, vol 34, no 8, pp 1332, 1998.

NTT Electronics. "FA1300DSF," <http://www.nel.co.jp/photo/fa/fa1300dsf.html>.

Ofelt G. S. "Intensities of crystal spectra of rare-earth ions," *Journal of Chemical Physics*, vol 37, pp 511, 1962.

Petreski B. P., Farrell P. M. and Collins S. F. "Cross-relaxation in praseodymium-doped fluorozirconate glass," *Optics Communications*, vol 132, pp 89, 1996.

Petreski B. P., Mitchell I. R. and Farrell P. M. "Measurement of lifetime in Pr<sup>3+</sup> doped ZBLANP," Australian Optical Society Conference, Brisbane 1995.

Petreski B. P., Schilders S. P., Farrell P. M. and Gu M. "Imaging concentration profiles of praseodymium-doped optical fibres," Electronics Letters, vol 33, no 10, pp 889, 1997.

Quimby R. S. and Miniscalco W. J. "Modified Judd-Ofelt technique and application to optical transitions in Pr<sup>3+</sup>-doped glass," Journal of Applied Physics, vol 75, pp 613, 1994.

Reisfeld R. and Jørgensen C. K. "Lasers and excited states of rare earths," Springer-Verlag, 1977.

Reisfeld R., and Jørgensen C. K. "Excited state phenomena in vitreous materials," Elsevier, 1987.

Remillieux A., Jacquier B., Linares C., Lesergent C., Artigaud S., Bayard D., Hamon L. and Beylat J. L. "Upconversion mechanisms of a praseodymium-doped fluoride fibre amplifier," Journal of Physics D: Applied Physics, vol 29, pp 963, 1996.

Shimada S. and Ishio H. (editors) "Optical amplifiers and their applications," John Wiley & Sons Ltd. 1994.

Siegman A. E. "Lasers," University Science Books, 1986.

Stanley A. T., Harris E. A., Searle T. M. and Parker J. M. "Upconversion in neodymium doped fluoride glasses," Journal of Non-Crystalline Solids, vol 161, pp 235, 1993.

Sugawa T. and Miyajima Y. "Gain and output-saturation limit evaluation in Pr<sup>3+</sup>-doped fluoride fiber amplifier operating in the 1.3 $\mu$ m band," IEEE Photonics Technology Letters, vol 3 pp 616, 1991.

Sun T., Zhang Z. Y., Grattan K. T. V. and Palmer A. W. "Intrinsic strain and temperature characteristics of Yb-doped silica-based optical fibers," Review of Scientific Instruments, vol 70, no 2, pp 1447, 1999.

Sun T., Zhang Z. Y., Grattan K. T. V., Palmer A. W and Collins S. F. "Temperature dependence of the fluorescence lifetime in Pr<sup>3+</sup>:ZBLAN glass for fiber optic thermometry," Review of Scientific Instruments, vol 68, no 9, pp 3447, 1997.

Svelto O. "Principles of lasers," 3<sup>rd</sup> edition, Plenum Press, 1989.

Tohman G., Sato H., Ohya J. and Uno T. "Thulium:ZBLAN blue fiber laser pumped by two wavelengths," Applied Optics, vol 36, no 15, pp 3381, 1997.

Tropper A. C., Carter J. N., Lauder R. D. T. and Hanna D. C. "Analysis of blue and red laser performance of the infrared-pumped praseodymium-doped fluoride fiber laser," Journal Optical Society of America B., vol 11, no 5, pp 886, 1994.

Webjorn J. and Waarts R. G. "Frequency doubling offers advantages for blue lasers," Laser Focus World, vol 34, no 5, pp 135, 1998.

Zellmer H., Plamann K., Huber G., Scheife H. and Tuennermann A. "Visible double-clad upconversion fibre laser," Electronics Letters, vol 34, no 6, pp 565, 1998.

Zhao Y. and Fleming S. "Theory of Pr<sup>3+</sup>-doped fluoride fiber upconversion lasers," IEEE Journal of Quantum Electronics, vol 33, no 6, pp 905, 1997.

Zhao Y., Fleming S. and Poole S. 22mW blue output power from a Pr<sup>3+</sup> fluoride fibre upconversion laser," Optics Communications, vol 114, pp 285, 1995.

# Publications, conference and meeting presentations,

arising from this work

**I. R. Mitchell**, P. M. Farrell, G. W. Baxter, S. F. Collins, K. T. V. Grattan and T. Sun.  
“Analysis of dopant concentration effects in praseodymium-based fluorescent fibre optic temperature sensors,” Submitted to Review of Scientific Instruments, June 1999.

**I. R. Mitchell**, V. K. Bogdanov and P. M. Farrell. “Energy Transfer in Praseodymium and Neodymium Co-Doped Fluorozirconate Glass,” Optics Communications, Vol 155, Nos 4,5,6 1998, p275-280.

**I. R. Mitchell** and P. M. Farrell. “Temperature Dependence of Judd-Ofelt Parameters for Pr:ZBLANP and Nd:ZBLANP Glasses,” Australian Conference on Optical Fiber Technology, Melbourne 1998.

**I. R. Mitchell**, B. P. Petreski, S. P. Schilders, P. M. Farrell, G. W. Baxter and M. Gu.  
“Imaging Concentration Profiles in Pr<sup>3+</sup> Nd<sup>3+</sup> Co-Doped ZBLANP Fiber,” Australian Optical Society Conference, Adelaide 1997.

**I. R. Mitchell** and P. M. Farrell. “Judd-Ofelt Parameters in Pr<sup>3+</sup> and Nd<sup>3+</sup> Co-Doped ZBLANP,” Australian Optical Society Conference, Adelaide 1997.

**I. R. Mitchell** and P. M. Farrell. “Cross Relaxation and Energy Transfer in Praseodymium and Neodymium Co-Doped ZBLANP,” Optical Guided Waves and Applications Meeting, Canberra 1997.

B. P. Petreski, **I. R. Mitchell** and P. M. Farrell. “Measurement of Lifetime in Pr<sup>3+</sup> Doped ZBLANP,” Australian Optical Society Conference, Brisbane 1995.

# **Publications, conference and meeting presentations,**

arising from this work

**I. R. Mitchell**, P. M. Farrell, G. W. Baxter, S. F. Collins, K. T. V. Grattan and T. Sun.  
“Analysis of dopant concentration effects in praseodymium-based fluorescent fibre optic  
temperature sensors,” Submitted to Review of Scientific Instruments, June 1999.

**I. R. Mitchell**, V. K. Bogdanov and P. M. Farrell. “Energy Transfer in Praseodymium  
and Neodymium Co-Doped Fluorozirconate Glass,” Optics Communications, Vol 155,  
Nos 4,5,6 1998, p275-280.

**I. R. Mitchell** and P. M. Farrell. “Temperature Dependence of Judd-Ofelt Parameters for  
Pr:ZBLANP and Nd:ZBLANP Glasses,” Australian Conference on Optical Fiber  
Technology, Melbourne 1998.

**I. R. Mitchell**, B. P. Petreski, S. P. Schilders, P. M. Farrell, G. W. Baxter and M. Gu.  
“Imaging Concentration Profiles in Pr<sup>3+</sup> Nd<sup>3+</sup> Co-Doped ZBLANP Fiber,” Australian  
Optical Society Conference, Adelaide 1997.

**I. R. Mitchell** and P. M. Farrell. “Judd-Ofelt Parameters in Pr<sup>3+</sup> and Nd<sup>3+</sup> Co-Doped  
ZBLANP,” Australian Optical Society Conference, Adelaide 1997.

**I. R. Mitchell** and P. M. Farrell. "Cross Relaxation and Energy Transfer in Praseodymium and Neodymium Co-Doped ZBLANP," Optical Guided Waves and Applications Meeting, Canberra 1997.

B. P. Petreski, **I. R. Mitchell** and P. M. Farrell. "Measurement of Lifetime in Pr<sup>3+</sup> Doped ZBLANP," Australian Optical Society Conference, Brisbane 1995.





